applied sciences

MDPI

Review

Review of Shape-Memory Polymer Nanocomposites and Their Applications

Rafiqul Islam [1,2], Sugandika Maparathne [1,2], Pailinrut Chinwangso [1,2] and T. Randall Lee [1,2,*]

[1] Department of Chemistry, University of Houston, 4800 Calhoun Road, Houston, TX 77204-5003, USA; spsmapa@gmail.com (S.M.); pchinwa3@central.uh.edu (P.C.)
[2] Texas Center for Superconductivity, University of Houston, 4800 Calhoun Road, Houston, TX 77204-5003, USA
* Correspondence: trlee@uh.edu

Abstract: Shape-memory polymer nanocomposites (SMPNCs) have emerged as a transformative class of smart materials, combining the versatility of shape-memory polymers (SMPs) with the enhanced properties imparted by nanostructures. Integrating these nanofillers, this review explores the pivotal role of SMPNCs in addressing critical limitations of traditional SMPs, including low tensile strength, restricted actuation modes, and limited recovery stress. It comprehensively examines the integration of nanofillers, such as nanoparticles, nanotubes, and nanofibers, which augment mechanical robustness, thermal conductivity, and shape-recovery performance. It also consolidates foundational knowledge of SMPNCs, covering the principles of the shape-memory phenomenon, fabrication techniques, shape-recovery mechanisms, modeling approaches, and actuation methods, with an emphasis on the structural parameters of nanofillers and their interactions with polymer matrices. Additionally, the transformative real-world applications of SMPNCs are also highlighted, including their roles in minimally invasive medical devices, adaptive automotive systems, 4D printing, wearable electronics, and soft robotics. By providing a systematic overview of SMPNC development and applications, this review aims to serve as a comprehensive resource for scientists, engineers, and practitioners, offering a detailed roadmap for advancing smart materials and unlocking the vast potential of SMPNCs across various industries in the future.

Keywords: shape-memory polymer nanocomposites (SMPNCs); nanofillers; actuation; mechanism; functional nanomaterials; shape recovery; shape fixity

Academic Editor: Roberto Zivieri

Received: 23 December 2024
Revised: 17 February 2025
Accepted: 18 February 2025
Published: 24 February 2025

Citation: Islam, R.; Maparathne, S.; Chinwangso, P.; Lee, T.R. Review of Shape-Memory Polymer Nanocomposites and Their Applications. *Appl. Sci.* **2025**, *15*, 2419. https://doi.org/10.3390/app15052419

1. Introduction

Nature's remarkable adaptability has long inspired the development of stimuli-responsive materials. For example, the Venus flytrap's rapid leaf closure (≤100 ms) to capture insects, triggered by mechanosensory hairs on its surface, exemplifies the potential of materials to respond dynamically to external stimuli [1]. Similarly, shape-memory polymers (SMPs) represent a fascinating class of smart materials that have garnered significant attention in recent years for their exceptional responsiveness to environmental triggers [2,3]. These materials can undergo changes in both their physical and chemical structure when exposed to external stimuli such as temperature variation [4,5], light exposure [6–8], mechanical force [9], magnetism [10,11], electric fields [12,13], and pH of the solution [14,15]. Compared to shape-memory alloys (SMAs) and ceramics (SMCs), SMPs offer several advantages, including highly recoverable strain, programmability and controllability of recovery behavior, low mass density, low cost, biocompatibility, biodegradability, ease of

processing, and tailoring of properties [16–18]. Despite offering these wide varieties of potential advantages, significant drawbacks of SMPs are associated with their relatively low tensile strength and stiffness, low recovery stress due to the low rubbery modulus, and actuation restricted primarily to heat-related treatment [19]. During actuation in the field of high-performance applications, the low recovery times are often responsible for their low thermal conductivity and inertness to electrical, light, and electromagnetic stimuli [20,21]. Furthermore, spatial or remotely controlled actuations are needed for specific applications, where SMPs fall short of satisfying the necessity of particular demand because their activation method largely depends on direct heating. The external heat sources are usually used to activate the thermally-induced SMPs directly, which is difficult to control due to low heat transfer and responsiveness.

By considering the challenges associated with SMPs, researchers introduced various types of functional fillers to develop a classical composite approach to mitigate these issues [3]. Numerous nanostructures, including nanoparticles (NPs), nanorods (NRs), nanotubes (NTs), nanocrystals (NCs), and nanofibers, along with microscale fillers and fibers, are commonly employed to enhance the properties of SMPs. Among these functional fillers, nanoarchitecture-embedded SMPs exhibit outstanding mechanical properties, including elevated elastic stiffness and high strength. These capabilities are attributed to the significant surface area-to-volume ratios of the nano additives, which surpass those of micro and macro additives [22]. The extensive surface area of the nanofillers ensures a strong interfacial interaction with the polymer matrix, promoting enhanced composite properties. Researchers found that the establishment of interfacial covalent bonds improves the uniform dispersion of the nanofiller due to adhesive forces between the polymeric matrix and the nanostructures [23]. This elevated dispersion, along with better interfacial interactions, not only facilitates favorable mechanical, electrical, and thermal properties but also enhances the stimulation of the nanocomposite materials, yielding a robust shape-memory effect (SME) with various actuation modes [20,24,25].

Incorporating nanofillers into SMPs has expanded their application domains, allowing nanotechnology to enhance adaptability to meet specific application requirements across various fields [24]. For instance, in biomedical technology, the addition of nanofillers with good electrical, magnetic, or luminous properties contributes to stimulation processes, which has led to the fabrication of various parts with shape-memory polymer composites (SMPCs) for endovascular thrombectomy devices, cardiovascular stents, artificial muscles, smart surgical tools, and laser-activated SMP microactuators for clot removal in blood vessels [18,26–28]. SMP composites are also promising candidates in the fields of flexible electronics, soft robotics, smart food packaging, textile, and more [25,29–31].

This review provides a comprehensive understanding of SMPNCs by detailing the foundational principles of shape-memory effects, the role of nanofillers, and the relationship between filler properties and material performance. A novel categorization of SMPNCs based on the type of incorporated nanofillers is introduced, offering valuable insights into their diverse applications, as outlined in Figure 1. It highlights the fundamental properties and mechanisms of SMPNCs, including the nanometric design of particulate-embedded structures, and showcases examples illustrating their enhanced thermal and electrical properties, mechanical integrity, and inherent advantages. The review begins with a concise introduction to SMPs and their working principles, followed by an exploration of various nanocomposites and their applications in biomedical technology, flexible electronics, soft robotics, and more. It concludes by highlighting emerging trends and future prospects in the synthesis and application of SMPNCs, charting a path for advancing smart material technologies to meet evolving industrial demands.

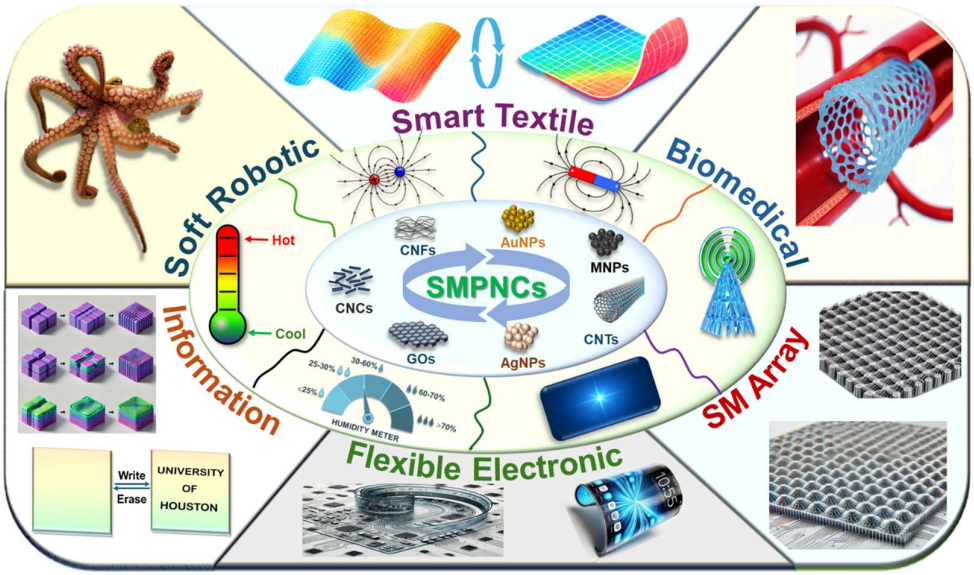

Figure 1. Schematic representation of SMPNCs, including types of nanofillers, activation methods, and applications.

2. Fundamentals of Shape-Memory Polymers (SMPs) and Shape-Memory Polymer Nanocomposites (SMPNCs)

2.1. Definition of SMPs

SMPs are a type of smart material and fall under the category of stimuli-responsive materials, which can change shape in response to environmental conditions, with temperature changes being the most prevalent trigger. The ability to remember their original shape is an intrinsic property of SMPs, allowing them to return to their memorized shape upon exposure to external stimuli multiple times without material degradation. This unique property of SMPs mainly arises from the capability to transition between shape-fixed and reversible phases, maintaining a temporary shape at lower temperatures and a permanent shape at higher temperatures [29]. The molecular structures responsible for these transitions are incorporated into the polymer matrix with different thermal properties to design SMP matrices. The matrix of SMPs comprises several materials, such as epoxy, polyvinyl alcohol, polystyrene, polylactic acid (PLA), thermoplastic polyurethane (TPU), polycaprolactone (PCL), polyimide (PI), and others. The combination of the fixed phase and reversible phase gives SMPs unique properties tailored to meet specific application needs [25].

The addition of nanofillers into neat SMP matrices results in SMPNCs, which exhibit enhanced mechanical, thermal, and shape-memory properties compared to their pure polymer counterparts due to the synergistic effects of the polymer matrix and the incorporated nanofillers. To achieve better dispersion of the nanostructures, researchers have developed various techniques to incorporate them into the polymer matrix, such as melt mixing, in situ polymerization, solution mixing followed by casting, chemical functionalization followed by cross-linking reactions, and ultrasonic dispersion [19,32,33]. As researchers delve into the synthesis and optimization of these SMPNCs, their applications span a wide array of fields, showing potential for innovative solutions in shape-changing and responsive materials.

2.2. Mechanisms and Shape-Memory Effects (SMEs)

Vernon first introduced the concept of the SME in polymers in a US patent published in 1941 [34]. The mechanism underlying the SME in SMPs is intricately linked to their molecular architecture and the interaction between the temporary shape and the original

(permanent) shape. When exposed to a suitable stimulus, SMPs can revert from their temporary shape to their permanent, memorized shape. In general, entropy variation can be used to describe this working cycle for thermally generated one-way SME (1W-SME) (Figure 2).

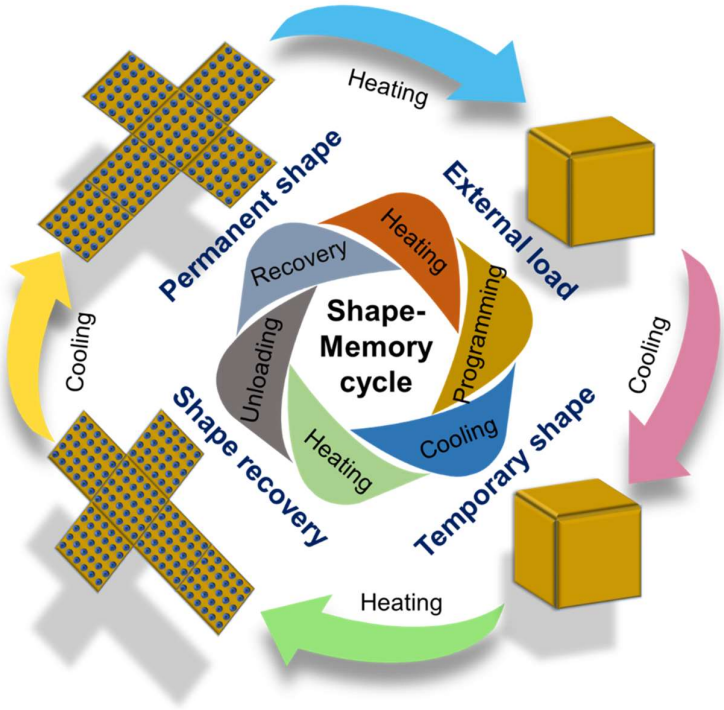

Figure 2. Schematic presentation of shape-memory cycle.

In the first step, initiating the temporary shape of SMPs is crucial during programming by heating the polymer to $T > T_{trans}$ (glass transition temperature T_g or melting temperature T_m). Elevated temperatures increase the entropy of the polymer, lower the energy barrier, and facilitate increased mobility of the molecular chains, making the polymer easier to manipulate [35]. Once the polymer is deformed into the desired temporary shape with an external load, it is cooled to a temperature below T_{trans} ($T < T_{trans}$) while maintaining the external stress to freeze the chains. At the molecular level, in the shape-fixing step, the chain segments in the polymer matrix align in an oriented manner, resulting in decreased entropy. This alignment stores entropic energy, or strain energy, placing the SMPs in a thermodynamically unstable state. The permanent shape of the polymer is recovered by heating it again to $T > T_{trans}$, allowing for chain relaxation and the release of stored entropic energy [36,37]. This entropic elasticity serves as the driving force for SMPs to transition from the low entropy-high energy state to the high entropy-low energy state, manifesting as a macroscopic shape [38].

To exhibit the SME, the polymer network structure must be composed of netpoints and switching domains [3,35,39]. The netpoints typically determine the permanent shape of the SMPs, arising from the crystalline phase, covalent (chemically cross-linked) or physical bonds (intermolecular interactions), molecular entanglement, or an interpenetrated network. Netpoints play a crucial role in preventing the movement of polymer chain segments during high-temperature programming, maintaining the stability of the entire system by generating a secure polymer network [19].

On the other hand, the switching segments establish the temporary shape of the SMPs, representing the flexible components responsible for reversible thermal phase transitions via thermal stimuli within the polymer network [29]. Switching domains are usually

involved in various mechanisms such as the crystallization/melting transition in the crystalline phase of polymers, vitrification/glass transition in the amorphous phase, liquid crystal anisotropic/isotropic transition in liquid crystalline polymers, reversible molecular cross-linking reactions like photodimerization, oxidation/redox reactions of mercaptan groups, Diels–Alder reactions, and supramolecular association/disassociation transitions such as hydrogen bonding, self-assembly of metal–ligand coordination, or β-CD self-assembly [3].

Macroscopic deformation in SMPs primarily results from the recoverable entropy change, preventing the dislocation of polymer chain segments. In terms of mechanical properties, SMPs demonstrate programmable mobility as the elasticity modulus drops dramatically at a temperature above their T_{trans}. The generation of a rubbery plateau signifies that netpoints can effectively hinder the slippage of chain segments within a defined range of force or temperature. Figure 3 depicts a schematic illustration of the entire architecture of SMPs, based on the evolution of molecular mechanisms.

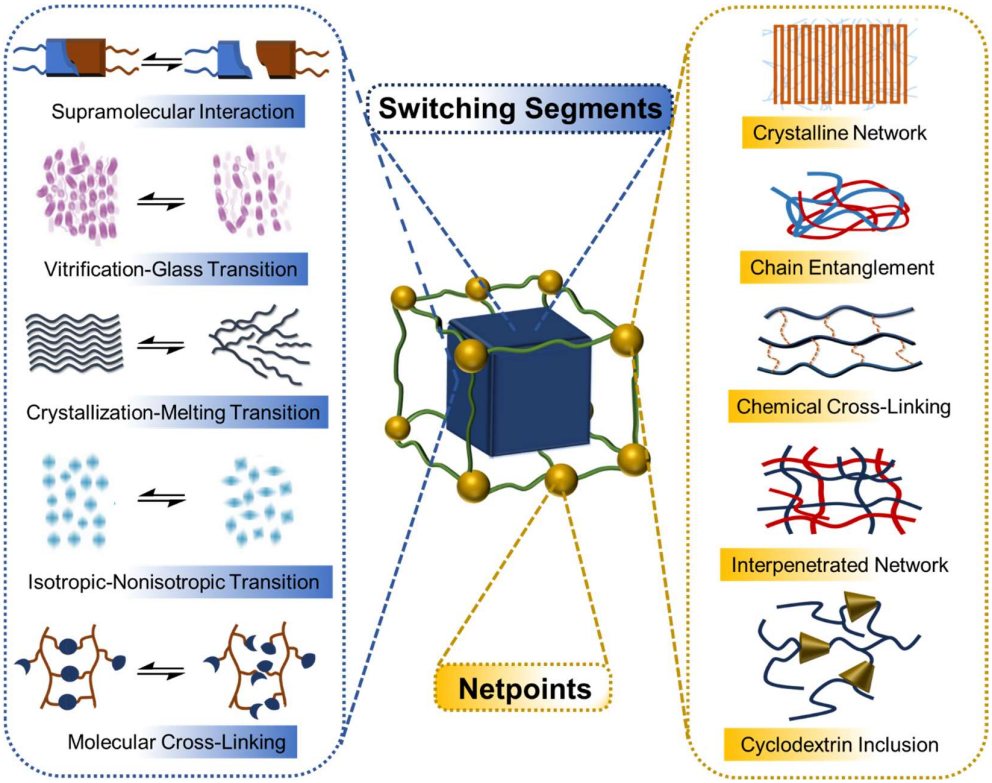

Figure 3. Schematic illustration of the molecular architecture of SMPs, composed of various types of netpoints and switching segments.

The mechanical properties of materials are also significantly influenced by their macrostructure, microstructure, and modulus. Adjusting the microstructure offers a viable approach to controlling these properties. SMEs provide a feasible method for structural control, and integrating an auxetic structure can enhance mechanical performance and active deformability. Given the complexity of auxetic foams, the initial structure of SMP foams should be auxetic to facilitate repeated deformation [40]. Auxetic SMP foams, characterized by a negative Poisson's ratio, exhibit superior mechanical resilience, energy absorption, and adaptability. Unlike conventional foams, auxetic SMP foams expand laterally under tension or become thinner when stretched or compressed longitudinally, enhancing durability, fracture resistance, and shape recovery [41].

2.3. Activation Techniques for SMPs and SMPCs

SMPs can be activated by several methods, broadly classified as heat, electricity, light, magnetism, moisture, pH, and so on [11,19,42,43]. The SME of thermally-responsive SMPs is immediately activated by the application of Joule heating, which is generated by a heat source such as hot gas or hot water. However, direct thermal actuation may not always be convenient for applications requiring remote or spatial activation. To address this problem, several functional additives, such as nanofillers and photochemical groups, are incorporated into the SMP to facilitate the activation of SMEs using diverse stimuli such as electricity, light, magnetism, and moisture [10,44].

SMPs induced using these techniques are inherently activated by Joule heating, which is generated through various indirect means. For example, when magnetic NPs are included in SMP nanocomposites and subjected to an external magnetic field, the composites are activated through inductive Joule heating in an alternating magnetic field. This process converts the electromagnetic energy from the high-frequency external field into heat energy. Similarly, light-activated groups can convert light energy into heat energy to trigger the activation of polymers for shape recovery. In the case of water- or solvent-driven SMPs, solvent molecules permeate the polymer sample. When the polymer is submerged in solution, the solvent molecules act as a plasticizer, reducing the transition temperature and helping the polymer recover its original form. This is an example of actuation indirectly caused by thermal changes. Specifically, the development of intrinsically light-induced SMPs involves the incorporation of reversible photoreactive molecular switches. This method of stimulation is not influenced by temperature, distinguishing it from the indirect actuation of thermally-responsive SMEs.

2.4. Classification and Types of SMPs

The categorization of SMPs and their nanocomposites relies on the criteria used for their specific assessments. According to thermally-induced phase changes, SMPs can be broken down into four types based on their netpoints and switching domains: covalently cross-linked glassy thermoset networks, covalently cross-linked semi-crystalline networks, physically cross-linked glassy copolymers, and physically cross-linked semi-crystalline block copolymers [5].

Depending on their response, SMPs can be divided into one-way SME (1W-SME), two-way SME (2W-SME), and multiple SME. 1W-SME is considered irreversible because the polymer chain fixation in its initial shape creates a specific structure without the ability to repeat SME. After recovering its initial state, it requires reprogramming to reactivate the effect [45]. In contrast, 2W-SME is different from conventional 1W-SME polymers. SMPs with reversible 2W-SME can spontaneously switch between two distinct shapes through external stimuli, eliminating the need for additional programming [25,46]. 2W-SMPs include liquid crystalline elastomers-based 2W-SMPs and semicrystalline polymers-based 2W-SMPs. For liquid crystal elastomers, the temperature shift below or above the transition temperature (T_{trans}) results in a transition between the anisotropic and isotropic phases, introducing the phenomena of crystallization-induced elongation (CIE) and melting-induced contraction (MIC) [47]. Above T_{trans}, the MIC effect dominates the molecular structure of the polymer matrix, while below T_{trans}, the CIE effect prevails, resulting in reversible contraction/extension behavior. Another type of SMP with 2W-SME can be obtained by introducing semicrystalline monomers into the polymer network. This type of SMP is considered a suitable candidate for soft actuators and sensors, artificial muscles, and soft robotics.

SMPs with multiple SMEs have multiple temporary shapes, allowing for multiple shape changes at different temperature intervals that can be fixed at a time, with the

recovery process carried out step by step [48]. The principle of this effect is to design an SMP with a wide range of thermal T_{trans} and multiple independent phases with different T_{trans}. Implementing this strategy is more complex because it requires comprehensive programming of the molecular structures of the polymer, with the number of temporary shapes determining the number of required programming steps [49].

Based on the external stimulus needed to trigger the shape-memory actuations, SMPs and SMPNCs are classified into various categories, including magnetic field [43,50,51], pH [14,15], water/solvent [52–54], electric [2,55], and light-responsive [8,56,57] SMPs. In this review, SMPNCs have been categorized and discussed based on the types of nanofillers incorporated into the polymer matrix.

3. Shape-Memory Polymer Nanocomposites (SMPNCs)

The primary objective in preparing SMPNCs is to enhance the electrical and thermal conductivity of SMPs while maintaining their mechanical properties. This enhancement is facilitated through the integration of metal or non-metal-based nanostructured fillers into the polymer matrix [42,58]. The inclusion of nanoarchitectures offers advantages such as a significant increase in surface area, greater confinement of polymer chains, elevated stiffness and tensile strength, higher tensile modulus, and enhanced flexural strength [59]. Additionally, conventional direct heating for SMP activation can lead to uneven temperature distribution due to low thermal conductivity, resulting in slow actuation. To address this issue, indirect heating methods such as electro-resistive and inductive heating are explored by designing SMPNCs, offering more uniform and efficient thermal activation. Below is a list of some common types of SMPNCs and the NPs or fillers that can be incorporated to enhance their properties. Additionally, Table 1 provides a summary of the key types of SMPNCs along with their corresponding nanofillers.

3.1. Metal-Based Nanocomposites

3.1.1. Fe_3O_4 Magnetic Nanoparticle (MNP) Nanocomposites

Magnetically activated SMPNCs represent a pioneering category of smart materials at the intersection of advanced engineering and materials science. These nanocomposites merge the inherent properties of SMPs with magnetic responsiveness through the incorporation of magnetic NPs or fillers, notably Fe_3O_4 NPs (MNPs). The choice of MNPs is predicated on their favorable magnetic characteristics, low toxicity, and biocompatibility [50,60]. Embedded within SMPs, these magneto-responsive NPs enable efficient, contactless activation when subjected to an external magnetic field [43]. This mechanism facilitates the shape-memory effect via inductive Joule heating, wherein electromagnetic energy from an alternating high-frequency magnetic field is converted into thermal energy [61]. The implications of this technology are vast, encompassing remotely controlled biomedical applications such as magnetically actuated SMP micro-actuators for thrombus removal, as well as innovations in smart textiles, aerospace, and robotics. By integrating magnetic components into SMPs, a new paradigm of responsive, adaptable materials is being forged, heralding an era of precision-engineered solutions responsive to magnetic stimuli.

Leungpuangkaew and colleagues pioneered the development of multistimuli-responsive SMPNCs by incorporating bio-based vanillin-furfurylamine benzoxazine/epoxy (V-fa/ECO) copolymers with MNPs (0–5 wt.%). [51]. These SMPNCs exhibit enhanced reconfigurability under the influence of both light and magnetic fields. The introduction of 3 wt.% MNPs improved the shape fixity ratio to 90%, an 8% increase over the unfilled polymer, attributed to the NPs serving as cross-linking points [62]. However, a reduction in mechanical properties was observed at 5 wt.% NP content, likely due to NP agglomeration [63]. The MNPs also facilitated rapid heat generation in a magnetic field

by aligning their magnetic dipole moments with the alternating magnetic field, resulting in accelerated shape recovery [64]. High concentrations of MNPs were effective in generating sufficient heat to surpass the glass transition temperature (T_g) of the copolymer, enhancing its shape-memory capabilities [65]. For instance, V-fa/ECO copolymers with 5% Fe_3O_4 NPs demonstrated significant shape-memory behavior, capable of moving objects by transitioning from straight to bent shapes under an alternating magnetic field (Figure 4a). Recently, they synthesized magnetic-responsive triple SMPNCs from bio-based vanillin-furfurylamine benzoxazine/polyurethane (V-fa/PU) polymers with incorporated MNPs [66].

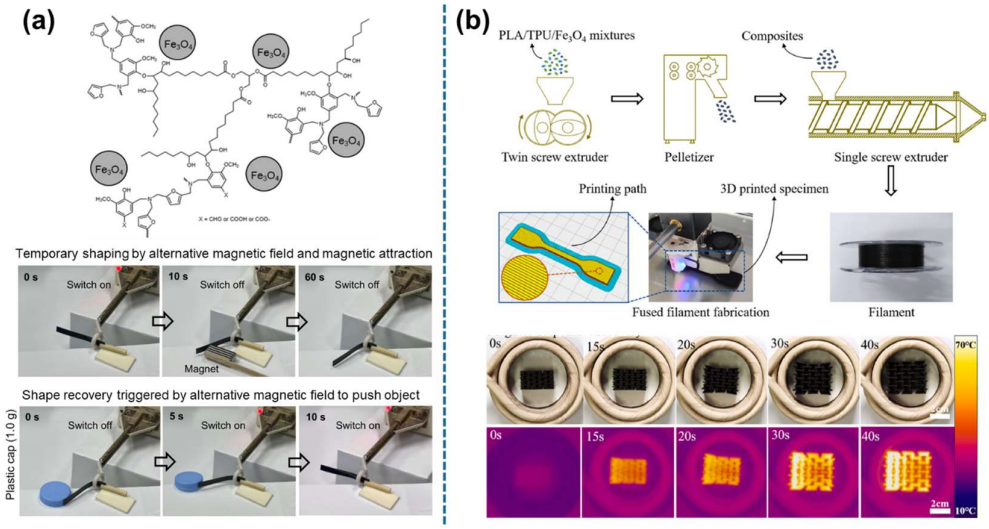

Figure 4. (**a**) Illustration of the structure of Fe_3O_4 NPs embedded in V-fa/ECO copolymers and object pushing actuation under a magnetic field using 5 wt.% NPs. Reproduced with permission from ref. [51]. Copyright 2023 Kingfa Scientific and Technological Co. Ltd. (**b**) Schematic of the manufacturing procedure for the composites used in 3D printing and the magneto-responsive shape-memory process of a honeycomb structure. Reproduced with permission from ref. [67]. Copyright 2022 Elsevier.

In another study, Liu et al. reported on 3D printable SMPNCs with enhanced mechanical strength and magnetic responsiveness, achieved by embedding Fe_3O_4 particles into polylactic acid/thermoplastic polyurethane (PLA/TPU) polymer blends [67]. The PLA/TPU/Fe_3O_4 composites showed nearly perfect shape fixity (~100%) and a high recovery ratio (96.4%) within 40 s, indicative of the homogeneous distribution of MNPs. As illustrated in Figure 4b, the shape-memory performance was demonstrated by designing various smart structures, such as a honeycomb and bionic flower-like model, which displayed complete recovery under a contactless magnetic field.

Babaie and colleagues developed a shape-memory polyurethane (SMPU) nanocomposite using Fe_3O_4 NPs modified with octadecyl isocyanate (OD), demonstrating outstanding thermo-responsive shape-memory properties [68]. The enhanced performance, including significant shape-recovery and fixity ratios, was attributed to the nanocomposite's crystallizable polycaprolactone (PCL) segments. Specifically, a nanocomposite with 10 wt.% OD-modified MNPs achieved rapid shape recovery in 90 s under a mild alternating magnetic field (350 kHz and 12.9 kA/m). In a separate study, Khasraghi et al. utilized silane-functionalized nanodiamond@Fe_3O_4 (S-NDF) hybrid NPs to create highly sensitive and multifunctional magnetic nanocomposites [69]. The resulting nanocomposites, with 9 wt.% S-NDF loading exhibited superior shape recovery (above 96%) in a small magnetic field (H = 0.76 kA/m), along with faster magnetic responsiveness compared to Fe_3O_4-loaded counterparts.

The SMPNCs filled with Fe_3O_4 NPs also demonstrated photothermal conversion capabilities, efficiently absorbing near-infrared (NIR) light to generate thermal energy [70,71]. This property enables non-contact actuation through NIR laser and magnetic attraction, offering a localized triggering mechanism for shape memory, distinct from traditional thermal activation methods [72–74]. Lu et al. synthesized a cellulose/PCL composite with notable strength, toughness, degradability, and multi-stimuli responsiveness by grafting soft PCL side chains onto a rigid cellulose backbone and incorporating a cross-linking network with hexamethylenediamine-modified MNPs [75]. This composite achieved exceptional toughness (up to 107 MJ/m^3), displayed significant thermal stability, and rapidly heated to 75 °C under 808 nm NIR light exposure, maintaining photothermal conversion efficiency and stability across multiple light on/off cycles. The shape-memory behavior of the composite was demonstrated by its significant ability to lift heavy objects and self-tightening knots under NIR light, suggesting potential for intelligent gripping applications (Figure 5a).

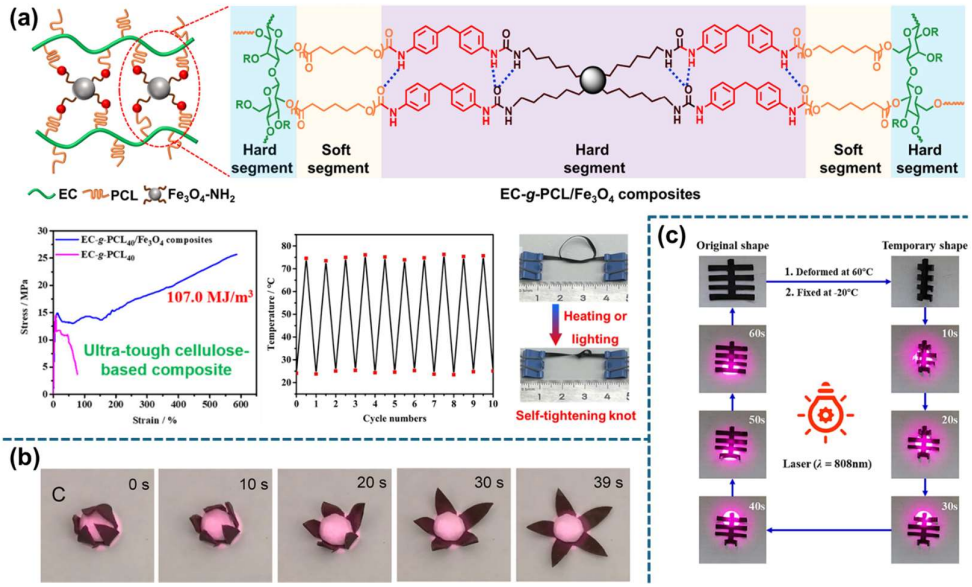

Figure 5. (**a**) Schematic diagrams illustrating the chemical composition of EC-g-PCL/Fe_3O_4 composites, stress-strain curves, the cyclic photothermal conversion process, and self-tightening knots of the composites. Reproduced with permission from ref. [75]. Copyright 2022 Elsevier. (**b**) Shape-memory behavior transitioning from a "bud" to a "blooming flower" of laser-triggered PHU-Fe_3O_4 nanocomposites containing 30 wt.% of PDOMA-grafted Fe_3O_4. Reproduced with permission from ref. [76]. Copyright 2021 Elsevier. (**c**) NIR-triggered shape recovery of a rectangular specimen. Reproduced with permission from ref. [77]. Copyright 2023 Elsevier.

Similarly, Li et al. developed polyhydroxyurethane (PHU)-based SMPNCs by integrating poly(2-oxo-1,3-dioxolane-4-yl)methyl methacrylate-modified Fe_3O_4 NPs, exhibiting shape-memory activation via non-contact NIR light exposure [76]. When subjected to NIR light, the pure PHU specimen failed to revert to its original shape even after two minutes of irradiation, while the nanocomposites displayed efficient recovery, transforming from a "bud" to a "blooming flower" shape within 39 s at a 30 wt.% filler content (Figure 5b). This suggests that the photothermal effect of Fe_3O_4 NPs effectively activates the shape-memory behavior in the nanocomposites.

Zheng et al. fabricated epoxy-based nanocomposites incorporating Fe_3O_4 NPs and poly(α-lipoic acid) as a cross-linker [77]. The resulting SMPNCs enable non-contact and photothermally induced shape recovery, exemplified by the rapid restoration of the extended rectangular specimen to its original shape when irradiated with an 808 nm NIR laser (Figure 5c). In another study, Chen et al. designed multiple-stimulus responsive SMPNCs

utilizing biocompatible PCL/TPU/Fe_3O_4@PDA [11]. The nanocomposites exhibited rapid response to light (5 s) and magnetic stimuli (1 s), essential for non-contact actuation in SMP applications.

3.1.2. Gold Nanoparticle (AuNP)/Nanorod (AuNR) Nanocomposites

Light-activated SMPs offer advantages of remote, spatial, and temporal control, contrasting with their thermally activated counterparts that require direct heating [78]. A conventional method to develop light-actuated SMPs involves incorporating photothermal fillers into thermally responsive SMPs [79]. Gold nanoparticles (AuNPs), gold nanorods (AuNRs), and gold nanospheres (AuNSs) are extensively utilized as nanofillers due to their distinctive photophysical properties and surface plasmon resonance (SPR) capabilities [80]. These nanostructures efficiently convert light, particularly at plasmonic or NIR wavelengths, into heat, facilitating remote and localized heating [81]. The significant photothermal heating capability of these NPs enables their use in SMPs for applications including therapeutic interventions [82], drug delivery [56], as well as polymer curing [83] and processing [84].

However, incorporation of NPs into SMPs introduces challenges such as NP clustering due to uneven dispersion, adversely affecting the material properties, and potential impacts on photothermal efficiency from surface modification [32]. To address these issues, Li et al. synthesized a cross-linked PCL polymer embedded with AuNPs/reduced graphene oxide (AuNPs/RGO) nanohybrids, achieving improved photothermal conversion and rapid NIR-light-driven shape recovery [85]. Graphene oxide (GO) acts as a carrier for effective nucleation and immobilization of AuNPs through ion-dipole interactions or metallic surface passivation, reducing NP aggregation and ensuring even distribution within the PCL matrix [86,87]. Comparative studies showed that PCL/AuNP-RGO composites exhibit faster, complete shape recovery in 53 s, outperforming PCL/AuNP (109 s) and PCL/RGO (87 s), attributed to the synergistic photothermal effects and uniform nanohybrid dispersion [88]. Additionally, the AuNP-RGO embedded nanocomposite demonstrated superior shape-recovery stress, effectively lifting a 10 g weight by 1.5 cm under NIR light, exhibiting enhanced heavy-lifting capabilities (Figure 6).

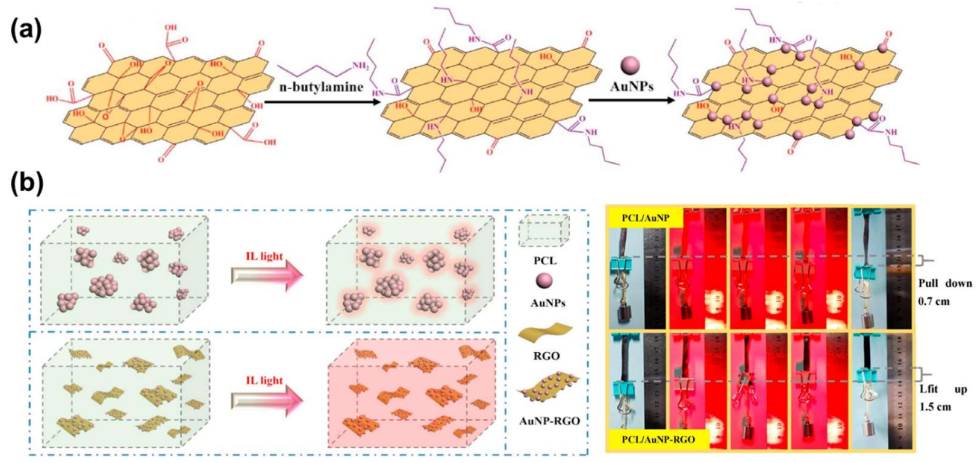

Figure 6. (**a**) Schematic diagram illustrating the synthesis of AuNP-RGO nanohybrids; (**b**) diagrams depicting the photothermal effect (left) and the ability of PCL/AuNP and PCL/AuNP-RGO to lift a 10 g weight under NIR light (right). Reproduced with permission from ref. [85]. Copyright 2019 Elsevier.

Wang and colleagues developed SMPNCs by integrating AuNPs as photothermal converters into acrylate-based composites, enabling adjustable transition temperatures [89]. These SMPNCs undergo shape transformation upon exposure to LED light, which is

facilitated by the conversion of light to heat through the AuNPs, reaching the polymer's T_g. This method results in exceptional shape-memory properties, with shape fixity and recovery ratios exceeding 95%. Zhang et al. designed a promising SMP that possesses optical healing capabilities in addition to light-triggered actuation [90]. This was achieved by chemically cross-linking a crystalline polymer with a minor concentration of AuNPs, enabling optically controlled shape memory and rapid healing through localized heating by the surface plasmon resonance of the AuNPs [91].

SMPs and elastomers containing plasmonic AuNPs exhibit inherent properties that vary with the arrangement of the NPs, which are influenced by their orientation or mutual coupling [92]. Yadav et al. investigated the plasmonic coupling of AuNPs in TPU SMPs, assessing changes pre- and post-mechanical stretching as well as thermal shape recovery [93]. Stretching the composite, as depicted in Figure 7a, induces a polarization-dependent optical response due to decreased interparticle distances along the stretching direction. This polarization effect disappears upon shape recovery. Additionally, simulations with AuNP dimers provide a method to estimate interparticle spacings, functioning similarly to a plasmon ruler. This suggests their potential utility in applications such as optical thermal history sensors.

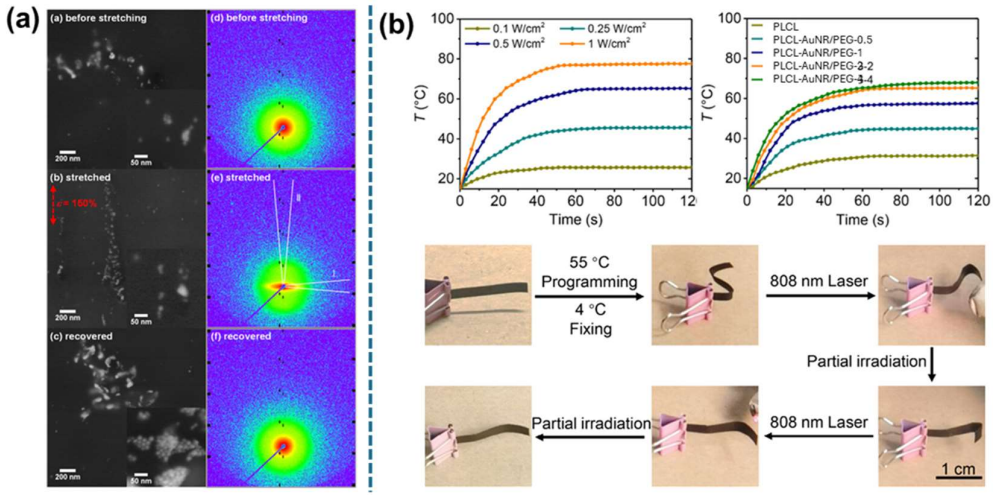

Figure 7. (**a**) SEM images using backscattered electrons and 2D SAXS detector images displaying the arrangement of AuNPs in the samples at various stages: before stretching, during stretching, and after shape recovery. Reproduced with permission from ref. [93]. Copyright 2021 American Chemical Society. (**b**) Graphs showing the temperature changes in response to varying NIR-light intensities and different AuNR concentrations, accompanied by sequential photos depicting the stages of the shape-recovery process for the PLCL-AuNR/PEG-2 nanocomposite. Reproduced with permission from ref. [80]. Copyright 2023 American Chemical Society.

AuNRs are widely employed as photothermal agents due to their biocompatibility and tunable SPR in the NIR region, which is achieved by adjusting their aspect ratio [94,95]. Utilizing this specific longitudinal SPR wavelength along with a polarizer enables polarization-selective photothermal heating in composites containing aligned AuNRs [96]. Consequently, Xiang et al. incorporated polyethylene glycol (PEG)-modified AuNRs into a poly(L-lactide-co-ε-caprolactone) (PLCL) matrix to introduce NIR responsiveness [80]. In the PLCL-AuNR/PEG composites, the T_g is critical for the transition between crystalline and amorphous phases, affecting the SME. The integration of caprolactone units into poly(L-lactide) (PLLA) enhances toughness and lowers the T_g of PLCL, which is further reduced by the addition of AuNR/PEG, thus facilitating SME activation at tissue-friendly temperatures [97]. However, achieving direct heating within a living organism is often challenging, which leads to the use of AuNR/PEG as a device to convert energy

from remote stimuli into thermal energy [80]. Under NIR light exposure, the heating rate and equilibrium temperature of the PLCL-AuNR/PEG composites increase significantly with higher light intensity and AuNR/PEG content. This results in enhanced thermal conductivity and rapid heat dissipation, crucial for the shape-recovery process [98]. As illustrated in Figure 7b, the PLCL-AuNR/PEG-2 composite (containing 2 wt.% AuNRs/PEG) demonstrated the ability to transform from a rectangular to an "S" shape under NIR light, exhibiting spatiotemporal control. In addition to NIR-induced heating, direct heating leads to excellent shape-memory performance, characterized by a decrease in the shape fixity ratio (R_f) and an increase in the shape-recovery ratio (R_r) with higher AuNR/PEG content. This indicates the role of AuNR/PEG as a physical cross-linking point that enhances stress storage for shape recovery [99].

Utilizing digital light processing (DLP) 3D printed technology (Figure 8a), Paunović and colleagues developed NIR-responsive biodegradable polymer composites based on *d*,*l*-lactide (LA) and ε-caprolactone (CL) by incorporating AuNRs [100]. These composites achieved a temperature of 55 °C within 20 s under laser exposure, demonstrating rapid and stable NIR responsiveness. The shape-memory properties of the printed cuboid shapes were assessed by evaluating the shape fixity (R_f) and shape-recovery (R_r) ratios through five cycles of deformation at 80 °C. These properties exhibited high consistency, with R_f and R_r values ranging from 97.6% to 100% and 83.1% to 100%, respectively, during one-minute exposure to an 808-nm laser (Figure 8a). In another study, Zheng et al. prepared light-induced shape recovery of deformed SMP micropillar hexagonal arrays containing AuNRs [101]. The pillars, bent to varying angles by applying force above their T_g and subsequently cooled to room temperature to fix the deformed structures, almost entirely recovered to their original straight state within 5 s under exposure to a 0.3 W green laser. This recovery efficiency was dependent on the AuNR loading and the exposure dosage.

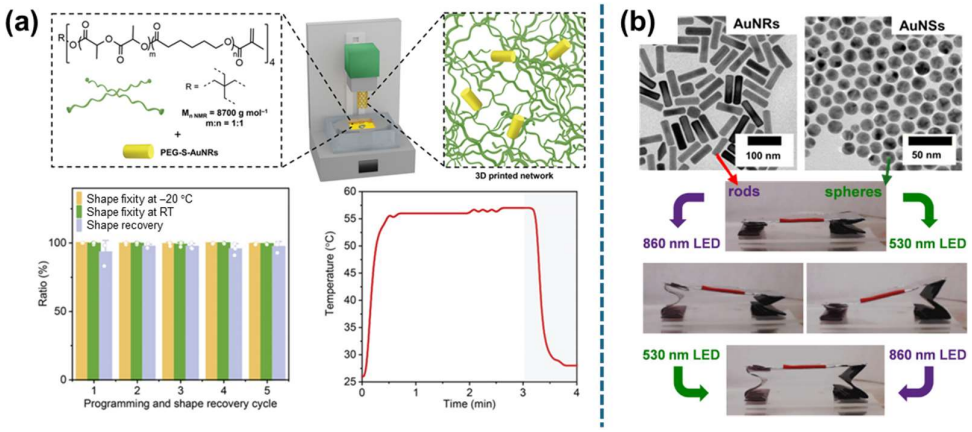

Figure 8. (**a**) Diagram illustrating the 3D printing strategy used for fabricating the composite materials, shape recovery, and fixity over five loading cycles, and the thermal response curve during and after NIR-light exposure. Reproduced with permission from ref. [100]. Copyright 2022 John Wiley and Sons. (**b**) Transmission Electron Microscopy (TEM) images displaying the structural details of AuNRs and AuNSs, alongside photographs that illustrate the wavelength-specific actuation of the composites, demonstrating controlled bending and straightening actions. Reproduced with permission from ref. [102]. Copyright 2018 American Chemical Society.

Mishra et al. introduced a wavelength-selective photothermally triggerable TPU SMP embedded with AuNSs and AuNRs [102]. Light-emitting diodes (LEDs) targeting the SPRs at 530 nm and 860 nm were employed for the sequential actuation of AuNS-TPU and AuNR-TPU composites. This selective heating facilitated controlled shape alterations by activating one type of AuNP without significantly heating the other. As illustrated in Figure 8b,

through alternating LED illumination at specific wavelengths, the extension sequence of accordion-shaped legs from the AuNR-TPU and AuNS-TPU films was controlled. This enabled precise manipulation of the lifting and tilting angles of the aluminum foil top. This capability demonstrated the potential for wavelength-controlled manipulation of SMPs, with applications in optically controlled stages capable of adjusting height and tilt angles using embedded AuNPs.

3.1.3. Silver Nanoparticle (AgNP) Nanocomposites

Silver nanoparticles (AgNPs) have attracted significant attention in recent years due to their promising characteristics, including superior thermal and electrical conductivity, chemical stability, and antibacterial properties [103–105]. Jouni et al. reported that incorporating 22% AgNPs into high-density polyethylene enhances thermal conductivity by approximately 4.5 times when processed via extrusion, simultaneously imparting electrical functionalities [106]. Dorigato and Pegoretti explored the effects of AgNPs on the shape-memory behavior of epoxy nanocomposites, produced through casting with in situ reduction of silver nitrate ($AgNO_3$), carbon black, and carbon nanofibers (4 wt.%) [107]. They demonstrated that applying 220 V to both the terminal and lateral zones of the material achieved the required temperature for activating the SME where $T > T_g$, within 60 s.

Reversible two-way SMPs utilized in soft actuators offer advantages such as significant output stress, low driven voltage, straightforward construction, and cost-effectiveness [108,109]. The key to achieving a two-way SME lies in generating internal stress within the polymer composites [110]. Additional factors, such as two-layer structures, cross-linked networks, three-dimensional structures with reversible covalent bonds, and materials with dual-crystal components, also contribute to reversibility [111–113]. Despite the merits of two-way SMP-based actuators, opportunities for improvement remain, including more stable multilayer structures, simplified multi-molecular network designs, and enhanced reversible deformation. Consequently, Xing et al. designed an AgNPs-integrated sandwich structure for a shape-memory soft actuator that features reversible electric and moisture actuation, along with strain sensing capabilities [44]. The actuator consists of a middle layer of AgNPs for electrothermal activation, sandwiched between a hygroscopically deformable polyvinyl alcohol (PVA) layer and a flexible shape-memory polymer (FSMP) layer (Figure 9a). The PVA-AgNPs-FSMP (PAF) composite, containing 6 mol/m^2 AgNPs, exhibited enhanced performance, particularly at 2 V, achieving recovery within 10 s at a 98% rate (Figure 9b). In a moist environment, the composite bends and returns to its original shape in 40–50 s under electric power below 2 V, demonstrating effective Joule heat generation for shape recovery (Figure 9c) [44].

Researchers also have a notable interest in AgNP-embedded nanocomposites due to the SPR properties of the NPs, which offer potential for light-triggered remote activation with precise spatial and temporal resolutions across a broad spectrum of light [114]. Yenpech et al. utilized in situ ring-opening polymerization (ROP) of thermoset polybenzoxazine (PmBz) and thermoplastic PCL composites embedded with plasmonic AgNPs for laser-triggered SMP applications [57]. Benzoxazine (Bz) is known for developing permanent cross-linking or network points in thermoset polymers, thereby enhancing the thermo-mechanical performance of SMPs [115,116]. It also plays a crucial role in forming the PmBz network and providing numerous hydroxyl groups for conjugation with the thermoplastic PCL [117]. The selection of AgNPs is based on their ability to be activated by a low-energy violet laser (408 nm, 780 mW) and surface modification with disulfide polycaprolactone (SS-PCL) to ensure high miscibility and easy dispersal in PCL matrices. An investigation into the impact of AgNP concentration on shape recovery revealed that

composites with varying AgNP weights exhibited no shape recovery at 0.001 wt.% after 40 s of laser irradiation, while those with 0.01 wt.%, 0.1 wt.%, and 0.3 wt.% AgNPs displayed clear SMEs (Figure 10a). This experiment determined that a minimal content of 0.01 wt.% AgNPs is required for the phenomenon to be visually observable [57].

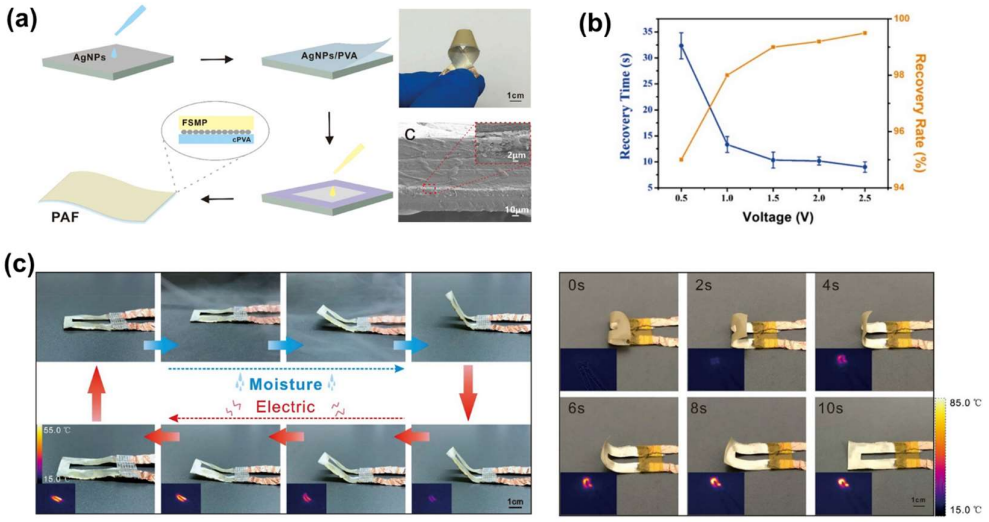

Figure 9. (**a**) Diagram illustrating the preparation process of PAF alongside images of its fractured surface. (**b**) Graph depicting PAF's recovery time and rate under various applied voltages. (**c**) Digital photos and infrared thermal images showing the electric/moisture actuation process and its recovery, with corresponding infrared images (left) and digital photos demonstrating the 10-s recovery process of PAF at 2 V (right). Reproduced with permission from ref. [44]. Copyright 2020 Elsevier.

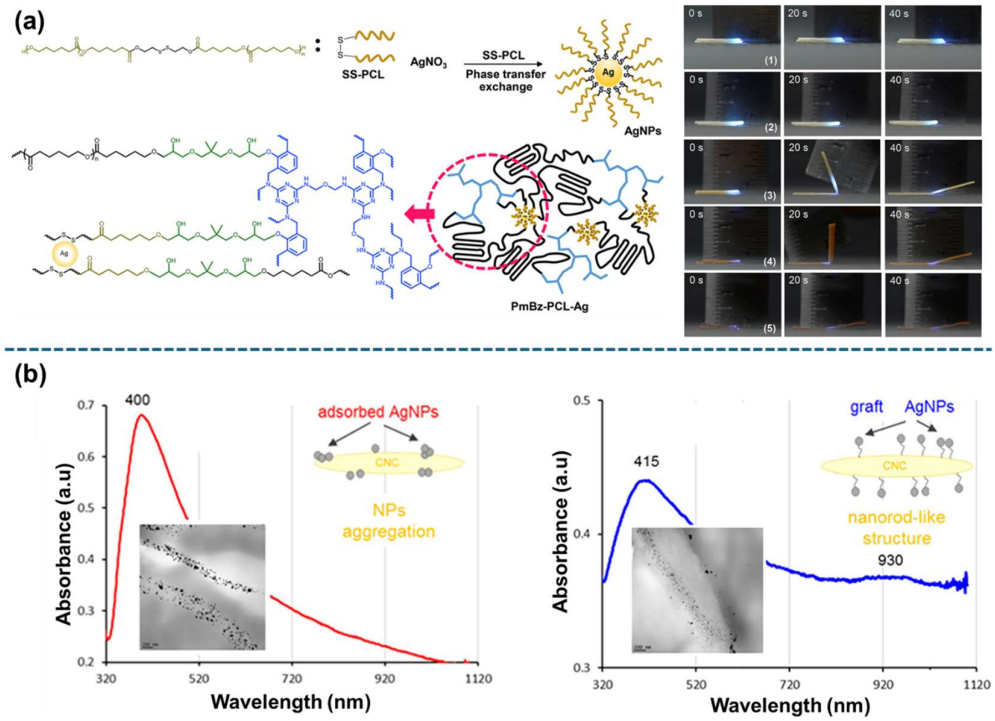

Figure 10. (**a**) Illustration of the network formation in the PmBz-PCL-Ag nanocomposite using SS-PCL modified AgNPs, along with photographs depicting the shape recovery of PmBz-PCL (1), PmBz-PCL-Ag0.001 (2), PmBz-PCL-Ag0.01 (3), PmBz-PCL-Ag0.1 (4), and PmBz-PCL-Ag0.3 (5) upon light activation. Reproduced with permission from ref. [57]. Copyright 2020 Elsevier. (**b**) UV−vis spectra of CNC-ad-AgNPs and CNC-g-AgNPs. Reproduced with permission from ref. [32]. Copyright 2018 American Chemical Society.

In another study, Toncheva et al. designed light-activated SMP composites by incorporating 1 wt.% AgNPs into PCL [32]. The study employed two methods for synthesizing plasmonic AgNPs: (i) adsorption of AgNPs onto the surface of cellulose nanocrystals (CNCs) through direct reduction of Ag ions with $NaBH_4$, labeled CNC-ad-AgNPs, and (ii) grafting of AgNPs onto CNCs after modifying the CNC surface with thiol groups, followed by subsequent Ag ion reduction, referred to as CNC-g-AgNPs. The light absorbance capability of the CNC-ad-AgNPs and CNC-g-AgNPs composites were illustrated in Figure 10b. CNC-ad-AgNPs exhibited a single absorption band at 400 nm, indicative of adsorbed spherical nanostructures. In contrast, CNC-g-AgNPs displayed a redshift of the band to 415 nm, suggesting plasmon excitation along the nanofiller's longer axis, and a second absorption band of low intensity at 930 nm, indicative of a nanorod-like structure. This design strategy for incorporating plasmonic AgNPs onto CNCs enables efficient, fast, and remotely triggered shape-memory actuation under IR light, demonstrating the potential of such systems for advanced applications.

Soto-Castro et al. employed a method to decrease the shape-memory recovery times and improve the recovery ratio of thermoplastic potato starch (PS) by incorporating AgNPs [118]. AgNPs act as anchor points within the starch matrix through hydrogen bonds between the hydroxyl groups of the starch and the AgNPs [119]. This interaction increased the shape-recovery ratio from 85% to 98% as the AgNP concentration increased from 0% to 2 wt.%, attributed to mechanical reinforcement and increased number of netpoints between the polymer chains [118]. Additionally, the presence of AgNPs reduced recovery times to two minutes for PS20AgNP with 2 wt.% AgNPs. Initial recovery of over 75% of the original shape occurred within the first 20 s for composites with lower AgNP content, while those with 2 wt.% AgNPs achieved over 85% recovery. After one minute, both the PS and the PS05AgNP with 0.5 wt.% AgNPs reached similar recovery ratios (85% and 87%, respectively), likely affected by water absorption. In contrast, composites with higher AgNP content (1 wt.% and 2 wt.%) exhibited higher recovery ratios (approximately 98%) and demonstrated lower water absorption n rates. In another study, Pekdemir et al. utilized a direct green synthesis technique to produce SMPNCs embedded with AgNPs [120]. The composite material was fabricated using a solution casting method, combining a PLA/PCL blend with AgNPs synthesized through the environmentally friendly reduction of silver salts using *Rubus caesius* L. leaves. It was observed that the shape-recovery properties of the nanocomposite films improved with increasing AgNP content.

The smart superhydrophobic surfaces of SMPs with tunable wettability have attracted extensive attention due to their widespread applications. Li et al. developed a superhydrophobic SMP microconed surface on a silver nanowire (AgNW) film, which allows for reversible transitions between pinned and roll-down states through in situ heating via voltage [121]. Remarkably, this reversible transition could be repeated over 100 cycles, demonstrating the efficient shape memory of the microcones under various applied voltages (4–11 V) in a short period of time (Figure 11).

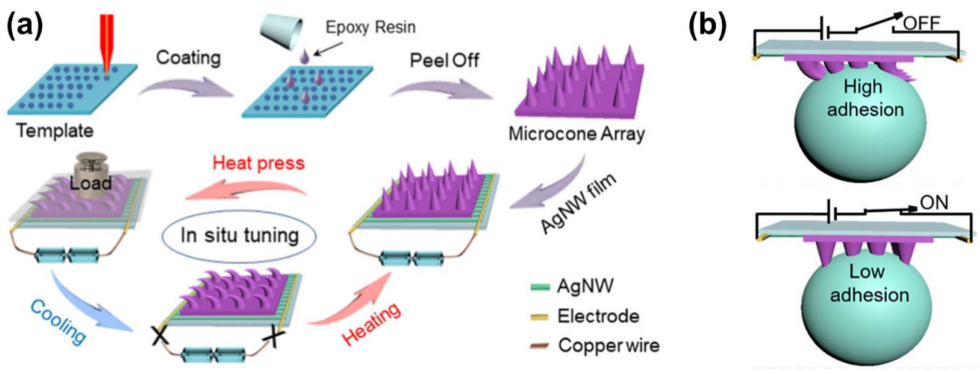

Figure 11. (**a**) Diagram illustrating the conventional preparation methods for SMP surfaces with microcone arrays; (**b**) the transfer of droplets without any loss during both the "captured" and "detached" stages. Reproduced with permission from ref. [121]. Copyright 2020 American Chemical Society.

3.1.4. Tungsten Oxide Nanowire Nanocomposites

Tungsten oxide nanocrystals (WO_{3-x}) exhibit broad absorption across the UV–vis–NIR region due to their intramolecular charge transfer and localized surface plasmon resonances (LSPR) absorption [122]. Their photothermal conversion efficiency is notably high, approximately 28.1%, which is comparable to carbon nanotubes (28%) and surpasses the efficiencies of AuNPs at 11% and reduced graphene oxide (rGO) at 12%, as previously reported [123]. Diverse nanostructures of WO_{3-x}, including nanofibers, nanowires, and spherical particles, have been prepared with tunable sizes. Among these, WO_{3-x} nanowires display superior NIR light absorption, highlighting their potential for advanced photothermal applications [124]. Zhou et al. introduced multi-photoresponsive SMP composites and chiral actuators incorporating oligo(ethylene glycol) (OEG)-modified $W_{18}O_{49}$ nanowires into cross-linked polyethylene glycol diacrylate (cPEGDA) matrices (Figure 12a) [72]. The integration of OEG-modified $W_{18}O_{49}$ nanowires facilitated chemical cross-linking through acrylate groups for shape fixity and utilized crystalline PEG segments as the reversible phase for shape memory [72]. The presence of OEG ligands on the $W_{18}O_{49}$ surface enhanced compatibility with cPEGDA via hydrogen bonding, ensuring even dispersion of nanowires and maintaining high crystallinity at loadings up to 4.0 wt.%. The cPEGDA/$W_{18}O_{49}$ nanocomposites exhibited rapid temperature increases due to the efficient photothermal conversion of $W_{18}O_{49}$ nanowires and effective heat transfer to the polymer matrix. As illustrated in Figure 12b, a composite with 2.0 wt.% nanowire loading reached a surface temperature of 74 °C under 365 nm UV light within one minute. Under 808 nm NIR laser irradiation (1.6 W cm^{-2}), the temperature escalated to 167 °C in 20 s and 214 °C in one minute. Similarly, under a 980 nm NIR laser (1.6 W cm^{-2}), the temperature reached 161 °C in 20 s, highlighting their potential for rapid and precise thermal actuation.

Tian et al. developed remotely and spatially controllable shape-shifting characteristics in SMP composites upon a laser-induced temperature gradient [125]. These composites were synthesized through a thiol-ene Michael addition reaction, using acrylate-terminated polycaprolactone (PCLDA) and a four-arm cross-linker to integrate OEGy-modified $W_{18}O_{49}$ nanowires as photothermal agents. The crystalline PCL phase within the composite underpins the SME, while the OEGy-$W_{18}O_{49}$ nanowires serve to absorb light and convert it into heat [125]. Upon exposure to a 100 mW/cm^2 laser, the composites rapidly exceed the melting temperature (T_m) of PCL, with the equilibrium temperature rising in tandem with the OEGy-$W_{18}O_{49}$ content at a constant laser intensity. A direct relationship was observed between laser intensity and peak temperature, which varied from 92.3 °C to 175.2 °C as the laser intensity increased from 0.1 to 1 W/cm^2. Following laser discontinuation, the composites cooled down to ambient temperature. These materials exhibited excellent

thermally induced shape-memory behavior, with shape fixity (R_f) and shape-recovery (R_r) ratios of 97.1% and 96.3%, respectively. Moreover, the composites enabled the creation of intricate 2D to 3D reversible shapes through targeted laser irradiation and stable helical shapes in both right-handed and left-handed configurations, demonstrating potential for sophisticated actuation applications.

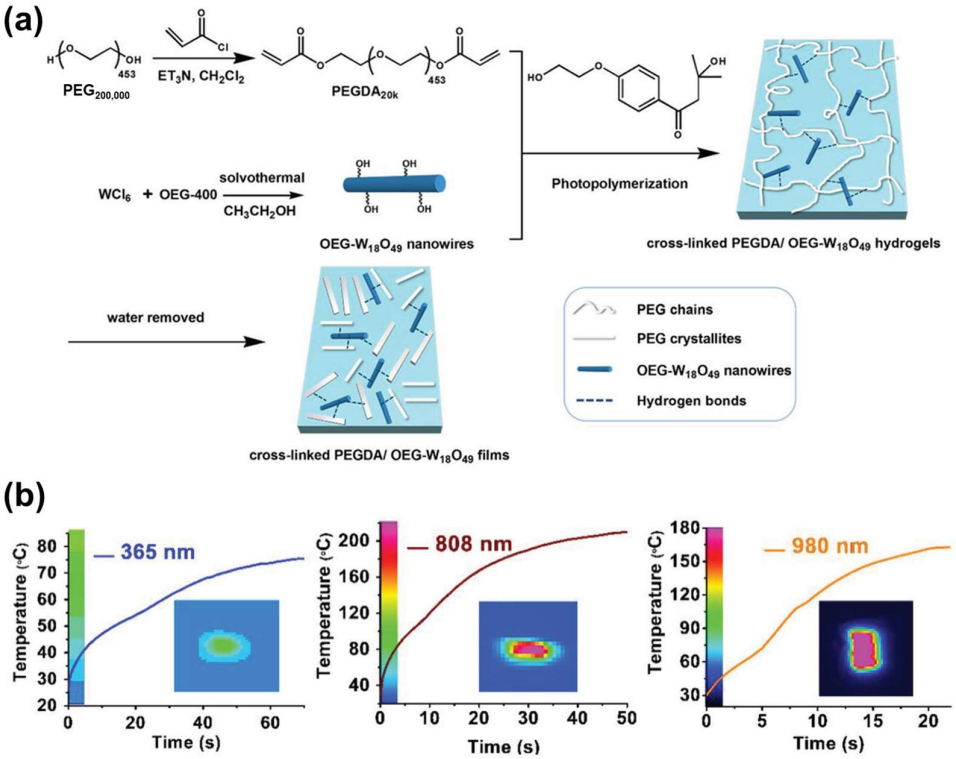

Figure 12. (**a**) Illustration of cross-linked networks in the PEDGA/OEG-$W_{18}O_{49}$ composite synthesis; (**b**) temperature vs. time plots for UV and NIR light irradiation at different wavelengths. Reproduced with permission from ref. [72]. Copyright 2019 John Wiley and Sons.

3.1.5. Other Metal Nanocomposites

Metal nanostructures, in addition to those previously mentioned, are also commonly used in the design of SMPNCs. Hu et al. developed an SMPNC by incorporating PCL-hybridized titanium dioxide (TiO_2) nanomaterials (PCL-TiO_2) into poly(L-lactide) (PLLA), resulting in a PCL-TiO_2/PLLA composite [126]. In this system, the TiO_2 component functions as a 'heat dispersion pump' within the switching phase, with PCL acting as a 'heat dispersion bridge'. This configuration establishes an effective heat conduction pathway within the PCL-TiO_2/PLLA composite, facilitating the transfer of thermal energy necessary to initiate the melting process, release stored elastic energy, and trigger the shape-memory behavior of the composite [126]. Additionally, the hybrid switching phase provides a plasticizing effect on the otherwise rigid PLLA matrix, optimizing the balance between stiffness and toughness [52,127]. The shape-memory function was demonstrated by deforming the composite into a spiral strip and bud shape at a transition temperature (T_{trans}), freezing the temporary shape by cooling to 15 °C, and then recovering the original shape by reheating to 57 °C (Figure 13). The PCL-TiO_2/PLLA composite exhibited superior reversible shape-memory properties compared to PCL/PLLA, with shape fixity (R_f) and shape-recovery (R_r) ratios of 93.9% and 94.4%, respectively, and achieved shape recovery in just 15 s [126].

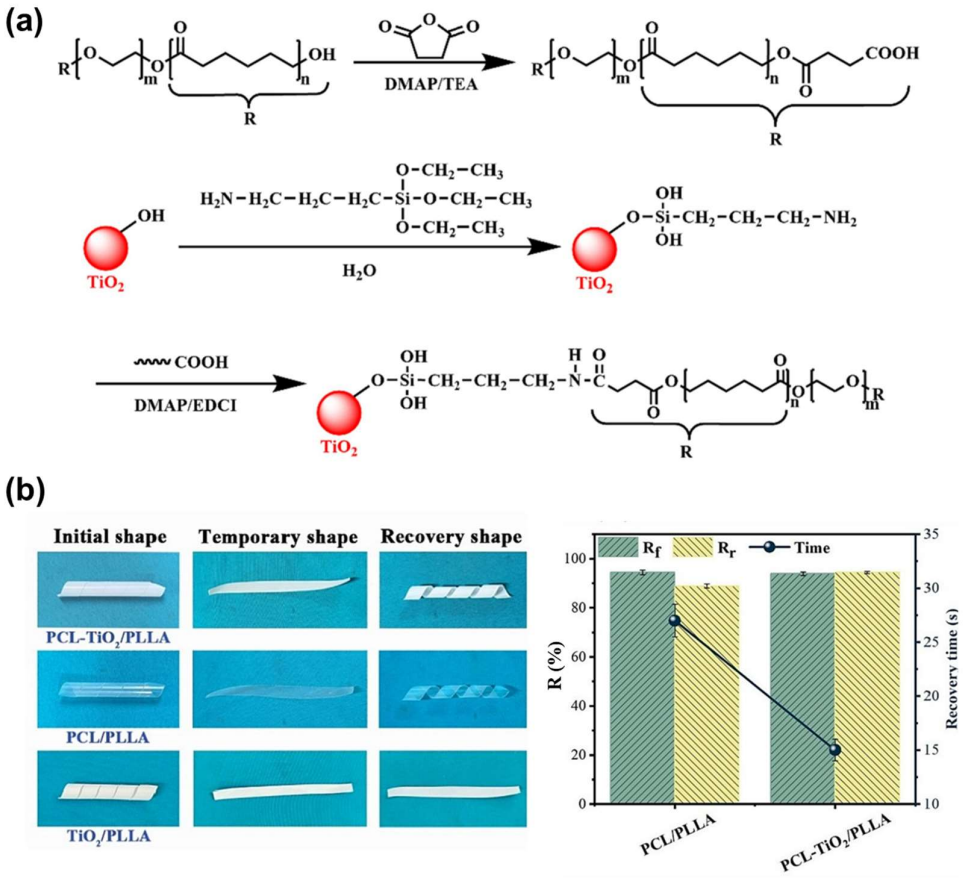

Figure 13. (**a**) Schematic of the PCL-TiO_2 synthesis process; (**b**) visual demonstration of shape-memory behavior (left) and shape fixity (R_f) and shape-recovery (R_r) ratios of the polymer composites (right). Reproduced with permission from ref. [126]. Copyright 2023 Elsevier.

Ishii et al. explored the use of titanium nitride (TiN) NPs as broadband plasmonic light absorbers in cross-linked PCL SMP composites [128]. Compared to gold or silver NPs, TiN exhibited higher optical absorption loss, resulting in a broader linewidth of its plasmonic resonance [128]. Analytical and experimental demonstrations revealed that the broad resonance of TiN NPs enhanced sunlight absorption efficiency [129]. The study assessed the shape-memory behavior of TiN-PCL composites with TiN concentrations ranging from 1 to 20 wt.% by programming temporary shapes through elongation above the melting temperature (T_m). Subsequent shape recovery was observed under five minutes of solar radiation at intensities of 100, 130, and 160 mW/cm^2. All composites exhibited a high and TiN concentration-independent shape-fixing ratio [128]. Under sunlight irradiance at 130 mW/cm^2, partial recovery occurred, while complete recovery was achieved at 160 mW/cm^2, suggesting a threshold irradiance for full shape recovery between these values. The incorporation of TiN NPs impacted the flexibility of the composites, with the 1 wt.% TiN-PCL sample exhibiting the most significant shape change. The biodegradable nature of PCL, combined with the chemical stability and light-responsive properties of TiN NPs, positions the TiN-PCL composite as a suitable candidate for biological and clinical applications, providing an energy-efficient approach to activating SMPs under sunlight [128]. In a related study, Pekdemir et al. prepared an SMP composite by solution blending, doping PCL and poly(vinyl chloride) (PVC) blends with various concentrations of titanium carbide (TiC) NPs [130]. This approach aimed to investigate the effects of TiC NPs on the shape-memory behavior and properties of the PCL-PVC composite.

Leonés and colleagues reported the incorporation of manganese oxide (MgO) NPs into PLA-based electrospun fibers at concentrations of 0.1, 0.5, 1, and 3 wt.% relative to

the PLA matrix, and introduced 20 wt.% oligomers as a plasticizer to adjust the glass transition temperature (T_g) (Figure 14a) [131]. The thermally-activated shape-memory behavior of these composites was examined at various temperatures to assess the effects of NP and plasticizer incorporation. At 60 °C, composites containing 0.1 and 0.5 wt.% MgO NPs did not exhibit shape-memory behavior, whereas those with 1 and 3 wt.% MgO NPs demonstrated excellent shape-memory responses, achieving shape fixity ratio (R_f) values over 97% for effective shape fixation. In contrast, at 45 °C, while neat PLA electrospun fibers lacked thermally-activated shape memory, the addition of MgO NPs within 0.1–3 wt.% range preserved the high shape-memory performance of the PLA matrix (20 wt.% oligomers), with consistent shape fixity (R_f > 99%) and shape-recovery ratio (R_r > 82%) values across multiple thermo-mechanical cycles [131].

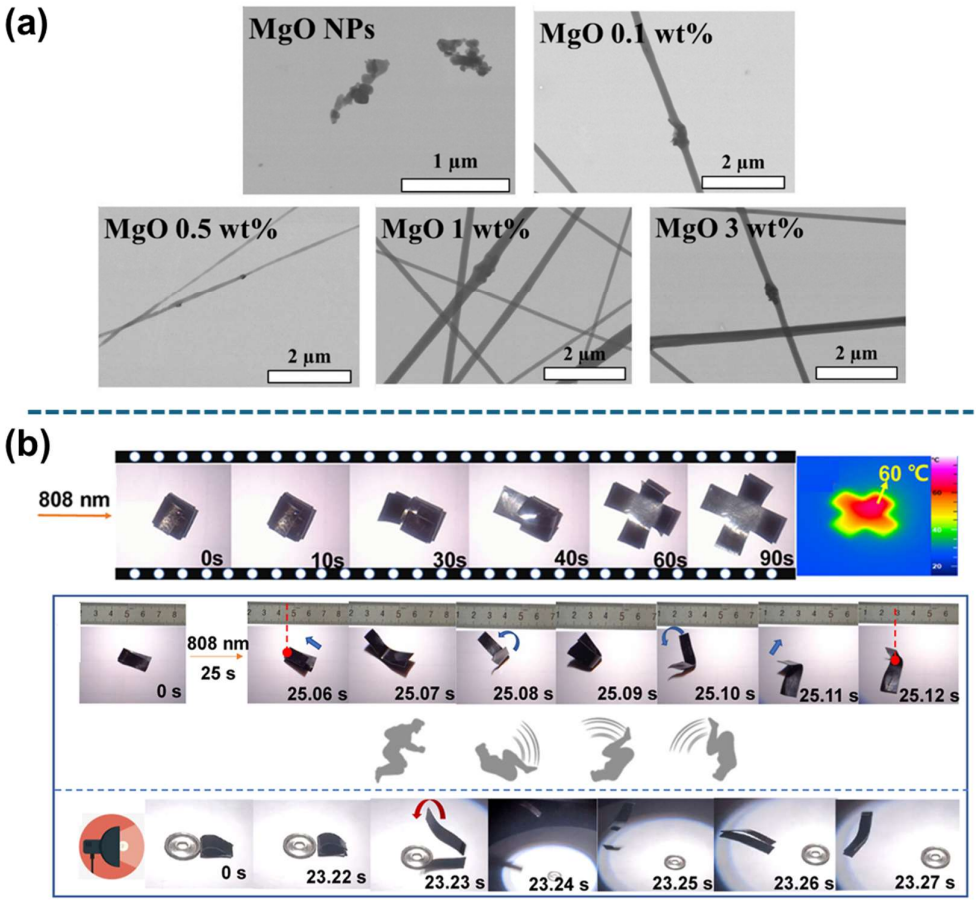

Figure 14. (**a**) FESEM images of MgO NPs with MgO-loaded electrospun fibers containing 0.1, 0.5, 1, and 3 wt.% MgO. Reproduced with permission from ref. [131]. Copyright 2022 MDPI. (**b**) Photographs depicting the shape recovery of a "box", as well as the processes of "Jump" and "Cross Obstacle" for a SMPU-PB material under 808 nm NIR light exposure. Reproduced with permission from ref. [132]. Copyright 2023 American Chemical Society.

By incorporating citric acid-modified Prussian blue nanoparticles (PBNPs), Wang and coworkers developed NIR-responsive shape-memory polyurethane (SMPU-PB) composites [132]. PBNPs are known for their cubic hexacyanoferrate structure, featuring a mixed valence state of Fe^{2+} and Fe^{3+}, which endows them with unique photophysical, magnetic, electrochemical, and electrochromic properties [133]. The cyano groups (C≡N) in their hexacyanoferrate cubic structure act as a coordination link between the iron ions [134]. Additionally, as an excellent NIR photothermal agent similar to AuNPs, PBNPs have strong absorption at 808 nm [135]. The incorporation of photothermal PBNPs into the polymer matrix allows the resulting composite to exhibit an NIR response, as evidenced by the

unfolding and recovery of a fabricated "box" shape upon NIR irradiation (Figure 14b). The material displayed consistent shape fixation and recovery ratios of 98.9% and 95.7% respectively, over five cycles, indicating its resilience to repeated shape-memory cycles, although it did not achieve 100% shape recovery due to potential permanent deformation in the thermoplastic composite. The study also explored a light-activated bionic "athlete" that exhibits a jumping motion initiated by NIR light for 25.6 s, covering 17 mm in 0.06 s, and demonstrated its ability to adeptly overcome obstacles with consistent "cross-obstacle" performance even after five iterations (Figure 14b) [132].

Copper sulfide (CuS) NPs are used as nanofillers to enhance the behavior of SMP composites. As a p-type semiconductor with a direct bandgap ranging from 1.2 to 2.0 eV, CuS exhibits notable photothermal conversion driven by the efficient d–d energy band transition of Cu(II) ions under NIR laser irradiation [136]. Li et al. developed a cost-effective, stable light-sensitive SMP composite by embedding CuS NPs, synthesized on modified cellulose nanocrystal (CuS NPs@MCNC) through chemical precipitation, into a polyurethane matrix [137]. The resulting composite demonstrated robust light-induced shape-memory capabilities, attributed to the highly efficient photothermal effect of CuS NPs. The polyurethane nanocomposite film containing 0.2 wt.% CuS NPs@MCNC achieved a R_r of 97.4% under NIR irradiation for 21 s, maintaining a ratio exceeding 85.7% after five repeated tests. This performance indicates the potential of such light-sensitive SMP composites, particularly those incorporating CuS NPs@MCNC, for use in medical devices and advanced packaging solutions.

3.2. Carbon-Based Nanocomposites

3.2.1. Carbon Nanotube (CNT) Nanocomposites

Carbon nanotubes (CNTs) are extensively studied within the carbon family for their ability to significantly enhance the mechanical, electrical, and thermal properties of SMP composites [138]. Their integration into SMP matrices not only provides superior flexibility compared to traditional fiber reinforcements but also aims to induce an electroactive SME via Joule heating, leveraging their intrinsic thermal responsiveness [139,140]. However, integrating CNTs within the SMP matrix is challenging due to their lack of uniform dispersibility [141]. To overcome this issue, several strategies have been employed, such as in situ polymerization, melt mixing, sol-gel, solution mixing followed by casting, solution mixing aided by ultrasonic dispersion, and chemical functionalization of CNTs followed by cross-linking [142–144]. These integration techniques are robust and effective approaches to enhancing the compatibility between CNTs and SMP matrices through physical and chemical interactions [19]. After preparing the polymeric matrix through conventional methods like extrusion or injection molding, it is subsequently programmed to deform and lock into the desired temporary configuration.

Electrically conducting SMP composites are developed to prevent localized heating in surrounding areas, enabling remote control and rapid actuation. For this purpose, CNTs are commonly used in non-conducting SMP matrices as conducting fillers [145]. CNTs can be categorized as single-walled (SWCNTs) or multiple-walled carbon nanotubes (MWCNTs) depending on their wall structure [146]. The latter is widely used for fabricating SMP composites due to its low bulk density and high aspect ratio, providing enhanced electrical and thermal conductivities, along with improved mechanical and shape-memory properties, compared to neat polymers [147,148]. Raja et al. enhanced the conductivity of polyurethane and poly(vinylidene difluoride) (PVDF) composites by incorporating modified MWCNTs through melt blending, achieving notable improvements in mechanical, dynamic mechanical, and electroactive shape-memory properties [149]. The inclusion of 10 wt.% MWCNTs enabled the composite to recover approximately 95% of its original

shape under a 40 V voltage. Similarly, Qi et al. developed a rapid-response electroactive ternary SMP composite combining MWCNTs, poly(propylene carbonate) (PPC), and poly(lactic acid) (PLA), achieving a conductivity of 10 S/m at 30 V, resulting in a surface temperature of 80 °C and 97% shape recovery within 30 s [150]. Employing digital light processing (DLP) 3D-printing technology, Cortés and colleagues created a photocurable, electroactive SMP composite by integrating MWCNTs into an amorphous thermosetting PEG diacrylate/poly(hydroxyethyl methacrylate) matrix [13]. This approach significantly improved the composite's electrical conductivity, enabling remote activation through Joule heating. The shape-memory functionality was demonstrated in a smart, 3D-printed butterfly structure, showcasing high shape fixity ($R_f \approx 100\%$) and shape recovery ($R_r > 95\%$), illustrating the potential for Joule-heated shape-memory activation.

Houbben and colleagues conducted a study on the development of covalently adaptable networks (CAN) using conducting poly(ε-caprolactone) (PCL-CAN), incorporating MWCNTs into a four-arm star-shaped PCL with maleimide and furan end-groups through melt blending [55]. Both conventional tensile testing and dynamic mechanical analysis confirmed the enhancement of the composite's mechanical properties, coupled with outstanding shape-memory characteristics, achieving recovery and fixity ratios of approximately 99%. To impart conductivity to the PCL-CAN network, 3% of MWCNTs were added to the matrix, although 1 wt.% was sufficient to enable current-driven heating [151]. In their experiments, a rectangular sample of the PCL-CAN composite network was stretched and then quickly returned to its original shape within two minutes through Joule heating, demonstrating efficient localized heating in stretched regions while avoiding overheating of the entire sample (Figure 15).

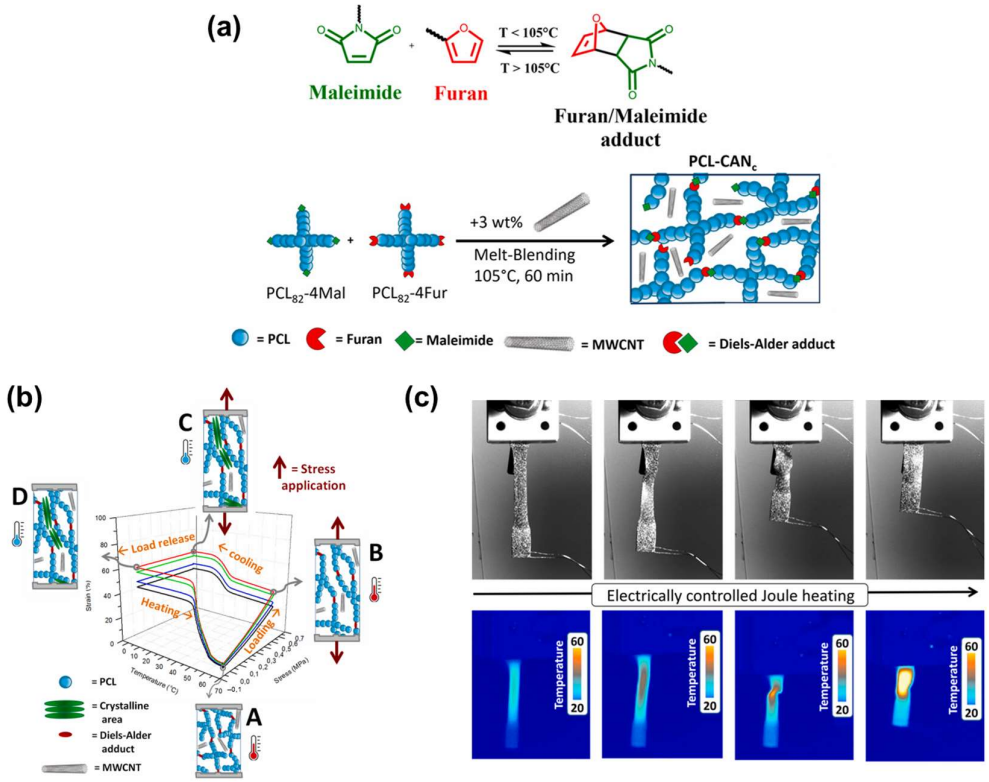

Figure 15. (**a**) Illustration of step-by-step network formation through maleimide-furan Diels-Alder addition; (**b**) shape-memory cycles of PCL-CAN, measured by DMA, starting from panels A to D; and (**c**) standard and infrared images illustrating the electroactive shape-memory recovery process driven by the Joule effect. Reproduced with permission from ref. [55]. Copyright 2023 Elsevier.

Zhou and coworkers fabricated a nanocomposite with fast healing capabilities based on dynamic bonds, utilizing carboxyl-functionalized $MWCNT_{-COOH}$ and a cross-linked polyurea (CPU) matrix through a facile two-step method. This method involved in situ photo-induced polymerization followed by hot compression [152]. The resultant nanocomposites exhibited exceptional photo-induced SME, capable of unfolding round-shaped films under NIR light irradiation within 20 s and returning them to their original shape in 120 s. In contrast, pure CPU films remained unchanged even after 120 s of exposure, highlighting the significant role of $MWCNT_{-COOH}$ in enhancing photo-induced SME through its photothermal properties. Furthermore, the self-healing capabilities under NIR light were investigated, revealing that while visible scratches on pure CPU matrices persisted even after prolonged NIR exposure, nanocomposites containing 0.5 wt.% and 1.0 wt.% $MWCNT_{-COOH}$ achieved rapid and complete scratch healing within 40 s, reaching a 100% self-healing efficiency (Figure 16). In another study, Feng and coworkers added polydopamine (PDA)-modified MWCNTs to an epoxy vitrimer to improve the interfacial interaction between nanofillers and the polymer matrix while maintaining high photothermal efficiency [153]. The incorporation of 1 wt.% MWCNTs resulted in shape-memory composites demonstrating initial shape fixity and recovery ratio 80.1% and 92.1%, respectively. This approach not only improved the performance of the composites but also underscored the synergy between material innovation and scientific advancement in the field of materials engineering.

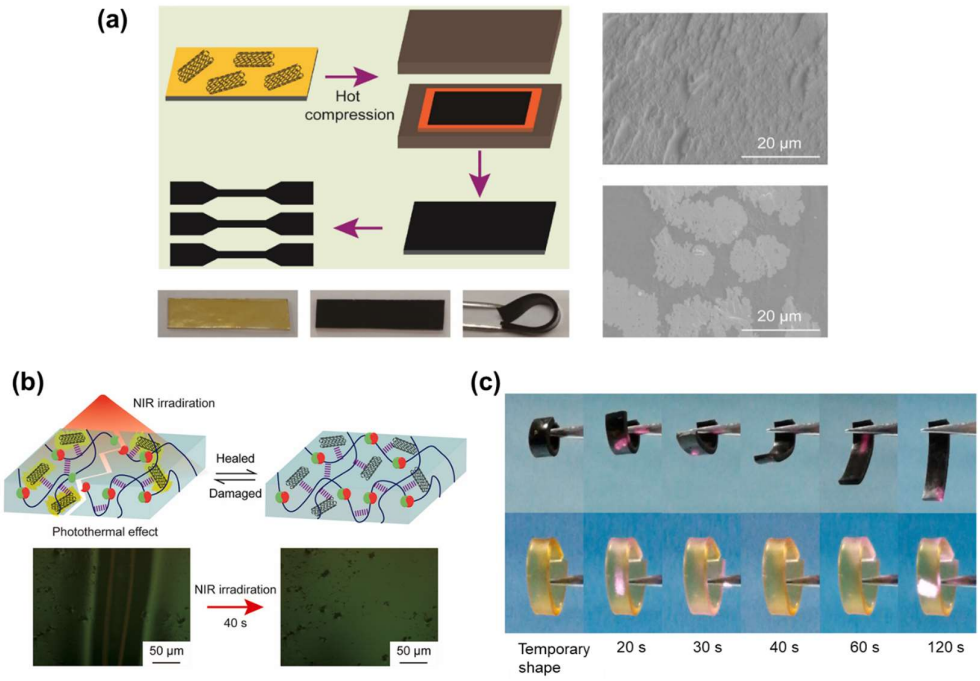

Figure 16. (**a**) Images depict the production process of CPU@CNT using hot compression, with photos of a pure polymer film and a nanocomposite film before and after bending, along with SEM images of the cross-sectional and surface views of CPU@CNT1.0; (**b**) illustration of the scratch-healing process under NIR light; and (**c**) images of shape recovery for CPU@CNT and pure CPU. Reproduced with permission from ref. [152]. Copyright 2022 Elsevier.

Li and colleagues utilized a sol-gel method to synthesize silica-coated multi-walled carbon nanotubes ($MWCNT@SiO_2$). These were subsequently incorporated into a cyanate ester-based SMPNC [154]. The optimal loading of 0.9 wt.% $MWCNT@SiO_2$ not only enhanced the moisture resistance but also significantly improved the mechanical properties, as evidenced by increased strength and toughness. Furthermore, the inclusion of $MWCNT@SiO_2$ facilitated an accelerated shape-memory process, with the composites demonstrating excellent

shape fixity (R_f) and recovery (R_r) ratios exceeding 98% after 10 testing cycles. In a related study, Namathoti et al. reinforced the mechanical and shape-memory characteristics of shape-memory polyurethane (SMPU) with a mixture of two types of nanofillers: MWCNTs and halloysite nanotubes (HNTs) [155]. This reinforcement strategy yielded composites with impeccable 100% shape recovery from their programmed temporary shapes, alongside a reduction in recovery time as the filler concentration increased.

Bo and colleagues developed SMPCs based on cardanol-based benzoxazine and CNTs, aiming to leverage their high conductivity for intelligent applications [156]. The SMP/CNT combination displays excellent sensitivity to changes in pressure and bending, along with commendable stability and recoverability. In another study, Sun and coworkers explored a reversible SME using a segregated CNT/poly(ethylene-co-vinyl acetate) (EVA) composite, achieving actuation at a remarkably low voltage of 15 V [157]. This segregated CNT/EVA composite was distinguished by its superior reversible actuation, evidenced by its capability to lift and lower a target object under low voltage application. Further advancing the application of shape-memory composites, Ma et al. utilized a CNT/EVA nanocomposite for the reversible actuation of 3D structures through a synergy of chemical and physical programming, facilitated by NIR irradiation [158]. Figure 17a depicted a locally reversible actuation, as demonstrated by the wings of a model responding to NIR irradiation with an upward swinging motion, which reverted to their original position upon cessation of the irradiation.

The addition of CNTs to polymer matrices significantly influences the crystallization behavior of the resulting composites, as documented in various studies [55]. This impact varies across studies depending on factors such as the nature of the polymer matrix, dispersion quality, CNT-polymer interactions, thermal treatment, and other variables [159–162]. Generally, MWCNTs have been identified as potent nucleation agents that expedite the crystallization process in polymers, affecting key parameters such as crystallization temperature, degree of crystallinity, and crystallite dimensions [163,164]. However, an increase in crystallinity can impede the elastomer phase from returning to its original shape, enhancing temporary shape retention and diminishing the shape-recovery ratio with increased MWCNT content [165–167]. This phenomenon is attributed to the displacement of MWCNTs during deformation and their subsequent failure to return to initial positions, potentially causing permanent deformation in the composite material [13,167].

In a related study, Tekay et al. developed SMPCs that respond to heat and electricity, consisting of poly(ethylene-1-octene) (PEO) and poly(styrene-b-isoprene-b-styrene) (SIS), with MWCNTs serving as fillers [168]. The resulting composite exhibited a noticeable rise in stiffness and brittleness, while tensile strength and elongation at break decreased with increasing MWCNT content, leading to restricted molecular mobility and premature fractures [169,170]. Although nanofillers can enhance polymer matrix stiffness, this often results in higher recovery stress levels but not necessarily improved shape recovery [171]. When assessing heat-induced actuators, “C-shaped” samples demonstrated that composites with increased MWCNT content exhibited longer recovery times due to hindered elastomer molecule mobility [169]. The 10CNT composite took 600 s to recover, twice as long as the blend, attributed to MWCNT-induced inhibition. In contrast, electrical voltage rapidly triggered shape recovery in the 5CNT and 10CNT composites, with the 5CNT outperforming due to a lower concentration of MWCNT aggregates, showcasing the efficiency of electrical stimulus compared to heat-induced recovery (Figure 17b).

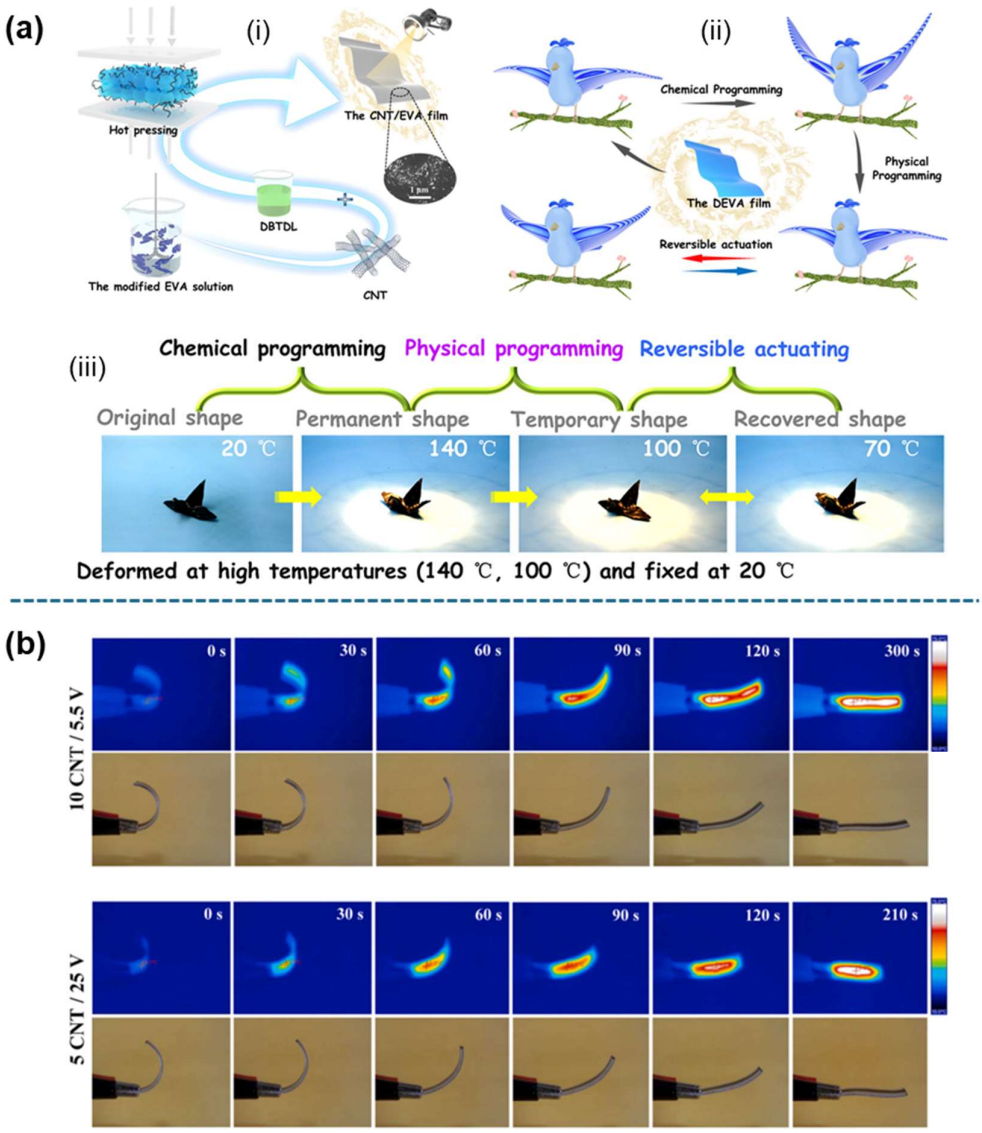

Figure 17. (**a**) Synthesis of CNT/EVA composites (i), locally reversible actuation demonstrated using a bird model (ii), and light-triggered reversible actuation of the composite (iii). Reproduced with permission from ref. [158]. Copyright 2023 American Chemical Society. (**b**) Electro-active shape-recovery images showing 10CNT at 5.5 V and 5CNT at 25 V. Reproduced with permission from ref. [168]. Copyright 2023 Elsevier.

Dong et al. developed continuous fiber-reinforced electro-induced shape memory auxetic composites (CFRSMCs) using a 3D-printed PLA/TPU/CNT blend [172]. Adding carbon fiber reduced the thermal recovery ratio (R_r) from 96.7% to 89.5% due to fiber-matrix slippage, despite enhancing shape recovery speed. Electrically, CFRSMCs achieved rapid recovery (R_r = 94% in 25 s at 10 V), demonstrating the efficiency of their conductive network. The printed auxetic structure exhibited a negative Poisson's ratio, with experimental results aligning with theoretical predictions, while the integrated carbon fiber-CNT network enabled precise electro-induced shape recovery and selective activation, enhancing functionality and adaptability [172]. These properties make them ideal for biomedical applications, enabling precise conformability to complex anatomical structures and enhancing bone regeneration and tissue integration, as well as for soft robotics, adaptive actuators, and smart protective materials.

3.2.2. Carbon Nanofiber (CNF) and Carbon Black (CB) Nanocomposites

Carbon nanofibers (CNFs) and carbon blacks (CBs) are widely accessible carbon-based nanomaterials known for their distinctive mechanical properties and applications [173]. These materials form excellent electrical conductivity networks and achieve uniform thermal distribution in polymer matrices [19]. Gopinath et al. engineered thermo-responsive SMPNCs by integrating CNFs into the matrix of PCL and polystyrene-block-polybutadiene-block-polystyrene (SBS) using a melt blending technique (Figure 18a) [174]. These nanocomposites exhibited an almost instantaneous recovery to their original configurations, with a shape-recovery ratio (R_r) approaching 100%, upon heating beyond their transition temperature (T_{trans}) to a predefined flower-like morphology. The concentration of PCL significantly influences the shape-memory performance by enhancing mechanical strength and reducing recovery time, while both PCL and CNF concentrations affect shape fixity and recovery efficiency. In another study, varying concentrations of CNFs were incorporated into a matrix of hydroxyl-terminated polybutadiene (HTPB) and polytetramethylene glycol (PTMG) cross-linked polyurethane [175]. This system utilized chemically cross-linked hard-phase components for stability and elastomeric soft-phase components for reversible shape transitions, emphasizing the importance of the hard-to-soft segment ratio and CNF concentration for optimal dispersion and SMPU composite quality. Notably, composites with 1 wt.% CNFs demonstrated a recovery time of 46 s to their original shape, while those with 5 wt.% CNFs achieved recovery in only 38 s, showcasing enhanced shape-memory properties.

In another study, Lu et al. developed an innovative approach to enhance both the electrical conductivity and the shape-recovery efficiency of SMPU nanocomposites by integrating self-assembled CNF nanopaper layers [176]. The multilayers of self-assembled nanopapers improved the interfacial bonding and mechanical properties of the polymer composite [177,178]. The greater the quantity of CNFs in the nanopaper, the higher the conductivity, which resulted in increased electric current amplitude and carrying capacity due to expanded conductive paths and reduced electrical resistance [179]. Consequently, SMPU nanocomposites containing four-layered CNF nanopaper demonstrated effective Joule heating-induced shape recovery upon the application of 30 V DC, achieving original shape restoration in 80 s, as confirmed by an infrared camera that captured a peak temperature of 102.5 °C.

Uranbey et al. demonstrated that SMPUs embedded with 20% carbon black (SMPU/20CB) achieved 88.8% shape recovery within 40 s under a 4 kV electric field This performance was attributed to the enhanced mobility of hard segments facilitated by the CB additive [180]. In contrast, in situ techniques had demonstrated even higher shape-recovery rates (R_r) at elevated temperatures, such as 100% recovery in 26 s under 60 V, but required a higher CB content for operation at lower voltages [181]. With increasing CB contents, the conductivity of the SMPU/CB blend was enhanced, owing to the strengthened electron tunneling effect [111]. The SMPU/20CB filament also exhibited increase temperature with rising voltage, indicating its responsiveness to electrical stimulation for shape-memory behavior. However, it burned at multiple points when exposed to 9 kV, indicating its voltage tolerance and heating limitations. In another study, Du et al. developed a conductive composite by integrating 10 wt.% CB into a polyolefin elastomer (POE) and lauric acid (LA) blend, achieving a volume resistance of approximately 23 Ω cm through CB percolation networks [182]. This electroactive nanocomposite demonstrated superior shape-memory capabilities, with a U-shaped sample regaining its original form within 75 s at 10 V, and within 20 s at 20 V, showcasing the tunability of the SME by adjusting CB concentration and applied voltage (Figure 18b). Ren et al. utilized fused deposition modeling (FDM) to create nanocarbon black/polylactic acid composites with SMPU, exhibiting remarkable shape recovery upon heat application [183].

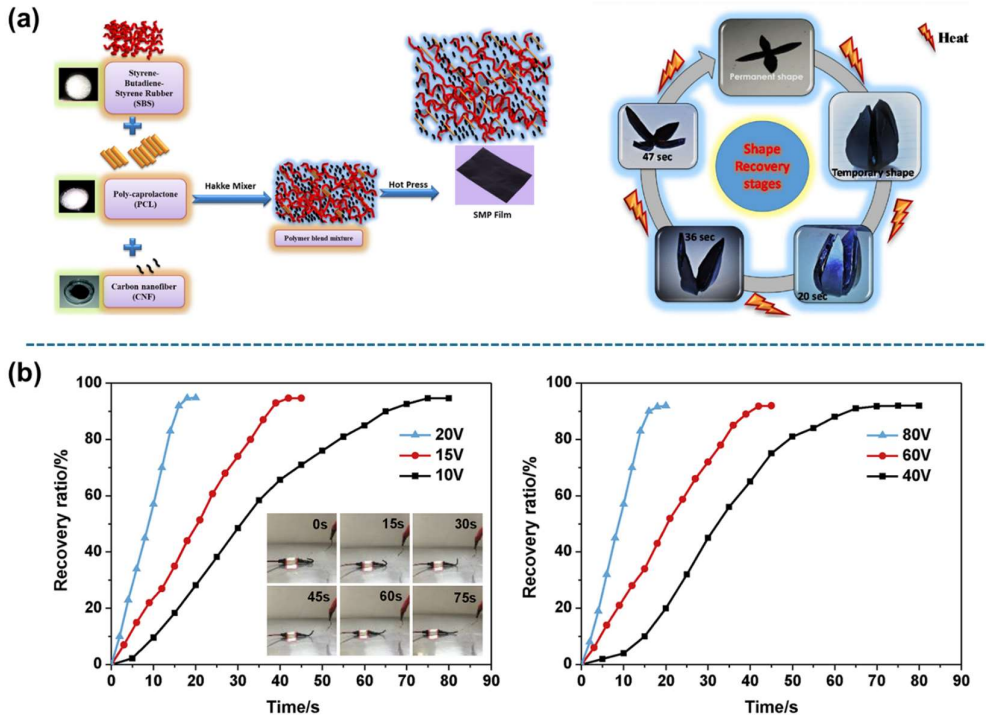

Figure 18. (**a**) Diagrams illustrating the fabrication process of nanocomposites from SBS, PCL, and CNF, as well as the shape-recovery cycle. Reproduced with permission from ref. [174]. Copyright 2019 Elsevier. (**b**) Plots showing the shape-recovery ratio vs. time for two distinct compositions: POE/LA/CB (50/50/20) (left) and POE/LA/CB (50/50/10) (right), under various voltage conditions. Reproduced with permission from ref. [182]. Copyright 2018 Elsevier.

3.2.3. Nanostructured Cellulose Nanocomposites

Incorporating nanofillers into polymer matrices is a prevalent engineering strategy to enhance material properties and introduce tunable functionalities in nanocomposites [184,185]. Cellulose nanomaterials (CNs), including cellulose nanocrystals (CNCs) and cellulose nanofibers (CNFs), are particularly valued as fillers or reinforcing agents in SMPs due to their affordability, high availability, low density, exceptional crystallinity, substantial aspect ratio, remarkable tensile strength and modulus, and biocompatibility [186–188]. The abundant hydroxyl groups on the surface of CN materials facilitate the formation of hydrogen bonds with the soft polymer matrix during polymerization, resulting in improved interfacial adhesion and increased stiffness [189,190]. Nevertheless, the fabrication of nanoarchitecture through direct physical encapsulation of CN materials within the polymer matrix is challenging.

To enhance the nanoscale dispersibility of CNs and overcome processing challenges, considerable attention has been directed towards implementing bottom-up surface modifications techniques such as chemical covalent bonding, surfactant treatment, wet compounding, polymer grafting, and wrapping [191]. Without undergoing any functional modification, CNs in their pristine state typically exhibit only modest improvements in their characteristics [192]. Recently, functionalized cellulose materials have been investigated as cross-linkers to fabricate nanocomposites with enhanced properties [193,194]. However, robust cross-linking often leads to decreased free volume and fewer active sites for hydrogen bonding, affecting water molecule diffusion within the microstructure and, consequently, the material's water-induced shape-recovery performance [195–197]. Hydrated cellulose nanopapers (CNPs), produced from CNFs, offer significant potential due to their nanoscale effects, high specific surface area, and hydrophilicity, making them excellent for functional applications [198]. Yet, their direct application in water-induced

shape-memory materials is limited due to susceptibility to swelling and dissolution, caused by water infiltration weakening the CNFs' interfibrillar hydrogen bonding [199–201]. This vulnerability restricts the application of CNPs in high humidity and water environments.

The preparation methods and characteristics of CNFs predominantly influence the structure and properties of CNP [202]. Formic acid (FA) hydrolysis is one of the clean and sustainable pre-treatment methods for CNF production, offering easy recycling due to the low boiling point of FA [203]. During this process, the introduction of ester groups on the surface of CNFs adjusts their polarity and hydrophilicity, allowing the preparation of flexible CNPs with appropriate hydrophilicity and wet strength [204]. A neutral amino-containing polymer, chitosan (CS), has also been explored to enhance wet strength in CNP as a cross-linker [205]. However, the increased brittleness associated with CS cross-linking poses a challenge for practical applications, limiting folding endurance [206]. Moreover, CS, reported as a shape-memory scaffold for drug delivery, exhibited a relatively low response to water and a rapid decrease in wet strength due to excessive swelling, highlighting the trade-off between water responsiveness and material durability [54].

In recent years, water-induced SMP composites have been investigated more deeply because of the mild and environmentally friendly nature of water as a stimulus [207]. Wu et al. addressed the inherent limitations of water-induced SMPCs through the integration of CS-modified CNP, which is derived from CNFs treated with FA hydrolysis to introduce surface ester groups [54]. This modification endowed the CNP with rapid responsiveness to water (<3 s) and humidity (<10 min) without compromising wet strength (Figure 19b). Notably, the composite exhibited a shape-recovery ratio (R_r) exceeding 90% across 10 cycles, indicating its durable shape-memory capability in aqueous environments. The observed behavior was attributed to the water-mediated disruption of hydrogen bonds and the reversible activity of CS chains, which facilitated the transition between its temporary folded state and its original configuration [208]. The response benefited from the combined hydration effects of CS and the water-resisting properties of CNFs with ester groups, which together prevented overhydration and enabled a swift shape recovery [204]. The CS-modified CNP further demonstrated significant folding endurance (exceeding 1190 cycles, Figure 19c), exceptional wet tensile strength (65 MPa), transparency, and superior barrier properties, underscoring its potential for diverse applications where water-induced actuation is desirable.

Utilizing CNFs, Meng and coworkers developed water-responsive SMPNCs via the evaporation-induced self-assembly (EISA) method, incorporating polyvinyl alcohol (PVA) and lignin as raw materials, and citric acid (CA) as cross-linker [209]. By adjusting the CNF to PVA ratio and the amount of added lignin, the cross-linked network structure was modified, affecting the microstructure, water responsiveness, and mechanical properties of the membrane. However, an increase in CNF concentration resulted in enhanced hydrogen bonding among CNF chains, potentially raising crystallinity and surface density, thereby increasing the hydrophobicity of the composite [210,211]. The nanocomposite membrane achieved nearly 100% shape recovery in 15 s upon water immersion, with its response time optimized to 3 s at a 20% lignin content, demonstrating exceptional water responsiveness (Figure 20a).

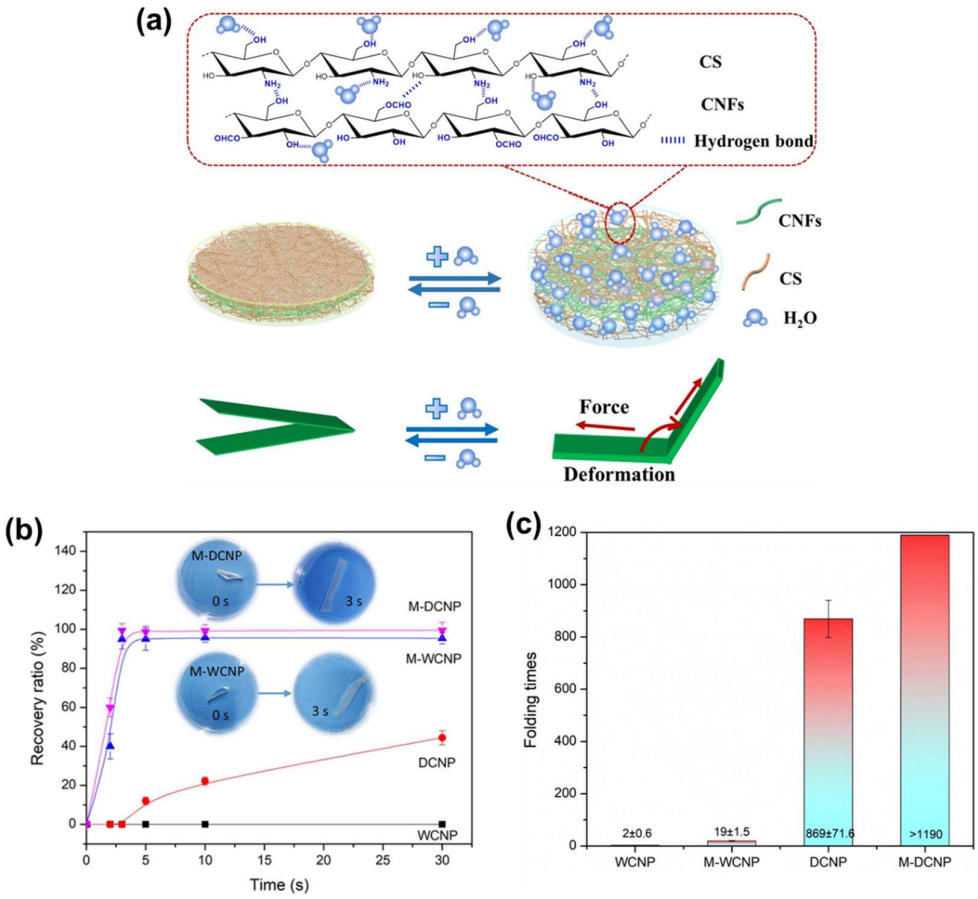

Figure 19. (**a**) Schematic diagram illustrating the synergistic hydration process of the composite; (**b**) shape-memory responses to water for various tape-like CNP samples; and (**c**) double folding times of various composites. (WCNP and DCNP were produced from the homogenization of CNFs in water and dimethylacetamide, respectively). Reproduced with permission from ref. [54]. Copyright 2019 Elsevier.

In another study, utilizing in situ polymerization technique, Hosseinnezhad and coworkers explored hybrid polymer-polymer nanocomposites using a three-component system (polylactide/polybutylene adipate terephthalate/CNFs) [212]. Unlike conventional polymer blends, the novel formulation exhibited a triple SME characterized by significantly superior strain recovery and fixity ratios, faster recovery rates, and enhanced mechanical properties. Gu et al. engineered 4D-printed thermally responsive SMPNCs by incorporating CNFs into polycaprolactone (PCL)/poly(butyleneadipate-co-terephthalate) matrix through wet melt blending method [213]. The resulting composite exhibited excellent shape fixation and recovery with good shape stability at the transition temperature. However, the incorporation of CNFs did not alter the shape fixity (R_f) and recovery (R_r) ratios but expedited the recovery process. Utilizing the nanocomposite filament, a flower model was printed and thermally programmed into a temporary shape, showcasing remarkable shape recovery and thus evidencing the achievement of 4D printing capabilities. (Figure 20b).

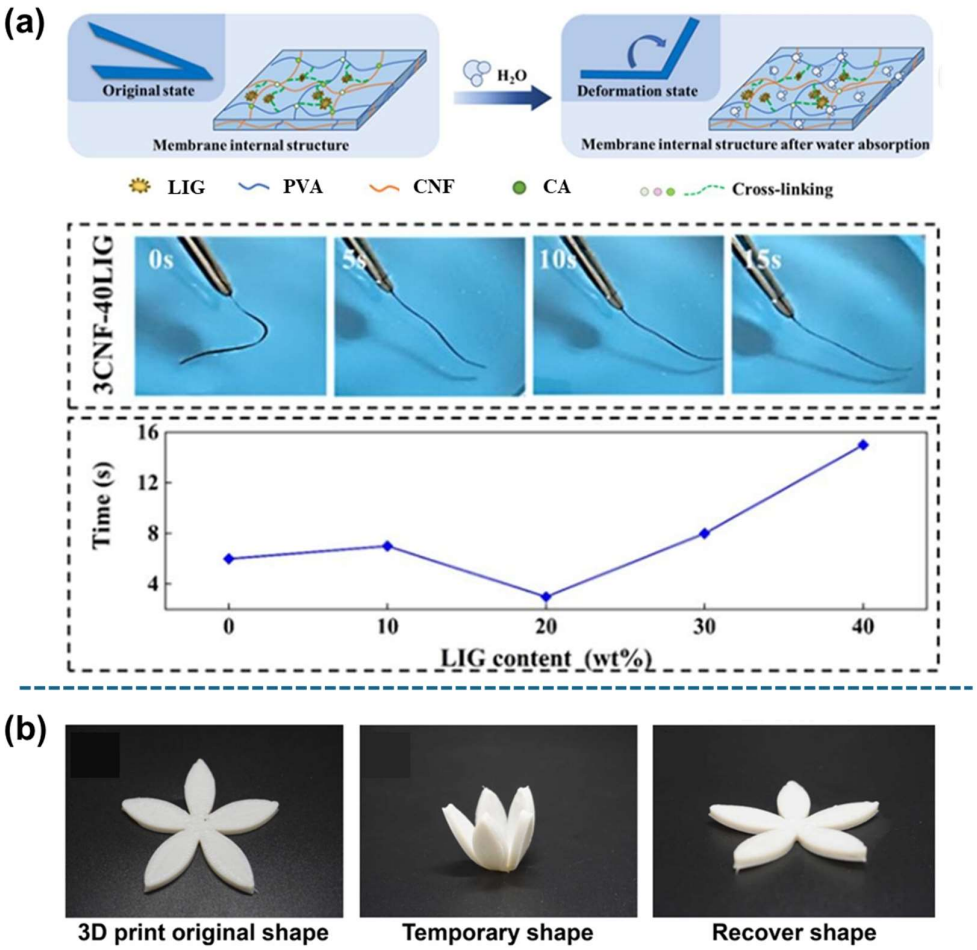

Figure 20. (**a**) Schematic diagram of the water-responsive mechanism, shape recover process, and lignin (LIG) content-dependent recovery time graph of the CA/LIG/PVA/CNF composite. Reproduced with permission from ref. [209]. Copyright 2022 Elsevier. (**b**) Shape recovery of a 3D-printed flower-like structure of CNFs embedded nanocomposite. Reproduced with permission from ref. [213]. Copyright 2023 Elsevier.

To achieve magnetic-responsive 3D-printed structures, Yue and coworkers added Fe_3O_4 and CNFs to poly(hydroxybutyrate)/poly(ε-caprolactone) (PHB/PCL) blends as functional particles and reinforcing agents [214]. The 3D printed snowflake model exhibited excellent magneto-responsive shape memory, gradually unfolding and recovering to its permanent shape within 35 s. This confirms the favorable magneto-responsive shape-memory property of the snowflake model.

Gupta et al. introduced cellulose nanocrystals (CNCs) to polycaprolactone (PCL)-based SMPU through in situ one-pot reactions [215]. The in situ incorporation of CNCs led to covalent bonding between PCL chains and the CNC surface, enhancing dispersion without the need for conventional pre-modification of CNCs (Figure 21a). Incorporating 10 wt.% CNCs significantly improved the mechanical properties, including tensile strength and modulus, without compromising elongation at break (Figure 21b). Additionally, the composite exhibited remarkable shape fixation and recovery qualities during a stretching test conducted on a 20 mL glass bottle, evidenced by its tight grip and rapid return to its original shape upon heating, highlighting its suitability for biological applications (Figure 21c).

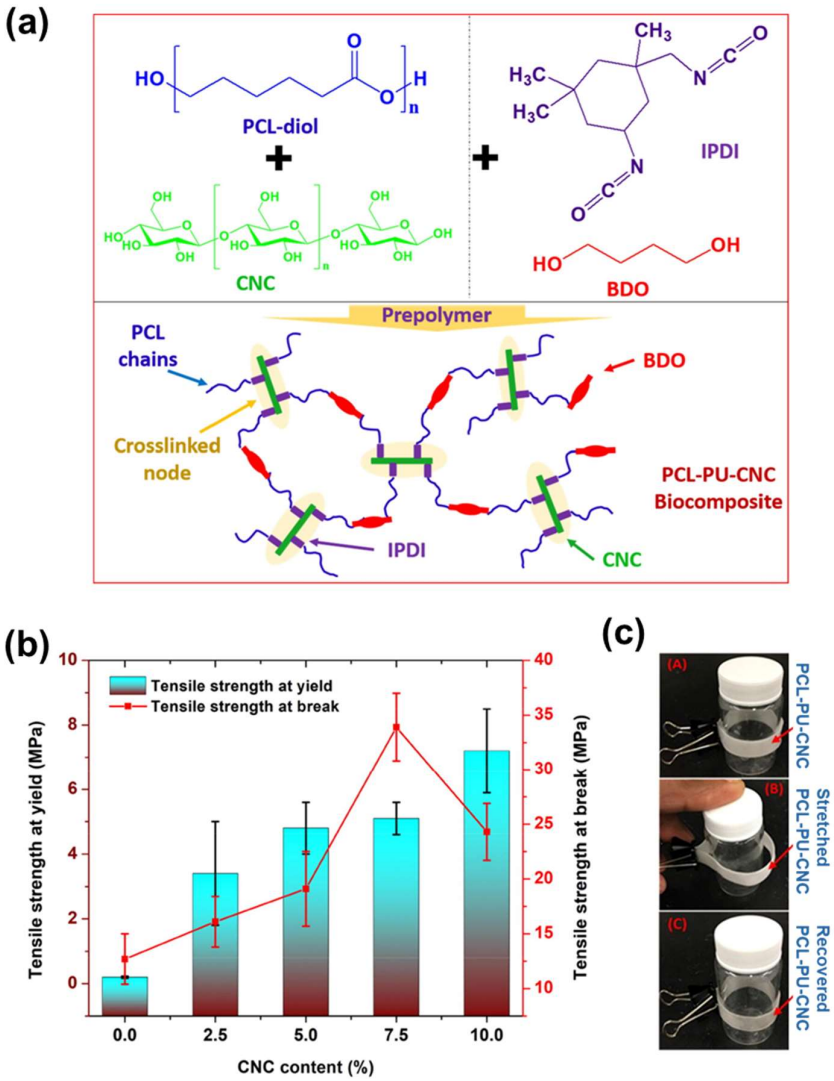

Figure 21. (**a**) Depiction of a possible interaction between PCL and CNC; (**b**) relationship between CNC concentration and tensile strength at yield and break; and (**c**) images of grippers taken at room temperature, following mechanical stretching, and after being heated to 40 °C. Reproduced with permission from ref. [215]. Copyright 2022 Elsevier.

Du et al. developed SMPCs by incorporating modified cellulose nanocrystals (MCNCs) with urethane and phosphorus-containing flame retardant units through an in situ polymerization method [216]. With a 3 wt.% inclusion of MCNCs, the nanocomposite exhibited excellent dispersibility within the polymer matrix and maintained shape fixity (R_f) and recovery (R_r) ratios above 90% over five cycles. Similarly, Fan et al. developed a shape-memory polyacrylamide/gelatin hydrogel, integrating 3-methacryloxypropyltrimethoxysilane modified MCNCs that acted as chemical-physical cross-links, enhancing the mechanical properties and swelling resistance [217]. Optimal performance was achieved with 2 wt.% MCNC addition; the hydrogel exhibited superior mechanical strength, excellent thermally induced shape-memory performance with 76.6% fixity and 96.5% recovery, and maintained cytocompatibility, marking its potential in biomaterial applications.

Recent advancements in SMPCs have shifted focus from the traditional reliance on a single triggering mechanism towards the exploration of multi-stimulus-responsive systems, significantly enhancing their applicability across various domains [218]. Wu et al. developed multi-responsive SMPNCs by integrating thermoplastic polyurethane (TPU) with carbomer (CB) and utilizing CNCs as a cross-linking agent [139]. This composite benefited

from the dual-phase structure of polyurethane, which facilitated thermo-responsive shape-memory behavior through its hard and soft segments, alongside a high concentration of -COOH groups (ranging from 56.0% to 68.0%) of CB, aiding in cross-linking via hydrogen and ester bonds [219,220]. The nanocomposite exhibited shape-memory behavior through molecular switches activated by stimuli such as water, heat, and pH changes, enabling the programming and recovery of temporary shapes (Figure 22). Chemical and microstructural analyses revealed that the optimal loading of CNCs at 5 wt.% significantly influenced the mechanical properties of the nanocomposites, facilitating the formation of quaternary ammonium ionic and hydrogen bonds. The application of combined water and heat stimuli enhanced the opening of these bonds in shape-fixed samples, yielding a more pronounced shape-recovery effect than when stimuli were applied individually [221].

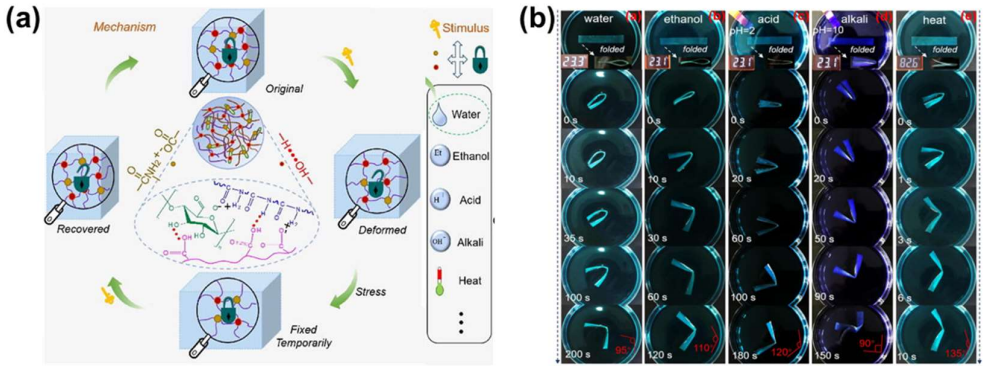

Figure 22. (**a**) A proposed switchable multi-stimuli shape-memory mechanism and (**b**) shape-recovery process for manually deformed TPU/CB/CNC-5 (5 wt.% CNC) strips under various conditions: water (23.0 °C), ethanol (23.0 °C), acid (23.0 °C, pH = 2), alkali (23.0 °C, pH = 10), and heat (82.6 °C). Reproduced with permission from ref. [139]. Copyright 2022 Elsevier.

In another study, Liu and coworkers synthesized a multi-stimulus responsive SMPNC networks by chemically cross-linking CNCs with biocompatible PCL and PEG, resulting in enhanced mechanical properties and notable thermo-induced and water-induced SMEs in water at 37 °C [222]. The nanocomposite film exhibited multi-responsiveness under various conditions, revealing its potential applications in drug delivery, flexible robotics, and electronics.

Bi and colleagues developed SMPCs with self-healing properties via a thermoreversible cross-linked network, utilizing Diels-Alder (DA) reversible covalent bonds and transient cross-links from TPU and PCL, with the addition of CNC as a cross-linking agent (Figure 23a) [223]. The DA-based matrix demonstrated outstanding transparency, thermal efficiency, and notable temperature-induced self-healing properties, effectively mending surface scratches via mild heat treatment [224]. Concurrently, the modification of CNC with furan (CNC-FA) and maleic anhydride (CNC-MAH) groups improved its compatibility with the TPU/PCL matrix, thereby enhancing the mechanical and thermal characteristics, and elevating self-healing efficiency of the composites (Figure 23b). These developments have rendered the composites mechanically robust and suitable for 3D printing, with potential applications in a wide range of devices, including durable conductive and biomimetic skin devices, flexible electronics, and encryption devices.

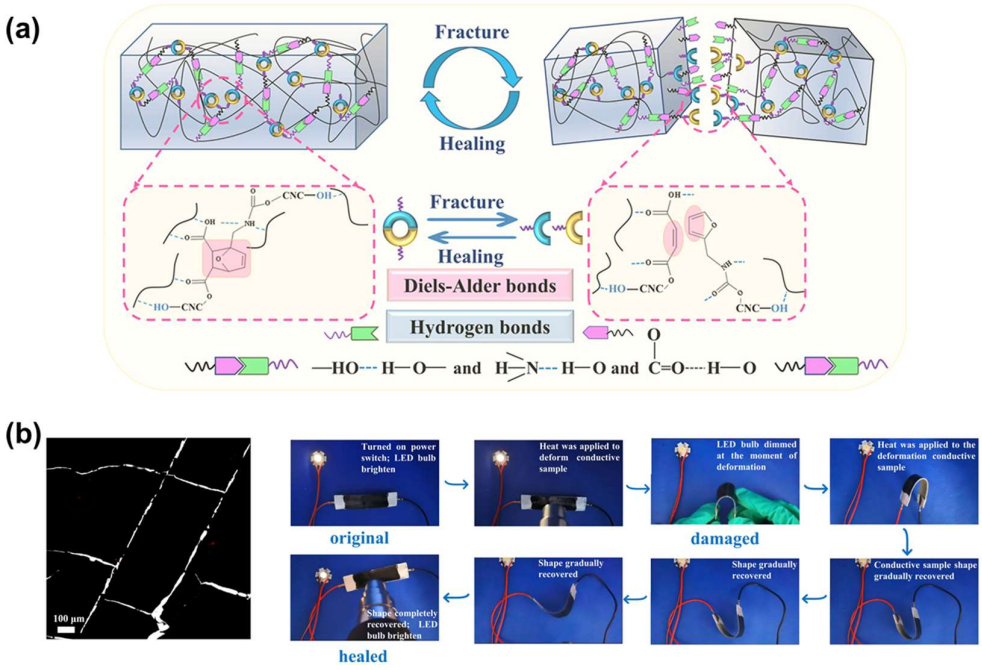

Figure 23. (**a**) Self-healing dynamic cross-linking network design; and (**b**) electrical healing process of the conductive device with an LED bulb. Reproduced with permission from ref. [223]. Copyright 2021 Elsevier.

3.2.4. Graphene Oxide Nanocomposites

Graphene, a unique two-dimensional nanostructure of sp^2 hybridized carbon atoms arranged in a well-organized honeycomb pattern, has garnered interest due to its outstanding electrical, optical, and thermal properties [225,226]. Its substantial surface area and aspect ratio make it an ideal candidate for enhancing the performance of SMPCs [226,227]. Furthermore, graphene and its derivatives have been effectively utilized as fillers in polymeric substrates, capitalizing on their superior heat and light absorption capabilities for light-controlled actuation and deformation [228–230]. For instance, Bai et al. developed SMPCs by incorporating graphene oxide (GO) into thermosetting polyurethane, demonstrating a photo-induced SME with 95% shape recovery upon NIR light exposure, as well as exhibiting solid-state plasticity and self-healing capabilities [73].

Among various synthesis methods, the chemical reduction of GO stands out as a widely recognized approach for producing substantial quantities of reduced graphene oxide (rGO) [231,232]. However, the limited dispersion capability of rGO in polymer matrices, attributed to the re-agglomeration of graphitic layers via strong π-π and van der Waals interactions, restricts its effective incorporation [233]. Consequently, enhancing stability and dispersibility necessitates the modification or functionalization of rGO. Punetha and colleagues utilized epoxy bisphenol A diglycidil ether (DGEBA)-functionalized rGO (DGEBA-f-rGO) to create cross-linked photothermal networks in hyperbranched polyurethane/epoxy (HBPU/EP) composites, enhancing their NIR light-driven actuation and mechanical properties (Figure 24a) [230]. Upon exposure to an 808 nm NIR laser, the composites displayed a significant increase in surface temperature and heating rate compared to the constant surface temperature of pure HBPU/EP. The DGEBA-f-rGO composites demonstrated superior photothermal performance and faster, more efficient shape recovery under NIR irradiation compared to their nonfunctionalized GO counterparts. Incorporating 1.0 wt.% DGEBA-f-rGO into the HBPU/EP matrix resulted in rapid shape recovery within 6 s and maintained a recovery ratio exceeding 95.0%, significantly outperforming DGEBA-f-GO composites.

Yoo et al. investigated the mechanical properties and shape-memory performance of PCL-based polyurethane nanofibers by integrating GO, PCL-functionalized f-GO, and rGO [234]. The composites containing f-GO and rGO exhibited enhanced actuation in shape-memory tests, achieving a recovery time of 8 s for 1 wt.% f-GO or rGO nanofibers, in contrast to 13 s for nanofibers with incorporated GO. This enhancement highlights the pivotal role of functionalized GO in improving interfacial interactions and enabling reversible cross-linking, thus optimizing the shape-recovery process [230].

Polyimide (PI) emerges as a key material in SMPs, notable for its excellent mechanical properties, thermal stability, and shape-memory functions [235]. Guo et al. developed thermosetting cross-linked polyimide SMP composites (TCPI/rGO) with a high transition temperature (T_{trans}), achieving rapid NIR light-induced shape recovery [236]. The addition of 1 wt.% rGO significantly enhanced the mechanical properties of the composites, achieving a breaking strain of 44.1% and toughness of 41.7 MJ/m^3. Upon exposure to 808 nm NIR light (1.5 W/cm^2), the TCPI-0.3/rGO-3% nanocomposites displayed a rapid temperature rise to approximately 300 °C within 10 s, while TCPI-0.3/rGO-1% reached 238 °C in 9 s, surpassing its glass transition temperature (T_g) of 221 °C. The rate of heating and the steady-state temperature exhibited a linear relationship with the rGO content, demonstrating that TCPI-0.3/rGO-1% could rapidly recover its original shape from a deformed π-shape within 7 s, with shape fixation (R_f) and recovery (R_r) rates exceeding 99% and 98%, respectively, due to the effective activation of macromolecular chains by localized NIR irradiation (Figure 24b).

Ghosh et al. utilized a simultaneous polymerization method to integrate functionalized reduced graphene oxide (f-rGO) into smart polyurethane and polystyrene, forming multi-stimuli responsive nanocomposites with interpenetrating polymer networks (IPN) [232]. Incorporating 1 wt.% f-rGO into IPN nanocomposites significantly enhanced their mechanical properties and thermal stability, and enabled efficient heat transfer, achieving 100% shape recovery within 33–44 s under microwave irradiation, surpassing the efficiency of sunlight exposure. In another study, they developed a functionalized-hydroxy iron oxide-anchored rGO nanohybrid to improve the thermal behavior of the nanocomposites, which exhibited faster shape recovery (20–40 s) with thermal heating than similar materials under sunlight exposure [237]. Additionally, these nanocomposites demonstrated exceptional chemical resistance, self-cleaning capabilities through surface hydrophobicity, and thermally actuated artificial muscle-like behavior [232,237].

Sofla et al. focused on electroactive SMPNCs composed of polyurethane/graphene nanosheets, where the polyurethane was synthesized from polycaprolactone, hexamethylene diisocyanate, and 1,4-butanediol through solution processing [238]. The incorporation of graphene into polyurethane significantly improved electrical conductivity, reaching a percolation threshold at 1.5 wt.%, where applying 75 V for 60 s facilitated shape recovery, although not complete at 1–1.5 wt.% graphene content (Figure 24c). Nanocomposites with 2–3 wt.% graphene nanofiller exhibited complete shape recovery within 60 s and showed enhanced shape fixity (83.4%) and recovery (100%) compared to neat polyurethane, underscoring the role of matrix-nanofiller compatibility in augmenting shape-memory performance. In another work, Wang et al. reported an epoxy-based SMPC utilizing reduced graphene oxide paper (rGOP) that achieved approximately 100% recoverability in just 5 s under 6 V, offering a more energy-efficient composite for applications purpose [239].

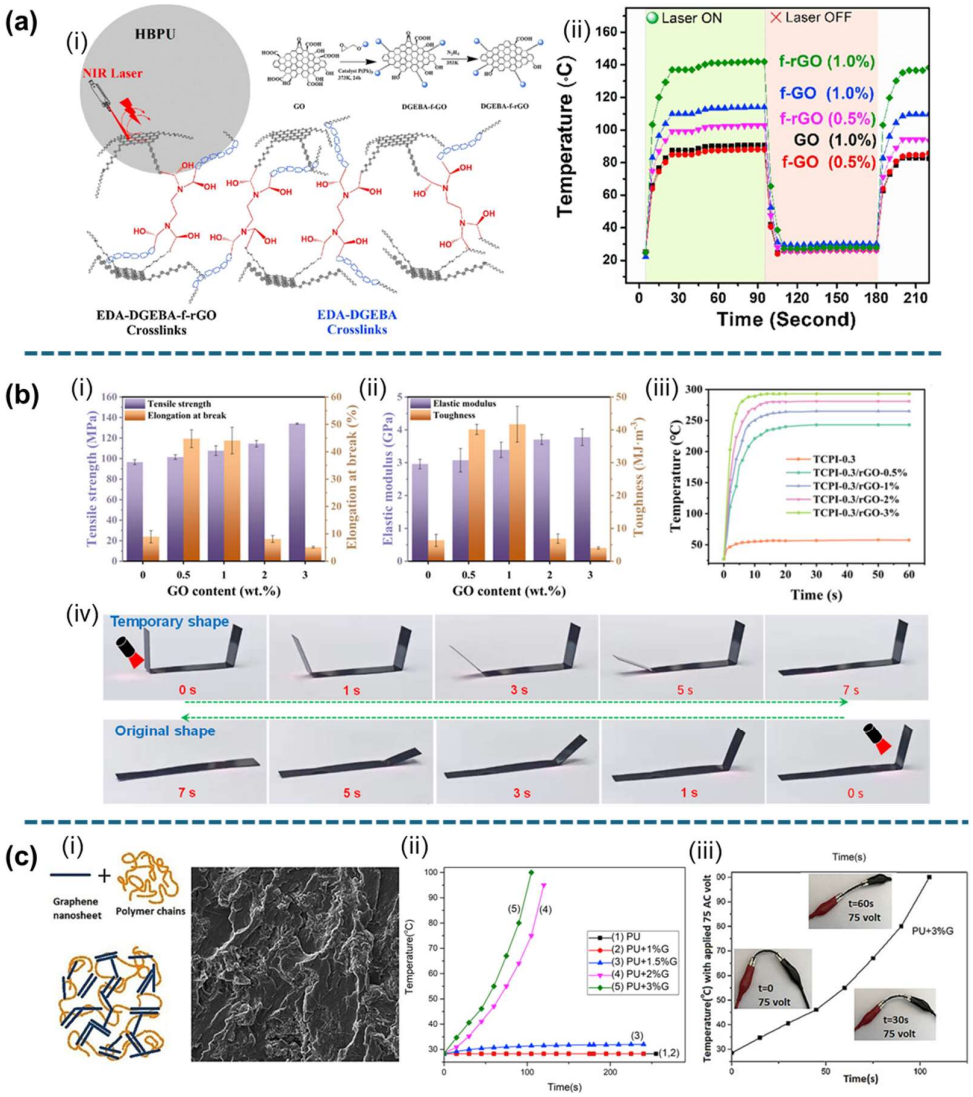

Figure 24. (**a**) (i) Schematic depiction of chemically bonded DGEBA-f-GO/EDA/DGEBA photothermal cross-links and (ii) surface temperature changes with varying nanofiller content in the HBPU/EP composite during NIR irradiation. Reproduced with permission from ref. [230]. Copyright 2020 Elsevier. (**b**) Graphical illustration of (i,ii) mechanical properties, (iii) temperature change as a function of GO content (wt.%) in TCPI/rGO composites, and (iv) the process of shape recovery of the TCPI-0.3/rGO-1% composite with a fixed π-shape under NIR irradiation. Reproduced with permission from ref. [236]. Copyright 2022 John Wiley and Sons. (**c**) (i) Graphene-incorporated FE-SEM image of polyurethane (PU) + graphene (G) nanocomposite, (ii) graphical representation of temperature vs. time for various GO content nanocomposites, and (iii) time needed for complete shape recovery for PU + 3 wt.% G composite at 75 V. Reproduced with permission from ref. [238]. Copyright 2019 Elsevier.

Falqi et al. utilized commercially available PVA/PEG to develop nanocomposites through solution casting, incorporating varying amounts of graphene, where the composite with 0.2 wt.% graphene achieved nearly 100% shape-memory recovery within 8 s [240]. However, increasing graphene content (0.5 and 1.0 wt.%) reduced the recovery ratio (R_r) to approximately 45% due to the enhanced brittleness hindering shape deformation [241,242]. Additionally, the inclusion of GO in PVA composites, facilitated by water as an athermal stimulus, significantly improved shape-memory properties by cross-linking within the PVA matrix, thereby improving response under various actuations [243].

3.2.5. Clay Nanocomposites

Nanoclays are two-dimensional, ideal reinforced nanofillers typically arranged in a stacked configuration, located at or in close proximity to the Earth's surface [244]. The concept of nanoclay originated in the 1990s, with seminal works by Usuki et al. and Okada et al., who investigated polyamide-6 filled nanoclay and referred to the composite as a hybrid material rather than a nanocomposite [245,246]. The incorporation of clay nanofillers into thermoset and thermoplastic polymers subsequently progressed, with a focus on montmorillonite (MMT), bentonite, mica, and hectorite. MMT became particularly favored due to its high aspect ratio and significant swelling properties in polar liquids [247–249]. Advances in material science have shown that nanoclays substantially enhance the mechanical, thermal, and shape-memory properties of nanocomposites by altering the crystal structure and improving the polymer matrix compatibility [250,251]. For example, Lourdin et al. developed starch/clay bio-nanocomposites using a melting process, showing that nanoclay addition significantly enhanced both the elastic modulus and shape-recovery ratio (R_r) [252].

Arash et al. enhanced the mechanical properties of PLA and TPU composites by incorporating cost-effective nano-clay particles through melt mixing, facilitating interactions with functional groups [253]. This modification not only improved the mechanical properties but also extended the biomedical applicability of PLA-TPU composites, including tissue engineering scaffolds and stent manufacturing [254]. The addition of 5 wt.% nanoclay resulted in significant enhancements in shape recovery and fixity ratios, increasing from 15.45% to 60.52% and from 95.81% to 99.76%, respectively, attributable to the uniform distribution of clay nanoparticles within the polymer matrix (Figure 25b). Another study demonstrated the fabrication of high-twist yarn using nanoclay-filled PLA/TPU composites to meet the demand for advanced actuators [59]. The yarn was coiled through mandrel annealing, exhibiting significant two-way SMEs and reversible contraction strokes within a low-temperature range [255]. This development of low programming temperature nano-reinforced PLA/TPU blends focuses on the shape-memory behavior of the composite, targeting applications in smart clothing, self-expandable stents, advanced medical devices, biomedical scaffolds, and SMPs for controlling proof marks in the frozen food industry [3,256,257]. Horastani et al. explored the thermal, structural, and shape-memory properties of PLA/TPU blends, which were fabricated using melt mixing on a twin-screw extruder and subsequent injection molding [256]. Figure 25a illustrated the distribution of nanoclay into the polymer matrix. PEG was incorporated as a plasticizer at a fixed loading of 10 wt.% to assess its influence on the programming stimulation temperature and SMEs, identifying an optimal blend ratio of 60/40 PLA/TPU for these applications. Thermal analysis confirmed the successful mixing and demonstrated a reduction in the glass transition temperature (T_g) with the addition of 5 wt.% nanoclay and 10 wt.% PEG, thus achieving the primary objective of the study.

The in situ inclusion of various modified nanoclays during nanocomposite synthesis enhances polymer chain intercalation, leading to increased interaction and reduced crystallinity compared to composites with pristine nanoclays. Biswas et al. incorporated both unmodified and organically modified nanoclays into polyurethane matrix through an in situ polymerization technique [258]. At physiological temperature (37 °C), the nanocomposite containing dimethyl dehydrogenated tallow ammonium cation modified nanoclay (HPL-15A) demonstrated superior shape recovery, attributed to the complete melting of the soft segment and the restricted flipping of the hard segment due to extensive interactions. In contrast, shape-memory behavior was diminished in unmodified nanoclay (HPL-Na) composites due to a lack of interaction (Figure 25c). The in situ inclusion of 4 wt.% organically modified nanoclay led to a 10% enhancement in shape recovery, whereas a 4%

decrease was observed with 4 wt.% unmodified MMT nanoclay in a hexamethylene diisocyanate (HDI) polyurethane matrix. Nevertheless, both the pure polyurethane polymer and its nanocomposites maintained high shape fixity, with values exceeding 94%.

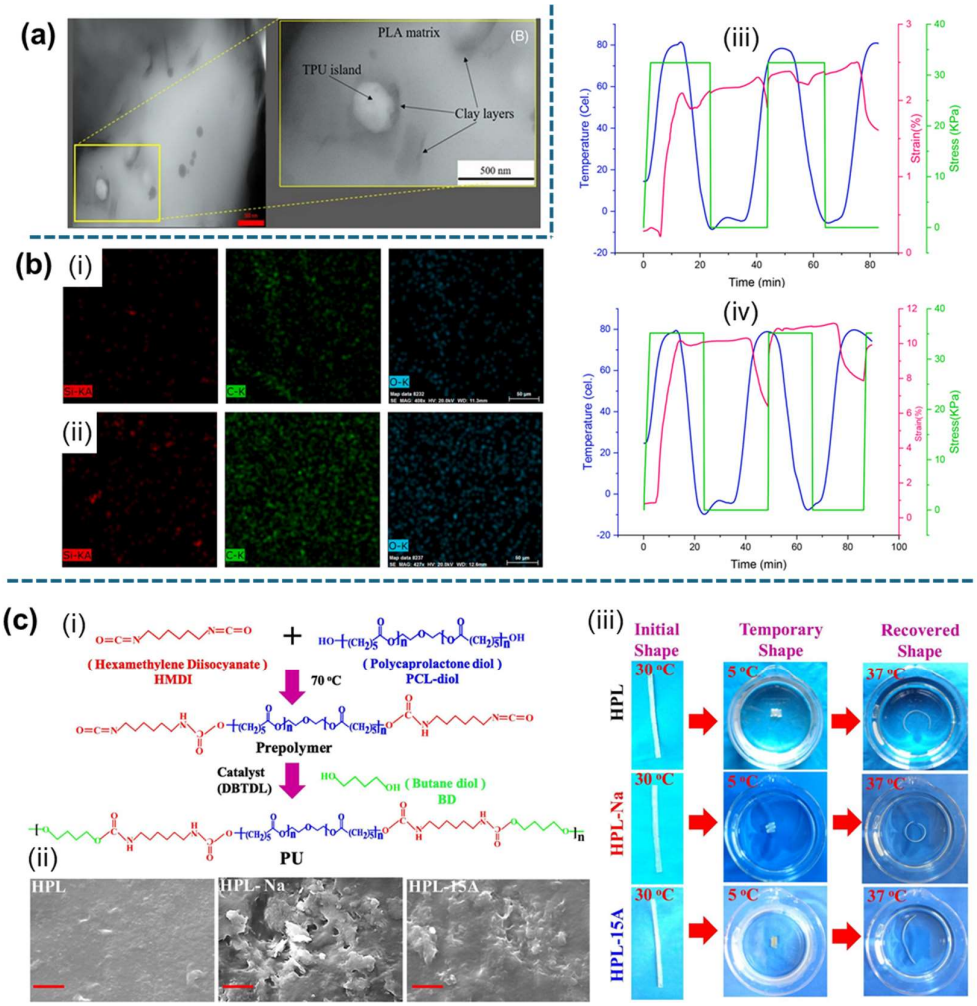

Figure 25. (**a**) TEM image of the clay-embedded polymer nanocomposite. Reproduced with permission from ref. [256]. Copyright 2022 John Wiley and Sons. (**b**) (i,ii) EDS images and (iii,iv) shape-memory cycle of PLA-TPU and PLA-TPU-5% NC, respectively. Reproduced with permission from ref. [253]. Copyright 2023 Elsevier. (**c**) (i) Two-step polymerization process, (ii) SEM images (scale bar ~10 μm), and (iii) illustration of comparative SMEs of pure HPL, HPL-Na, and HPL-15A. Reproduced with permission from ref. [258]. Copyright 2019 Elsevier.

Feng et al. fabricated dual-responsive SMP/clay nanocomposites (MDx-NCn) through in situ polymerization by incorporating exfoliated clay nanoplates into a 2-methoxyethyl acrylate (MEA) and N,N′-dimethylacrylamide (DMAA) mixture, where MDx-NCn is defined by the molar fraction of DMAA and the clay concentration [259]. The nanocomposites demonstrated enhanced mechanical properties due to a robust physical cross-linking network, formed by strong hydrogen bonding between polymer chains and clay platelets, enabling the material to lift loads up to 200 times its own weight under infrared light exposure. By varying the DMAA ratio via a two-step polymerization method, they successfully adjusted the T_g, facilitating the creation of advanced triple shape-memory materials. The introduction of clay into composites, particularly MD50-NC2, significantly enhanced their hydrophilicity, leading to excellent water-responsive shape-recovery behavior, with rapid recovery times.

A wide range of polymer/clay nanocomposites have been documented, and their current commercial and potential uses in packaging, coating and pigment, electrical materials, and especially in the biomedical field have been developed [259].

3.3. Other Non-Metal Nanocomposites

Various types of non-metallic nanofillers have been employed to enhance the properties of SMPNCs to meet specific application requirements. Dai et al. developed novel polyurethane-based NIR light-activated SMPCs by incorporating polydopamine nanoparticles (PDANPs) with polycaprolactone (PCL), hexamethylene diisocyanate (HDI), and 1,4-butanediol (BDO) [260]. The abundant benzene rings, catechol, and amine groups in PDANPs facilitate both covalent and noncovalent interactions with the polymer matrix, such as hydrogen bonding, coordination, and π-π stacking, thereby enhancing compatibility [261]. Due to its exceptional thermal stability and photothermal properties, PDA serves as an ideal photothermal agent for the construction of NIR light-triggered thermally-sensitive SMPCs, particularly suited for biomedical applications [262]. The PCL-PDA polyurethanes, containing 0.17 wt.% PDANPs, exhibited nearly 100% NIR light-triggered shape recovery within 20 s at laser intensities of 0.66 and 1.00 W/cm^2, while a lower intensity of 0.33 W/cm^2 required approximately 60 s for full recovery (Figure 26a). Further tests under an 808 nm laser at 0.33 W/cm^2, adhering to the American National Standard for safe skin exposure [263], confirmed the composite's precise and controllable shape recovery, achieving complete shape restoration within 60 s. In another study, Chen et al. synthesized SMPCs by incorporating PDA nanospheres as a photothermal filler into the PCL/TPU matrix via solution blending [264]. The light-responsive SME of the PCL/TPU/PDA nanocomposites was examined under visible light at a fixed intensity of 200 mW/cm^2, revealing that the shape-recovery rate accelerated with an increase in PDA nanosphere content. Specifically, the composite (PCL/TPU/PDA) with 3 wt.% PDA (P/T/D-3) achieved 100% recovery within 50 s, demonstrating the efficacy of PDA nanospheres as light-absorbing fillers for efficient light-to-heat conversion.

Polypyrrole (PPy), a conjugated organo-polymeric NP, has garnered significant interest for its technological applications, including roles in electrodes, electronic devices, sensors, actuators, biomaterials, and light-to-heat conversion materials, due to its unique properties and functionalities [265]. Chen et al. enhanced the ethylene-vinyl acetate copolymer (EVA)/PCL composite by incorporating PPy NPs as photothermal fillers, achieving exceptional photo-induced shape-memory performance with a 100% recovery ratio (R_r) [266]. In samples containing less than 0.5 wt.% PPy, rapid and complete shape recovery was observed under laser exposure, with the recovery time diminishing as the PPy content increased, culminating in full recovery within 7 s at a concentration of 1 wt.% PPy. Additionally, the nanocomposite demonstrated the capability for precise and selective self-healing of damaged areas, without adversely affecting the performance of intact regions. Once healed, the cut sample resisted re-fracture, even after repeated bending, and could support a weight of 3846 times its own, without significant deformation or damage. (Figure 26b) [266]. In another study, Wang et al. developed PPy NP-filled PLA/PCL nanocomposites, exhibiting exceptional triple shape-memory properties, with shape-recovery rates (R_r1, R_r2, and R_r3) of 92%, 87%, and 93%, respectively, in an 80:20 PLA/PCL blend [267]. The study revealed that under constant NIR irradiation, the surface temperature of composites increased, and the shape-recovery time decreased with higher PPy content, demonstrating the significant photo-induced SME of PPy NPs selectively distributed in the PCL component.

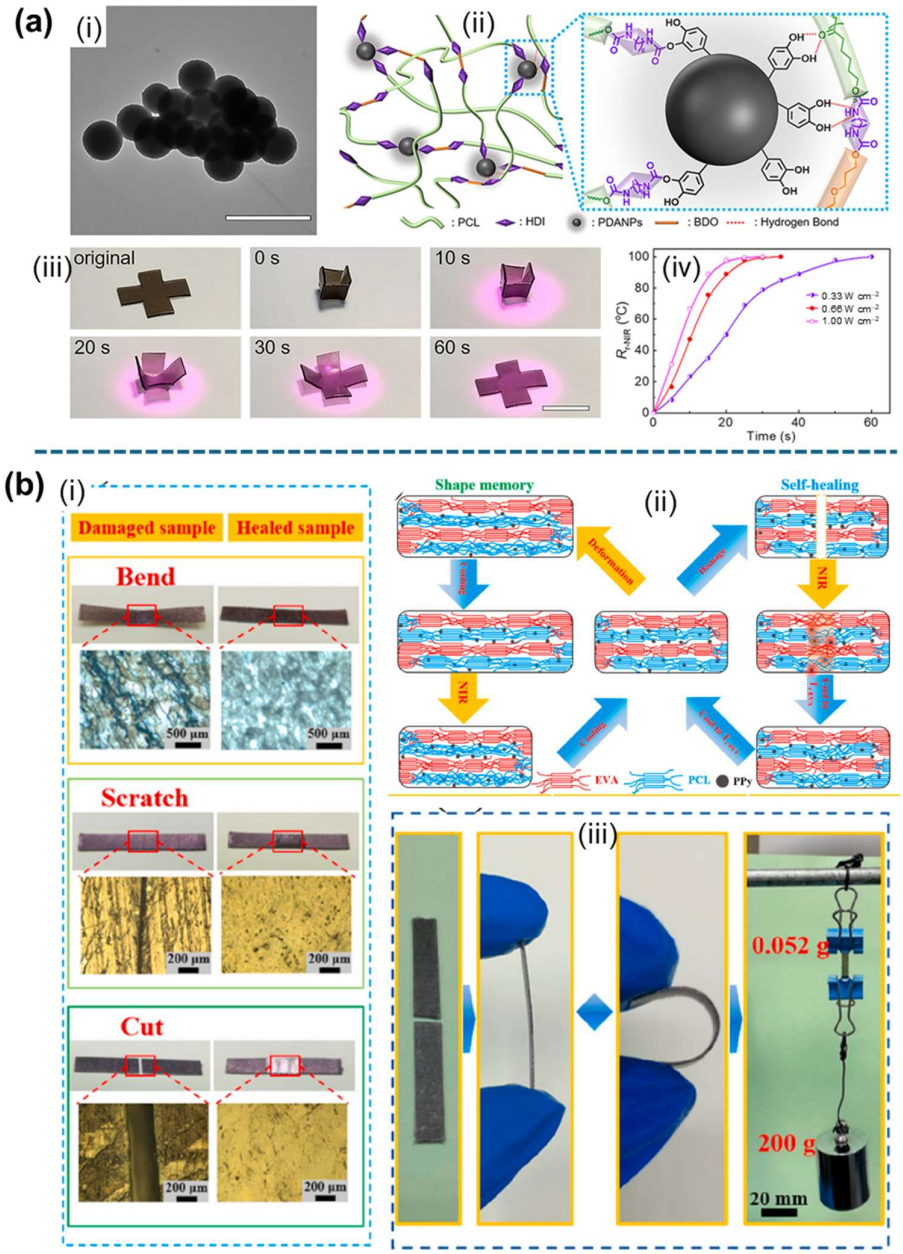

Figure 26. (**a**) (i) TEM image of PDANPS (scale bar: 1 μm), (ii) schematic of the chemical structure of PDANPs incorporated PCL-PDA polyurethane nanocomposite, (iii) NIR-responsive shape-recovery behavior of the nanocomposite, and (iv) recovery ratio variations for PCL–PDA with increasing irradiation time under 808 nm laser at intensities of 0.33, 0.66, and 1.00 W/cm^2. Reproduced with permission from ref. [260]. Copyright 2022 American Chemical Society. (**b**) (i) Digital photographs and optical microscope images illustrating the appearance of the damaged and healed samples, (ii) illustrations showing the photo-induced shape-memory and self-healing mechanisms in EVA/PCL/PPy blend composites, and (iii) mechanical performance of the healed nanocomposite. Reproduced with permission from ref. [266]. Copyright 2021 Elsevier.

Lashkari et al. synthesized SMPU nanocomposites by incorporating modified silica nanoparticles (SNPs) into polyurethane using an in situ two-step polymerization method. The introduction of SNPs created multifunctional cross-links and reinforced fillers, significantly enhancing the mechanical and shape-memory properties [268]. However, the high surface area to volume ratio of SNPs posed challenges in forming organic-inorganic nanocomposites due to poor dispersion within organic polymer matrices. To address this, chemical surface modification of SNPs was employed to improve interfacial interac-

tions between the organic matrix and inorganic SNPs [269]. Consequently, the modified SNP-SMPU nanocomposites exhibited enhanced shape-memory stability, maintaining a shape-recovery ratio (R_r) of over 80% even after three test cycles.

Table 1. Comparative analysis of key functional parameters of shape-memory polymer nanocomposites (SMPNCs).

Nanofillers	Polymer Matrix	Temperature (T_{rans}) °C	External Stimuli	Shape Recovery (R_r) %	Shape Fixity (R_f) %	Shape Recovery Time (t) s	Reference
Fe_3O_4	bio-based benzoxazine	–	magnetic field, light	99	93	26	[51]
	polylactic acid (PLA)/thermoplastic polyurethane (TPU)	80	magnetic field	96	~100	40	[67]
	polyurethane (PU)	42	magnetic field	>96	–	90	[68]
	cellulose/polycaprolactone (PCL)	75	thermal, NIR	96	98	–	[75]
	polyhydroxyurethane (PHU)	–	magnetic field, NIR	–	–	39	[76]
	polyurethane acrylate (PUA)	45	magnetic field	99.5	>97	130	[69]
AuNPs	PCL	56	NIR	–	–	53	[85]
	PCL	–	light	>95	>95	–	[89]
	poly(L-lactide-co-ε-caprolactone) (PLCL)	~55	NIR	84.3	93.1	–	[80]
	d,l-lactide (LA) and ε-caprolactone (CL)	57	NIR	~100	~100	–	[100]
AgNPs	PUA-PCL	–	electric/moisture	98	~100	10	[44]
	polybenzoxazine (PmBz) and PCL	57	laser	99.10	99.81	40	[57]
	potato starch (PS)	31	thermal	~100	~100	120	[118]
$W_{18}O_{49}$	polyethylene glycol diacrylate (cPEGDA)	~61	NIR	98.42	99.54	10	[72]
	PCL	~50	laser	96.3	97.1	–	[125]
TiO_2	poly (L-lactide) (PLLA)	57	heat	94.4	93.9	15	[126]
MgO	PLA	45	heat	>82	>99	–	[131]
CNTs	PU and poly(vinylidene difluoride) (PVDF)	40	electricity	95	–	15	[149]
	poly(propylene carbonate) (PPC) and PLA	–	electricity	97	–	30	[150]
	poly(ethylene glycol) diacrylate/poly(hydroxyethyl methacrylate)	–	electricity	>95	~100	204	[13]
	PCL	43	electricity	~99	~99	–	[55]
	epoxy polymer matrix	~40	heat and NIR	92.1	80.1	–	[153]
	cyanate ester/epoxy resin	–	heat	>99	99.5	92	[154]
	cardanol-based benzoxazines	70	microwave	100	>98	57	[156]
CNFs	PCL and Polystyrene-block-Polybutadiene-block-Polystyrene (SBS)	–	heat	100	100	47	[174]
	hydroxyl-terminated polybutadiene (HTPB) and polytetramethylene glycol (PTMG)	–	heat	>95.5	–	38	[175]
CB	PU	~40	electricity	100	–	26	[180]
	polyolefin elastomer (POE)/lauric acid (LA)	65	heat, electricity, solvent	95	–	20	[182]
CNs	chitosan	–	water	90	–	<3	[54]
	polyvinyl alcohol (PVA)/lignin (LIG)/citric acid (CA)	–	water	100	–	4	[209]
	PCL	40	heat	98.6	94.1	–	[215]
	TPU/carbomer	60.8	water, pH, heat	83.98	79.85	–	[139]
	polyacrylamide/gelatin	–	heat	96.6	76.6	–	[217]

Table 1. *Cont.*

Nanofillers	Polymer Matrix	Temperature (T_{rans}) °C	External Stimuli	Shape Recovery (R_r) %	Shape Fixity (R_f) %	Shape Recovery Time (t) s	Reference
GO	hyperbranched polyurethane/epoxy (HBPU/EP)	–	NIR	>95	–	6.5	[230]
	Cross-linked polyimide	>200	NIR	98	99	7	[236]
	Polystyrene (PS)/TPU	51.7	heat	100	100	22	[237]
	PU	~36	electricity	100	83.4	60	[238]
	polyvinyl alcohol (PVA)	–	heat, microwave	100	84	9	[240]
Nanoclay	PLA/TPU	170	heat	60.62	99.76	–	[253]
	PU	37	heat	76	94	–	[258]
PDA NPs	PCL/hexamethylene diisocyanate (HDI)/1,4-butanediol (BDO)	45	NIR	~100	100	20	[260]

Liu et al. developed a multifunctional, thermo-irritated SMP, poly(ethylene-co-vinyl acetate) (EVA), doped with non-close-packing SNPs. This composite exhibited reversible transparency changes during shape deformation due to light scattering in the internal cavities formed between the NPs and the polymer matrix [270]. Furthermore, the composite demonstrated excellent stability, enduring at least 20 stretch/reverse cycles without degradation.

Other types of non-metallic NPs, such as lignin nanotubes [271], hexagonal boron nitride (HBN) NPs [272], poly (9,9-dioctylfluorene-alt-benzothiadiazole) (F8BT) NPs [273], and hydroxyapatite (HA) NPs [274], have also been occasionally used to improve the mechanical and shape-memory properties of nanocomposites.

4. Applications

4.1. Biomedical Applications

SMPCs exhibit significant potential in biomedical applications due to their inherent nontoxicity, biocompatibility, and ease of processing. These properties facilitate the use of SMPNCs in a range of biomedical applications, including tissue engineering, drug delivery, stents, biological sutures, and minimally invasive surgery, where they transition from a compact temporary structure to their original expanded shape in response to external stimuli. Moreover, SMP-based scaffolds excel in self-healing and self-adaptation, allowing them to precisely conform to defect boundaries upon shape restoration, further underscoring their versatility and effectiveness in medical applications.

Congenital heart diseases (CHDs) are the most prevalent congenital anomalies that seriously threaten human health and life [26]. Interventional therapy, which utilizes occluders for percutaneous nonsurgical closure, has emerged as an effective treatment modality for CHDs [27]. However, the use of nondegradable materials such as nitinol (Ni-Ti) alloys and polyethylene terephthalate (PET) fabric in occluders has raised concerns regarding long-term foreign body reactions and associated complications [275]. Although nitinol-based occlusion devices are clinically effective in isolating the left atrial appendage (LAA), their limited biocompatibility, non-degradability, and mechanical property mismatch with adjacent tissues may lead to complications, including allergies, corrosion, tissue wear, and perforation [276,277]. Lin and coworkers designed a 4D-printed biocompatible and absorbable left atrial appendage occluder (LAAO) that can match the deformation of LAA tissue to minimize complications [278]. The LAAOs were fabricated through 4D printing from shape-memory PLA-based magnetic nanocomposites (PLA-MNCs), where incorporating MNPs facilitate self-heating and enable remote-controlled 4D transformation. A feasibility test for transcatheter closure of the LAA was performed using a 13 Fr catheter, which successfully and minimally invasively delivered the double-layer LAAO into a

freshly isolated swine heart. The LAAO exhibited excellent magnetic response, supporting its remote-controlled magnetism-induced 4D transformation and affirming its suitability for minimally invasive transcatheter closure in an isolated swine heart (Figure 27a) [278]. In another study, a 4D-printed biodegradable occlusion device for the treatment of atrial septal defects was developed by incorporating Fe_3O_4 particles into a shape-memory PLA matrix, enabling magnetically remote controllability post-implantation (Figure 27b) [279]. These biodegradable occluders emerge as a next-generation solution designed to overcome complications associated with non-degradable implants by offering a temporary mechanism that promotes in situ tissue regeneration and addresses issues related to permanent foreign bodies [280]. Upon endothelialization, the devices gradually decompose into benign substances that are metabolized, featuring self-expandable double-umbrella structures to facilitate healing within the heart defect [80].

In a related study, Xiang and coworkers incorporated polyethylene glycol-modified gold nanorods (AuNR/PEG) into poly(L-lactide-co-ε-caprolactone) (PLCL) to fabricate biodegradable occluders using PLCL-GNR/PEG nanocomposites [80]. The addition of 10% caprolactone (CL) structural units to PLCL enhances toughness and lowers the T_g to a level more suitable for tissue acceptance. The occluders, featuring a "double umbrella" structure, were designed for easy catheter loading and selective spatiotemporal expansion under NIR light to occlude defects (Figure 27c). The biocompatibility of these composites was confirmed by both in vitro and in vivo studies, with PEGylated AuNR improving hemocompatibility through increased hydrophilicity. Additionally, blood compatibility, cytocompatibility, and histocompatibility of the PLCL-AuNR/PEG composites were investigated and reported to be in acceptable levels [80].

Biodegradable SMPC-based stents represent a promising option for the treatment of cardiovascular and tracheal diseases. Drug-eluting nonvascular stents designed for local tumor treatment in tubular organs such as airways or the esophagus require both mechanical and therapeutic performance considerations. Paunović et al. developed a biodegradable digital light processing (DLP) 3D-printed SMPNC by incorporating AuNRs into a polyester copolymer, designed for stent fabrication [100]. This research included a clinically relevant demonstration where a human-sized meshed stent (H 12 mm, Ø 16 mm, thickness 1.6 mm) was implanted in a porcine intestinal segment, showing rapid expansion under 808 nm NIR light exposure within 40 s, highlighting its potential for on-demand deployment and NIR light-triggered expansion in biodegradable stent applications (Figure 27d). In parallel, Dai and colleagues utilized a shape-memory polycaprolactone-polydopamine (PCL-PDA) nanocomposite to create a biomedical tubular sample, which demonstrated efficient NIR light-triggered shape-memory behavior, reverting to its original configuration within 60 s during in vitro tests [260]. Further in vivo evaluations confirmed the non-cytotoxicity and excellent biocompatibility of the PCL-PDA polyurethane, as it did not inhibit cell proliferation or induce significant inflammatory responses.

Utilizing direct writing printing technology, Wei et al. developed stents from Fe_3O_4 NPs incorporated UV cross-linked shape-memory PLA ink [281]. The resulting stents demonstrated remote non-contact actuation, as exemplified by a spiral structure expanding from a 1 mm to a 2.7 mm inner diameter within 10 s when exposed to an alternating magnetic field (Figure 27e). In another study, Zhao et al. developed a bio-designed tracheal scaffold using 4D printing technology, utilizing a shape-memory PLA/Fe_3O_4 composite. These bioinspired scaffolds, activated by an alternating magnetic field, facilitate implantation in a temporarily deformed state and subsequent deployment into their predefined shapes, offering enhanced support and fixation within the trachea [282].

Polymer-based scaffolds for bone regeneration require materials that are non-toxic, biocompatible, and, in certain applications, biodegradable, characterized by high strength

and a porous structure to facilitate tissue integration [283,284]. The incorporation of active components to stimulate osteogenesis is essential, with polymers exhibiting a SME emerging as promising candidates for developing self-fitting scaffolds in tissue engineering. However, traditional bone tissue scaffolds encounter challenges, including brittleness, inadequate osteoinductive properties, and difficulties in implantation via minimally invasive procedures, underscoring the imperative for innovative approaches [25]. Zhao et al. engineered porous bone tissue scaffolds using shape-memory PLA/Fe_3O_4 composite, inspired by the microstructure of lotus roots and cellular co-continuous-like structures through 3D printing technology (Figure 27f) [285]. Exhibiting a porosity of 60%, these scaffolds demonstrated a strength of approximately 27 MPa, exceeding that of clinical artificial bone and thus offering significant support for bone defects. Designed for minimally invasive implantation in a compact form, these scaffolds are capable of expanding to their operational state under remote non-contact actuation, such as by a magnetic field, facilitating their application in bone regeneration. In another study. Zhang et al. developed a series of shape-memory PLA/Fe_3O_4 composite scaffolds utilizing 4D printing technology, enabling remotely controlled actuation for bone tissue engineering [286]. These scaffolds, composed of PLA/Fe_3O_4 composite filaments with 15% Fe_3O_4 NPs, were initially compressed to a smaller size while retaining the memory of their original, larger dimensions for injection into the implant site. Upon exposure to a magnetic field at 27.5 kHz, the compressed scaffolds expanded in situ to their predetermined shape and size, facilitating precise and minimally invasive implantation (Figure 27g). Bone fracture implantation was achieved using 4D-printed porous honeycomb structures, fabricated from a composite of PLA, polymethyl methacrylate (PMMA), and Fe_3O_4 NPs, as demonstrated by Doostmohammadi et al. [287].

Liu and coworkers created a bone morphogenetic protein-2 (BMP-2) loaded, porous smart nanocomposite scaffold, utilizing chemically cross-linked poly(ε-caprolactone) (c-PCL) and hydroxyapatite nanoparticles (HANPs), designed for the controlled release of growth factors [288]. This shape-memory scaffold is capable of returning from a compressed to its original shape within 10 min. The extended recovery time observed in vivo, a result of reduced heat transfer in air compared to water, provides a practical advantage for the implantation process of the scaffold. Hu and colleagues developed polyurethane/hydroxyapatite-based SMPNCs as a bone repair foam, characterized by its exceptional self-fitting capacity [289]. They demonstrated that the foam could perfectly match the defect site upon in vivo implantation, showcasing its potential for precise bone repair applications [289].

SMPCs offer a platform for developing controllable drug delivery systems, capable of targeting therapeutic drugs to specific sites and ensuring optimal therapeutic effects. Vakil et al. engineered magnetically responsive SMPCs by incorporating iron oxide magnetic nanoparticles (MNPs), enabling the activation of SMEs via an alternating magnetic field for controlled drug release [290]. These materials not only demonstrated favorable shape-memory properties and cytocompatibility but also allowed for the tunable release of drugs such as doxorubicin, 6-mercaptopurine, and rhodamine, with over 75% cytocompatibility. The ability to adjust polymer chemistry, MNP content, and shape-memory properties facilitated the customization of drug release profiles, illustrating the system's versatility in delivering dual drugs with enhanced precision.

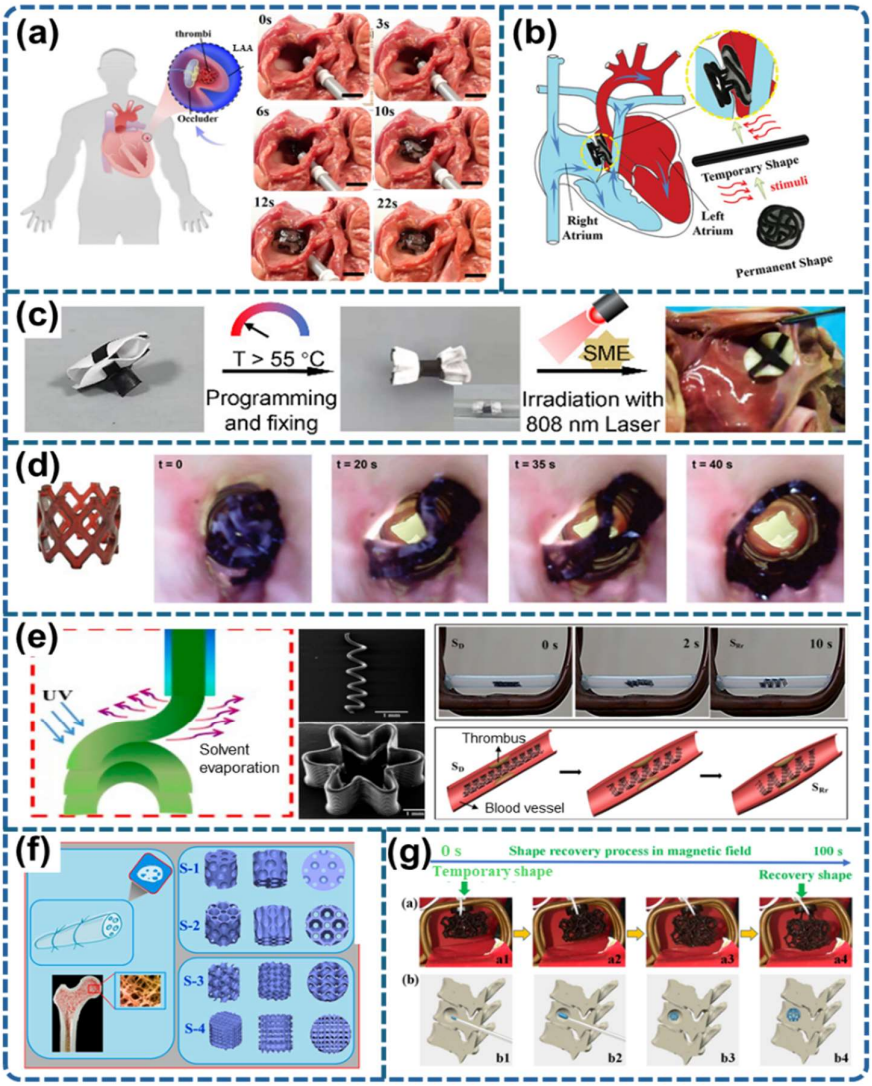

Figure 27. (**a**) Schematic illustration of LAA with thrombi and the magnetic-induced 4D transformation process of transcatheter LAA closure (scale bar = 10 mm). Reproduced with permission from ref. [278]. Copyright 2021 American Chemical Society. (**b**) Magnetically activated shape-recovery process of 4D printed occlusion devices. Reproduced with permission from ref. [279]. Copyright 2019 John Wiley and Sons. (**c**) Illustration of NIR controlled shape-memory "double umbrella" structure atrial septal defect (ASD) occlusion device in an isolated pig heart. Reproduced with permission from ref. [80]. Copyright 2023 American Chemical Society. (**d**) 3D-printed stent showing shape recovery ex vivo within a porcine intestinal segment using NIR light irradiation. Reproduced with permission from ref. [100]. Copyright 2022 John Wiley and Sons. (**e**) Schematic representation of the direct writing printing technique and the shape-recovery process of the 4D intravascular stent controlled by a magnetic field. Reproduced with permission from ref. [281]. Copyright 2016 American Chemical Society. (**f**) Design and fabrication of bone tissue scaffolds using 4D printing technology. Reproduced with permission from ref. [285]. Copyright 2020 Elsevier. (**g**) Magnetic field-stimulated the shape-recovery process of scaffolds for bone repair. Reproduced with permission from ref. [286]. Copyright 2019 Elsevier.

4.2. Flexible Electronics

Conductive and flexible materials have garnered attention for their conductivity, stretchability, and tensile strength. SMPNCs have emerged as promising candidates in the field of flexible materials in electronics, offering unique properties that can revolutionize various electronic applications [291]. These materials can adapt to curvilinear surfaces by changing shape or modifying physical properties like stiffness, enabling specific functions

in diverse applications [29,292]. The incorporation of nanofillers imparts multifunctionality of SMPs, boosting performance and responsiveness in electronic systems.

In the context of wearable electronics, semitransparent conductors play a vital role, enabling integration into various devices and applications such as artificial skins, photovoltaics, and touchscreens [292]. Notably, a visibly semitransparent SMP/Ag composite, combining cross-linked SMP polycyclooctene with electrospun Ag nanofibers, has been developed for such applications [293]. Furthermore, flexible semitransparent electrodes, incorporating silver nanowires (AgNWs) in a mercapto-ester-based ultraviolet-curable polymer, have been utilized in organic photovoltaic devices and wearable heaters [294,295]. Booth et al. designed a conductive, semitransparent SMP composite with UV-curable resin and AgNWs, showcasing its potential as a strain sensor and electronic skin capable of detecting touch, pressure, and bending (Figure 28a) [292]. Additionally, Luo et al. used AgNWs to create a temperature-sensing device, where AgNWs formed a conductive network within the SMP matrix, enabling dramatic resistance reduction upon thermal-induced shape recovery [296].

Zhang et al. developed a rubber-based electrically conductive strain sensor using epoxidized natural rubber (ENR), carboxymethyl chitosan (CMCS), dopamine (DA), and multi-walled carbon nanotubes (CNTs) [297]. The composite, affixed to the index finger joint with tape as shown in Figure 28b, demonstrated changes in the recorded current signal during finger movements, indicating the sensor's potential for monitoring body motions.

In another study, Li and colleagues utilized CNTs as conductive filaments in thermoplastic polyurethane fibers to create a wearable strain sensor, demonstrating reliable and repeatable performance with superior sensitivity across a wide tensile strain range (0.1% to 50%) [298]. This sensor architecture detected various deformation modes—including tension, bending, torsion—and human motions such as finger bending, breathing, and phonation. Utilizing multifunctional shape-memory RGO/ethylene-vinyl acetate composites, Qi and coworkers developed strain sensing by the swelling-ultrasonicating and one-step twisting method [46]. This composite demonstrated exceptional stretchability up to 130% strain, high sensitivity (gauge factor of 7.3), and a broad linear working range up to 70% strain [46].

Alipour et al. engineered a flexible strain sensor from a shape-memory hydrogel composite embedded with Fe_3O_4 nanoparticles, demonstrating the ability to control the illumination of an LED system through stretching, indicating higher sensitivity than its non-magnetic counterpart [299]. The composite exhibited reliable performance, maintaining its strain sensing capabilities over 500 cycles before and after its initial shape recovery.

In a separate study, Ren and colleagues developed a smart tactile sensor using 4D printing technology, capable of adjusting its measuring range, sensitivity, and shape to accurately sense unstructured objects [183]. This 4D-printed tactile sensor (4DPS) demonstrated superior performance over traditional devices by effectively adapting to both spherical dome and saddle surfaces (Figure 28c). The sensor's ability to program temporary shapes during the shape-memory process enabled it to adjust sensing performance for various complex body parts and joints, demonstrating enhanced versatility and applicability.

Yu and colleagues developed highly flexible electrodes using silver nanowires (AgNWs) on transparent polyacrylate substrates, capable of bending up to 16% while maintaining low surface resistance [300]. This composite was employed as a substitute for conventional indium-doped tin oxide (ITO) substrates in light-emitting diode devices, demonstrating enhanced flexibility and repeated bending capability. A similar technique was utilized to create light-emitting devices from a CNT/poly(tert-butyl acrylate) composite, which possessed a glass transition temperature (T_g) of approximately 56 °C [301].

The resulting device exhibited up to 45% linear strain stretchability while retaining its electroluminescent properties at 8 V, demonstrating its flexibility and functional durability.

SMP composites are also widely used to construct electric switches for various devices. Guo et al. developed a thermosensitive switch using a thermosetting shape-memory polyimide (PI)/reduced graphene oxide (rGO) nanocomposite (TCPI/rGO) for high-temperature warning devices [236]. As illustrated in Figure 28d, the nanocomposite film, initially set in a temporary shape with one end bent, was integrated into a circuit. Upon exposure to high temperature or NIR light, it reverted to its original two-dimensional shape, completing the circuit to light a bulb and signal an alarm. This demonstrates the potential application of these films in intelligent high-temperature early warning systems.

Using rGO/SMPU/polyurethane foam, Wang and coworkers engineered a temperature sensor that demonstrated a swift response to temperature changes, as indicated by the rapid dimming of a bright yellow light (within 1 s) emitted by a bulb [302]. This dimming occurred as the sensor expanded due to heating, resulting in an increase in electrical resistance, reflecting its practical and efficient temperature detection capabilities.

Liu and coworkers also designed a high-temperature warning circuit based on the transparency and shape-changing properties of a nanocomposite [270]. In their demonstration, a stretched, opaque SiO_2/EVA composite film was connected to a switch via a thin wire in a circuit with a lightbulb and battery. Upon exposure to hot air at 85 °C, the composite film gradually shrunk and increased in transparency. This shape recovery triggered the circuit, serving as a visual high-temperature alert.

In a separate investigation, Wang and colleagues developed an electric switch from a flame-retardant, shape-memory supramolecular PTAZ/GO nanocomposite, integrating cross-linking zinc ions, carboxyl graphene, and poly-(thioctic acid) via self-polymerization [303]. The nanocomposite exhibited a bending shape at −10 °C, leading to LED deactivation due to a break in the conductive path. With a temperature increase to room conditions, the polymer chains swiftly extended, re-establishing contact with the conductive copper sheet and consequently re-illuminating the LED.

Wang et al. engineered a stretchable shape-memory self-soldering conductive tape featuring reversible adhesion controlled by temperature, achieved through a polymer matrix embedded with a conductive network of AgNPs (Figure 28e) [304]. Above its melting temperature (T_m), the tape softened and formed strong adhesion with a rough copper substrate upon cooling, while this adhesion significantly decreased upon reheating, facilitating the closing and opening of circuits at high temperatures via the SME and reversible adhesion.

Polarized luminescence systems are being used in areas such as information storage, catalytic reactions, 3D displays, and anti-counterfeiting devices [305]. Xu et al. developed a luminescent cellulose nanocrystal shape-memory polymer (CNC-SMP) system featuring mechanically responsive circularly polarized luminescence (CPL) emission for optical anti-counterfeiting [306]. Utilizing hot-embossing to imprint various shapes on the CNC-SMP surfaces, the patterned samples demonstrated distinct color contrasts corresponding to changes in the helical pitch, observable under left-circularly polarized light (L-CPL). The embossed areas of the SMP samples exhibited specific CPL contrasts, rendering them effective for anti-counterfeiting applications (Figure 28f).

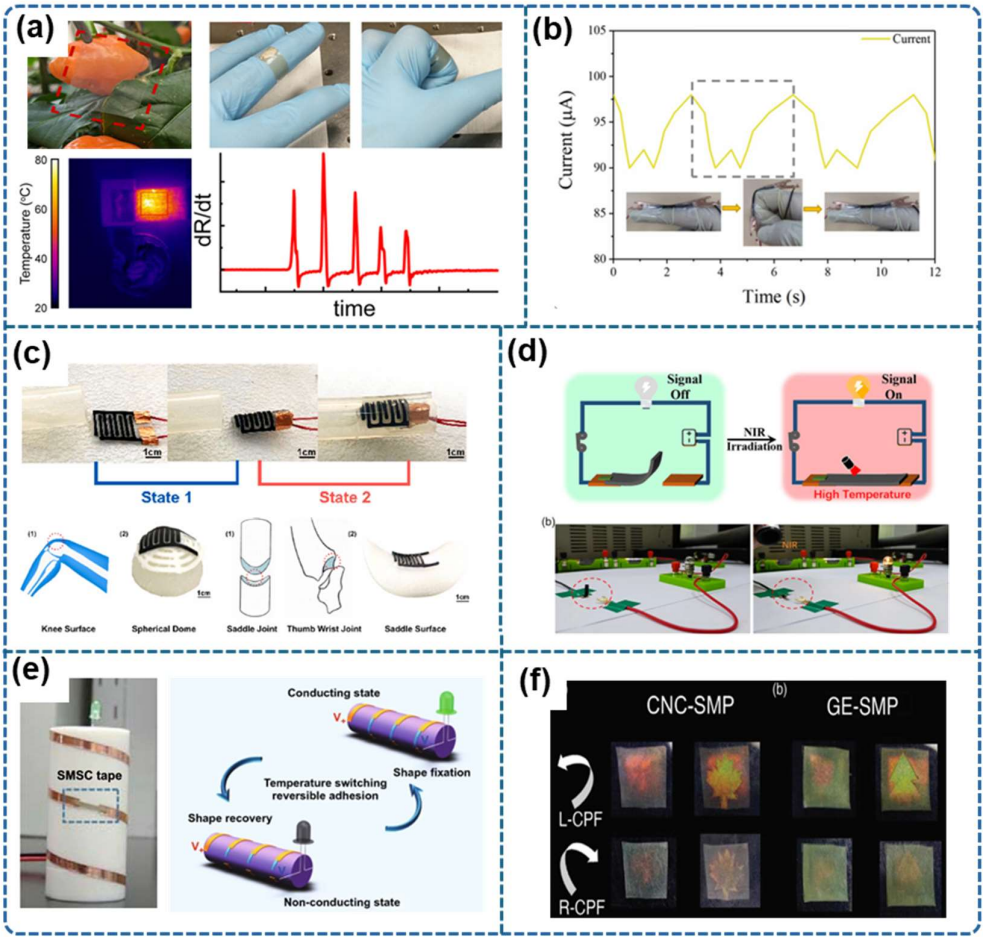

Figure 28. (**a**) Illustration of wearable touch, tape, and flex sensor using SMP:AgNWs composite. Reproduced with permission from ref. [292]. Copyright 2022 American Chemical Society. (**b**) The current signals and photos (inset) of the composite sensor while detecting finger bending. Reproduced with permission from ref. [297]. Copyright 2022 Elsevier. (**c**) 4D-printed tactile sensor (4DPS) tested through the application on both spherical dome and saddle surfaces. Reproduced with permission from ref. [183]. Copyright 2023 Elsevier. (**d**) Schematic and experimental demonstration of the application of the nanocomposite in high-temperature warning devices. Reproduced with permission from ref. [236]. Copyright 2022 John Wiley and Sons. (**e**) Optical image of the conductive SMPC tape circuit used to light an LED. Reproduced with permission from ref. [304]. Copyright 2021 Springer Nature. (**f**) Photographic illustration of unpressed and patterned CNC-SMP and GE-SMP for optical anti-counterfeiting. Reproduced with permission from ref. [306]. Copyright 2023 John Wiley and Sons.

4.3. Soft Robotics

Since their inception, robots have become indispensable in various sectors, including manufacturing, space exploration, biotechnology, and agriculture, due to their advanced technologies. However, traditional rigid robots, typically constructed from steel, face challenges such as the need for advanced protection, heavy weight, and limited maneuverability and adaptability. These limitations have spurred the exploration of novel materials, leading to the rise of soft robotics, which aims to mimic human behavior and overcome the constraints of conventional robots [29]. Soft robots are crafted from materials like rubber, polymers, and silicon, offering advantages such as lightweight, cost-effectiveness, high flexibility, and mechanical compliance. These attributes enable soft robots to excel in applications where rigid robots fall short, such as drug delivery, search and rescue, and human assistance.

The shape-memory gripper, a straightforward soft robot, performs gripping and lifting actions through programmed bending and recovery behavior facilitated by SMPCs. Wang et al. engineered a light-activated, 3D-printed morphing structure using AuNPs embedded in acrylate-based SMPs, demonstrating exceptional gripping capabilities [89]. Upon brief light exposure, the gripper initiated a return to its original shape, effectively securing a screw in an upward motion, highlighting its potential as a remotely activated actuator for soft robotics that responded to visible light (Figure 29a).

Gu et al. enhanced the NIR light and magnetic response of SMP nanocomposites by incorporating Fe_3O_4 NPs into a "hydrogen bonding–metal-phenolic" sacrificial network, aiming at applications in hazardous chemical operations [307]. The engineered nanocomposites demonstrated exceptional SMEs, facilitating shape programming, folding, and gripping actions crucial for soft robotics in chemical engineering. Under external stimuli, these soft robots performed precise and controlled movements, enabling the sequential addition of different chemicals within a reaction setup, as illustrated in Figure 29b. The durable shape-memory performance across multiple cycles underscores the potential of soft robots to mitigate operator risks in dangerous chemical experiments through remote control. Utilizing 3D printing technology and inspired by plant climbing mechanisms, they also designed a thermos-responsive soft gripper by incorporating CNFs into a polycaprolactone (PCL)/poly(butylene adipate-co-terephthalate) matrix [213]. The composite exhibited pre-programmed spiral structures to emulate vine transformation behaviors from straight to spiral forms during climbing. These self-deforming structures, designed with top filling angles of 45° and 0°, mimic the natural mechanism of plants for wrapping around objects. Upon thermal stimulation, the printed samples deform to encircle and securely grasp objects, demonstrating stability by withstanding forces up to 30 times their weight and achieving rapid deformation and wrapping within 3 s at 60 °C (Figure 29c). This showcases the potential of these 4D-printed, self-deforming bionic structures for application in soft robotic grippers.

Liu and colleagues developed a reconfigurable, remotely actuated soft robot based on SMPCs, utilizing simultaneous magnetic actuation and photothermal heating to achieve magnetic and photo-controlled manipulation [308]. In another study, Chen et al. developed bionic soft robots using a biocompatible PCL/TPU/Fe_3O_4@PDA nanocomposite film, employing light and magnetic fields for versatile actuation [11]. By modifying the shape of the films, various robots were created, including a flower-like robot with reconfigurable petals and a palmate robot functioning as a smart gripper. The flower-like robot achieved reversible shape transformations between lifted and flat positions, controlled by light and magnetic fields. Similarly, the palmate robot, mimicking an artificial hand, could soften under light, grasp a foam cube with magnetic fields, and release it upon reheating, demonstrating effective "grab" and "release" actions.

Wei and coworkers engineered an electroactive gripper based on highly conductive nanocomposite by incorporating hybrid Ag-coated CNFs (Ag@CNFs) as conductive fillers [309]. The 3D printable PLA/CNT/Ag ink with high electricity (>2.1 $\times$ 10^5 S/m) enabled the gripper to produce rapid responses at different voltages, evidenced by gripping a 5 g bolt within 20 s. Kim et al. designed an untethered millirobot based on MNPs containing shape-memory hydrogel that can simultaneously perform gripping motion and locomotion through an integrated electric and magnetic field system [310].

Nasseri et al. synthesized pH-responsive shape-memory hydrogel nanocomposites incorporating zwitterionic monomers and cellulose nanocrystals (CNC), demonstrating their utility for small-scale robotic applications [31]. They constructed a robot capable of remotely navigating and steering through confined spaces to transport light cargo, utilizing a magnetic field for movement as depicted in Figure 29d. This cargo robot was magnetically

guided through a maze, where an elevated pH caused it to twist and secure the cargo. Upon navigation completion, a subsequent pH increase allowed the robot to release the cargo by reverting to its original shape, showcasing the potential for precise control in targeted delivery applications.

Xu and colleagues demonstrated a soft robot capable of complex motion states by incorporating CNTs into a poly(ethylene-co-octene) matrix, fabricating a leopard-type robot that operated under low voltage ($\leq$36 V) or IR light irradiation [311]. The resulting robot exhibited movements involving the opening and closing of its legs, enabling it to advance 1 cm in 109 s, mimicking the pedaling motion of a leopard (Figure 29e). In a separate study, Sun et al. developed a walking robot based on a CNT/ethylene-co-vinyl acetate (EVA) composite, requiring just 15 V driving voltage [312]. As Figure 29f demonstrates, the robot mimics animal-like continuous walking by alternating the activation of its legs, covering a distance of 3.7 cm in 48 s. Utilizing double-layer CNT–SMP composites capable of bidirectional actuation, Peng and coworkers designed an inchworm robot consisting of two metal plates as moving legs [313]. The track was fashioned as a metal sawtooth with a right-triangle structure, and the front leg end was curved back to securely latch onto the metal sawtooth.

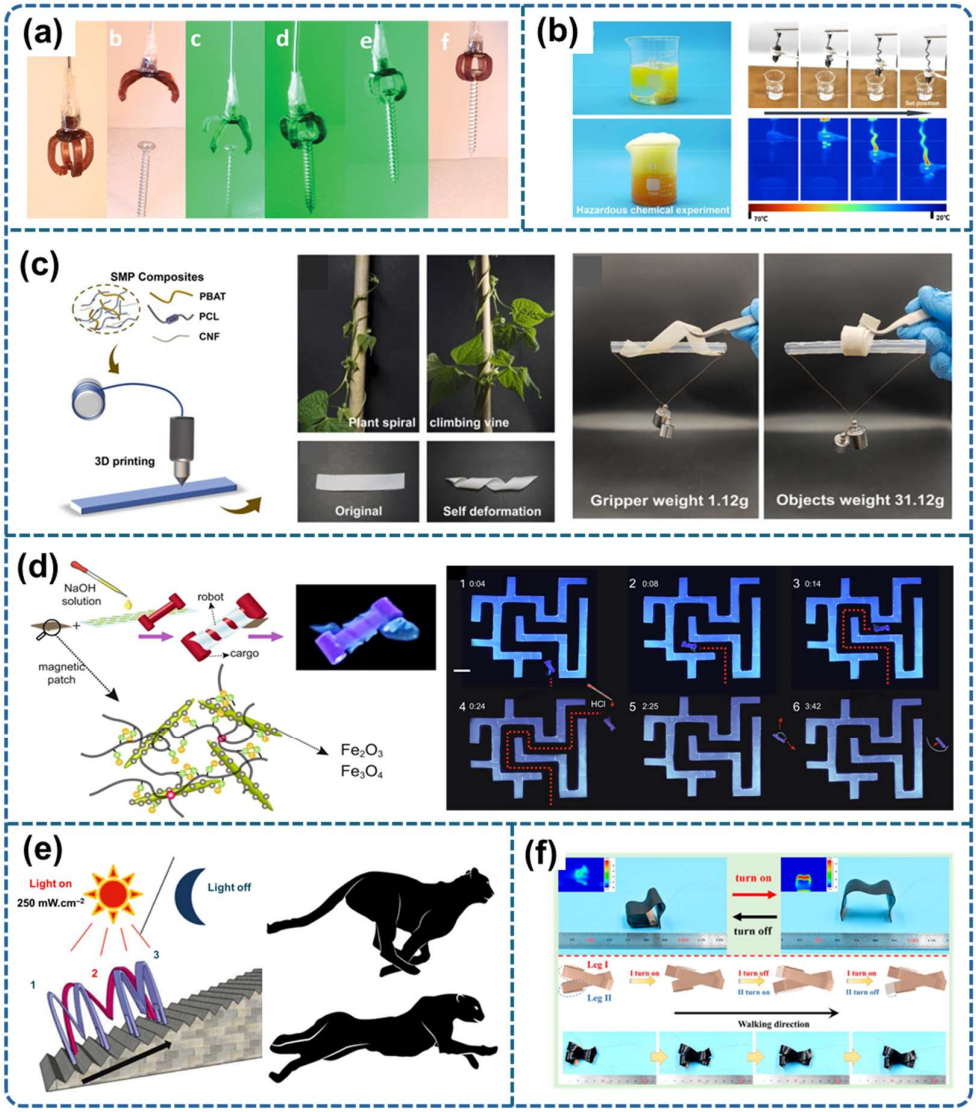

Figure 29. (**a**) Illustration of a DLP-printed gripper activated by light, serving as a soft robotic hand to grab objects. Reproduced with permission from ref. [89]. Copyright 2021 John Wiley and Sons.

(**b**) Illustration of a 4D-printed soft robot folded by magnetic stimulation during hazardous chemical handling. Reproduced with permission from ref. [307]. Copyright 2023 Elsevier. (**c**) Schematic of a 3D-printing technique and photographs of thermos-responsive soft grippers. Reproduced with permission from ref. [213]. Copyright 2023 Elsevier. (**d**) Demonstration of a magnetically controlled micro-robot navigating and transporting an I-shaped cargo by rotating around it in response to pH changes. Reproduced with permission from ref. [31]. Copyright 2023 Springer Nature. (**e**) Schematic illustration of a crawling robot, inspired by leopard locomotion, walking on stairs according to steps 1–3 with IR light sequentially switched on and off. Reproduced with permission from ref. [311]. Copyright 2019 American Chemical Society. (**f**) Photographs of a low voltage-driven walking robot. Reproduced with permission from ref. [312]. Copyright 2021 American Chemical Society.

4.4. Other Applications

Bacterial infections are prevalent health issues worldwide, necessitating materials with antibacterial properties to mitigate infection risks. The production of non-biodegradable materials has contributed to environmental pollution, underscoring the need for innovative, biodegradable, and biocompatible antimicrobial materials for applications such as food packaging and biomedical devices [314]. Pekdemir et al. utilized a surface Fe_3O_4 embedded PLA-PEG blend via a solution casting method to develop a nanocomposite [315]. This nanocomposite inhibited the growth of *Candida albicans*, a eukaryotic opportunistic pathogen harmful to human health, with antimicrobial activity increasing at higher MNP ratios. In a subsequent study, a direct green synthesis technique was employed to create an SMPNC incorporating AgNPs, which displayed significant antibacterial activity against both Gram-positive and Gram-negative bacteria [120]. Hu and coworkers designed organic-inorganic hybrid PCL-TiO_2/PLLA nanocomposites with antibacterial properties [126]. While PLLA exhibited no antibacterial activity, as indicated by the absence of inhibition zones, the PCL-TiO_2/PLLA nanocomposites demonstrated significant antibacterial effects against *Bacillus subtilis*, *Bacillus licheniformis*, and molds, attributing the antibacterial role to uniformly distributed PCL-TiO_2 in the PLLA matrix (Figure 30a).

Smart textiles have swiftly evolved due to consumer demands for high performance, functionality, and adaptability to both wearer physiology and environmental conditions. Memiş et al. engineered smart polyester fabric for sportswear with temperature and water/moisture responsive shape-memory performance [316]. The nanocomposite structure, comprising an SMPU matrix and hydrophilic nanowhiskers (CNWs), was applied to polyester fabric as a finishing treatment. The thermoregulation performance of the resultant composites was evaluated under varying temperatures and relative humidity conditions, demonstrating the textiles' ability to actively regulate temperature by adapting to dynamic environmental conditions of water vapor pressure and air permeability. Qi et al. developed smart gloves using a "swelling-ultrasonicating" and one-step twisting procedure with shape-memory RGO/EVA composite [46]. The RGO/EVA composite yarns were integrated into commercially available fabrics, such as silk fabrics and cotton gloves, using a simple sewing method (Figure 30b). This approach, particularly advantageous for practical applications, offers enhanced convenience over traditional flexible fiber sensors that rely on adhesive tapes, underscoring the potential of RGO/EVA composite yarns in smart textiles, wearable devices, and artificial muscles. In a study by Horastani and colleagues, nanoclay reinforced polylactic acid/thermoplastic polyurethane was used to produce highly twisted yarn, introducing a key innovation for smart breathing textiles [59].

Recent research efforts have been directed towards developing rewritable paper to mitigate the environmental impact of the traditional pulp and paper industry, focusing on sustainable alternatives. Xie and colleagues introduced an ink-free rewritable paper utilizing a core-shell NP-based photonic crystal, specifically ferroferric oxide-carbon (Fe_3O_4@C), combined with a bistable electroactive polymer (BSEP) [317]. This innovation allows for

electric field-induced switching of reflection colors, enabling the storage of vivid color images without ink and ensuring image stability for over a year under ambient conditions. Remarkably, the images on this rewritable paper can be overwritten up to 500 times without degradation, as demonstrated on a seven-segment numerical display (Figure 30c). Wu and colleagues utilized stepwise emulsion polymerization to integrate monodisperse NPs into a poly(ethylene terephthalate) (PET) film [318]. These core-interlayer-shell NPs were efficiently dispersed within the PET matrix to form photonic crystals, where the reflection color of the photonic crystals/PET composite was dynamically adjustable during shape programming and recovery processes due to changes in lattice spacing with strain.

Smart superhydrophobic SMP surfaces characterized by adjustable wettability have attracted considerable attention due to their wide range of applications. Li et al. developed a superhydrophobic SMP microconed surface on an AgNW film, which exhibited reversible transitions between pinned and roll-down states via in situ heating induced by voltage, highlighting the potential for adjustable wettability (Figure 30d) [121]. In another study, Zheng et al. prepared a light-induced shape recovery of deformed SMP micropillar hexagonal arrays with gold nanorods (AuNRs) [101]. The versatile microconed or micropillared SMP surface finds applications in droplet manipulation, reprogrammable fog harvesting, and more, owing to its robust and reversible morphology transitions.

In a recent study, SMP composites were used as information carriers without additional electronic elements. Wang et al. engineered electric- and light-driven information carriers utilizing a carbon nanotubes/ethylene-co-vinyl acetate (CNTs/EVA) SMPC, incorporating Morse code encoding and encryption for information transmission [319]. The study successfully established two modes of information transmission, leveraging the electricity and NIR light-responsive behaviors of the SMP-based composites for dynamic and versatile communication applications. In another study, Li et al. developed an epoxy-based SMPC embedding various Morse codes within a single specimen through imprint lithography, incorporating four functional components—Fe_3O_4, CNTs, p-aminodiphenylimide, and neat epoxy polymer—into distinct regions of the epoxy substrate (Figure 30e) [320]. The multicomposite specimen, designed with language code patterns, executed a programmable recovery process, showcasing the capability of the material to follow a predefined recovery route of temporary patterns via a multistage curing and stimulus command procedure. Each Morse code, linked to a specific embossed area, triggered the activation of corresponding sections when subjected to UV light, electromagnetic, or radiofrequency fields, thus illustrating the precise control over the language code recovery process within the shape-memory cycle.

Gopinath et al. synthesized thermo-responsive anti-corrosive SMPNCs by integrating CNFs into a cross-linked polyurethane matrix composed of hydroxyl-terminated polybutadiene (HTPB) and polytetramethylene glycol (PTMG) [175]. These nanocomposites demonstrated superior shape-memory properties and anti-corrosion capabilities in seawater environments, attributed to the hydrogen bonding between adjacent polymer chains [321]. Addressing the significant impact of corrosion on metallic industrial applications, the researchers employed HTPB and PTMG to produce co-polymer-based nanocomposites. In these nanocomposites, hard-phase components chemically cross-linked to form a stable system, while soft-phase components created an elastomeric network enabling reversible shape transitions [322]. The optimal ratio of hard to soft segments, along with the inclusion of CNFs, is critical for achieving high-quality SMPU composites with improved dispersion [323].

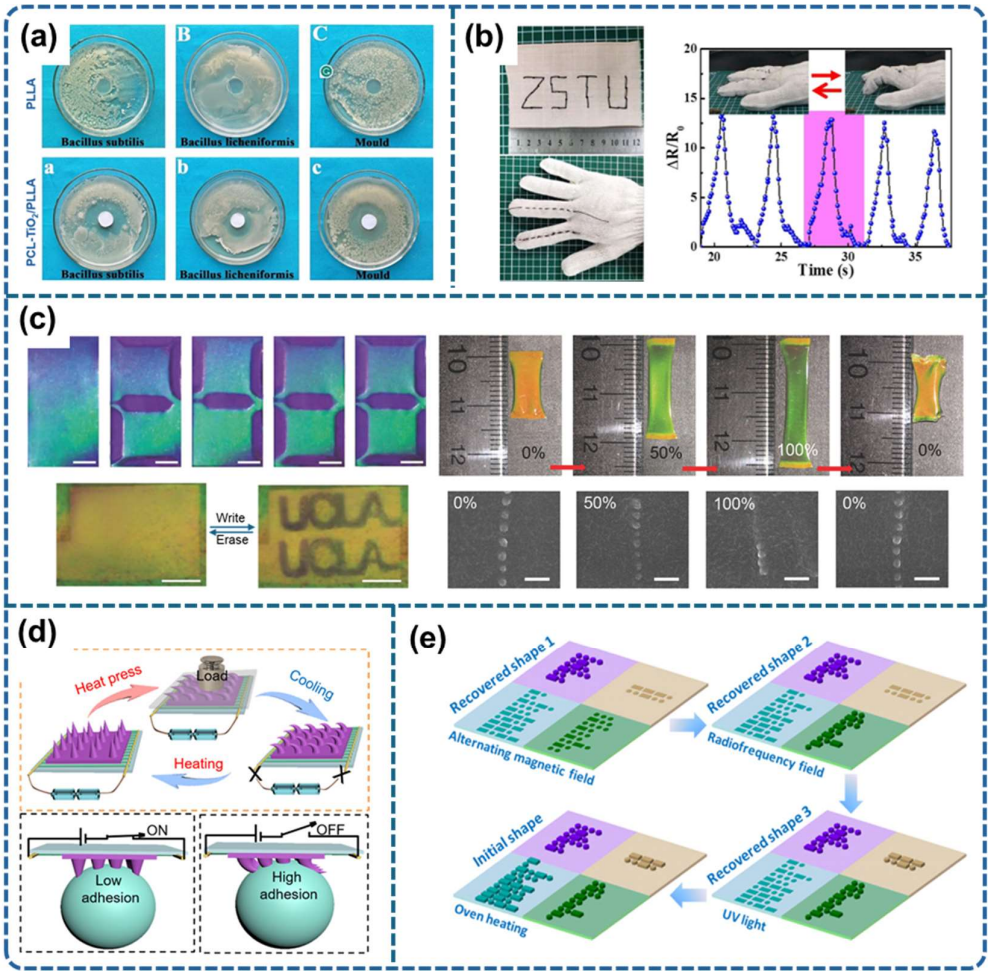

Figure 30. (**a**) The antimicrobial properties of PLLA and PCL-TiO_2/PLLA were tested against *B. subtilis*, *B. licheniformis*, and mold. Reproduced with permission from ref. [126]. Copyright 2023 Elsevier. (**b**) Photos of the 5f-t667 yarn sensor sewn onto silk fabric and a cotton glove, alongside relative resistance changes in the sensor when attached to a bending finger. Reproduced with permission from ref. [46]. Copyright 2023 Elsevier. (**c**) Illustration of rewritable photonic papers, along with optical and SEM images of a red photonic nanocomposite under 0%, 50%, and 100% tensile strain. Reproduced with permission from ref. [317]. Copyright 2018 John Wiley and Sons. (**d**) Fabrication of microcone arrays involved assembly procedures and showing the lossless transfer of droplets in both the "captured" and "detached" conditions. Reproduced with permission from ref. [121]. Copyright 2020 American Chemical Society. (**e**) Illustration of the shape-recovery procedure using several Morse codes based on different activation techniques. Reproduced with permission from ref. [320]. Copyright 2017 American Chemical Society.

5. Discussion

The advancement of SMPNCs represents a significant step forward in the development of smart materials with enhanced mechanical, thermal, and actuation properties. This review has extensively examined the fundamental aspects of SMPNCs, including their structural composition, mechanisms of shape recovery, and diverse applications across various fields such as biomedical technology, robotics, electronics, and automotive systems. While SMPNCs have demonstrated superior performance compared to conventional SMPs, certain challenges and limitations still persist, necessitating further exploration.

One of the key challenges in the field of SMPNCs is achieving uniform dispersion of nanofillers within the polymer matrix. The effectiveness of nanofillers in enhancing the properties of SMPs depends on their homogeneous distribution and strong interfacial

adhesion with the polymer chains. However, agglomeration of nanoparticles, particularly at high concentrations, can lead to non-uniform mechanical and thermal properties, negatively impacting the shape-memory performance. To address this, advanced fabrication techniques, such as surface functionalization of nanofillers, in situ polymerization, and the use of compatibilizers, have been investigated to improve the dispersion and interaction of nanofillers within SMP matrices.

Another significant consideration is the mode of actuation. While thermally triggered SMPNCs are the most widely studied, they often require direct heat sources, which can be challenging for remote or spatial control applications. Recent developments have focused on alternative actuation methods, including electrical, magnetic, and light-based stimuli. Magnetic and photothermal activation have shown promise in enabling remote actuation, but challenges such as the efficiency of energy conversion and potential overheating need to be addressed. Moreover, achieving multi-stimuli responsiveness in SMPNCs remains an area of active research, as integrating multiple activation mechanisms could lead to more versatile and application-specific material responses.

In biomedical applications, the biocompatibility and biodegradability of SMPNCs are critical factors that must be considered. Although certain nanofillers, such as gold and iron oxide nanoparticles, have demonstrated compatibility for medical applications, concerns remain regarding long-term stability, cytotoxicity, and potential accumulation in biological systems. Extensive in vivo studies and regulatory evaluations are required to ensure the safe implementation of SMPNC-based medical devices.

Additionally, the long-term durability and fatigue resistance of SMPNCs under cyclic loading conditions are crucial aspects that need further investigation. Many applications, such as deployable structures and wearable electronics, require repeated shape transformations, and maintaining performance over multiple cycles is essential for commercial viability. Studies on degradation mechanisms, structural integrity under stress, and the development of self-healing SMPNCs are ongoing to improve material longevity.

Overall, while SMPNCs have opened new avenues in smart material applications, continued research is necessary to optimize their fabrication, actuation efficiency, biocompatibility, and long-term performance. Addressing these challenges will be key to unlocking their full potential for next-generation adaptive and responsive materials.

6. Prospects and Emerging Trends

In recent times, there has been a significant surge in the scientific community's interest in SMPs and related composites (SMPCs), as evidenced by the upward trend in the number of scientific publications over the past few decades, as illustrated in Figure 31. The extensive research on SMPs and SMPCs, focusing on new mechanisms, fabrication methods, fillers, and responsiveness to stimuli, highlights their potential for a plethora of future applications. The successful implementation of SMPCs in future prospects depends on their ability to adopt new mechanisms and environments effectively, overcoming challenges such as lack of thermal stability, reduced mechanical strength, brittleness, material degradation due to aging, and associated production costs [324,325]. This review outlines some areas where a surge in research is anticipated.

4D printing is a relatively new prototyping technology that can replace traditional mechanical components in modern engineering equipment and biomedical devices, which can change their certain shapes [325]. Although 4D SMPCs have attracted significant interest, there is still a need to acquire substantial knowledge on better reprogramming, limitations in the printing process, and the ability to perform multi-material printing. While one-way 4D SMPCs have shown excellent properties, research focused on multi-way SMPs is also required. Furthermore, developing 4D-printed SMP-based sustainable

composites for biomedical devices is crucial to realizing the true importance of this novel technology [326].

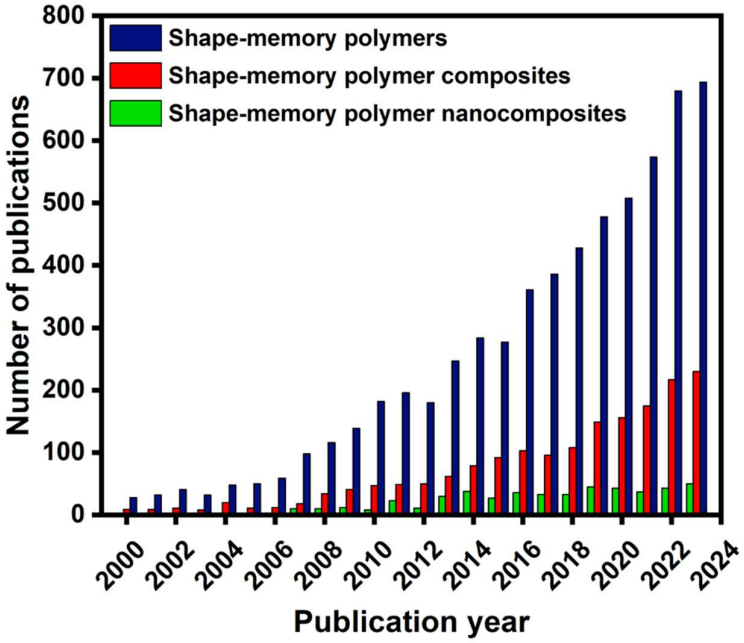

Figure 31. Illustration of the yearly quantity of scientific publications since 2000, obtained by employing the search phrases "shape-memory polymer", "shape-memory polymer composites", and "shape-memory polymer nanocomposites". The data analysis was conducted with the Scopus search system on 29 January 2024.

The addition of nanofillers significantly improves the properties of SMPCs. The composition, concentration, shape, and distribution patterns of the fillers determine their interactions with the polymer matrices. However, adding higher fractions of additives may interfere with the performance of SMPCs. Therefore, novel SMPCs need to be designed with a delicate balance between properties and additives, focusing on intended applications [325]. While SMPC-based electronics, storage devices, and energy harvesting devices are popular, there is room for improvement for their commercial applications. Fabricating materials with broad transition temperature changes, deploying two-way or multiple-way SMEs, and developing new fabrication methods utilizing advanced structures combined with different actuation mechanisms will pave the way for their commercial availability [30]. Future research is expected to focus more on remote actuation techniques rather than traditional techniques to achieve safer and better control over the recovery process. This can be achieved by designing composites with embedded fillers responsive to light and ultrasound, further enhanced by burrowing mechanisms from nature [30].

In extreme applications such as aerospace engineering, the mechanical strength of SMPCs can be compromised during thermal processes since they could be exposed to temperatures exceeding the glass transition temperatures (T_g). Therefore, enhancing mechanical properties that can withstand higher temperature changes is crucial [327].

To further optimize and tailor the properties of SMPNCs, the incorporation of machine learning (ML) and computational simulations offers transformative potential to predict, optimize, and design material properties with unprecedented accuracy and efficiency [328]. By utilizing large datasets of material behavior, ML algorithms can identify complex correlations between nanocomposite compositions, external stimuli, and shape-memory effects. This data-driven approach can significantly reduce the time and cost associated with experimental processes, enabling the rapid prototyping of customized SMPNCs [329].

Additionally, ML can model dynamic responses under multi-stimuli conditions, enhancing the design of applications in biomedical devices, aerospace components, and flexible electronics. The application of ML in this domain represents a critical step toward establishing fully predictive frameworks for advanced material design.

7. Conclusions

The development of SMPNCs has emerged as a groundbreaking class of smart materials, overcoming the limitations of traditional SMPs. By integrating functional nanofillers into SMP matrices offering enhanced thermal and electrical properties while maintaining mechanical integrity. This review underscores the diverse advancements achieved through the integration of metallic nanoparticles, carbon-based materials, and cellulose nanostructures, enabling SMPNCs to respond to diverse stimuli such as magnetic fields, light, electricity, water/solvents, and pH. These multi-responsive capabilities and inherent advantages, such as higher stiffness, strength, and biodegradability, position them as prime candidates for diverse applications, including smart medical devices, soft robotics, engineering structures, energy devices, electronics, and textiles. Specific examples, such as Fe_3O_4 NPs for magnetic actuation, gold and silver NPs for precise photothermal control, and carbon-based fillers for enhanced electrical conductivity, underscore the versatility and performance of SMPNCs in meeting the demands of advanced engineering and technology applications.

SMPNCs are traditionally categorized based on thermal-induced phase changes, response mechanisms, and the type of external stimuli triggering shape-memory actuation. However, this review introduces a novel categorization of SMPNCs based on the types of reinforced nanostructures incorporated into polymer matrices, offering a unique perspective on their design and functionality. Despite the challenges associated with incorporating nanostructures, such as aggregation and surface modification effects, innovative techniques have been developed to achieve better dispersion and interfacial interactions within polymer matrices to explore enhanced mechanical and thermal properties. Unlike traditional SMPs that rely solely on thermal activation, SMPNCs' ability to respond to a broad range of stimuli further expands their potential for next-generation applications. Therefore, future research must focus on achieving an optimal balance between nanofillers and polymer matrices, developing advanced actuation mechanisms, and enhancing remote control capabilities of shape-memory effects. By addressing these challenges and expanding their application potential, SMPNCs have the capacity to redefine smart material technology, offering sustainable, adaptive, and dynamic solutions for a wide array of industries.

Author Contributions: R.I., S.M., P.C. and T.R.L. discussed, commented on, and wrote the manuscript. All authors have read and agreed to the published version of the manuscript.

Funding: This research was generously supported by the Air Force Office of Scientific Research (AFOSR FA9550-23-1-0581; 23RT0567) and the Robert A. Welch Foundation (Grant Nos. E-1320 and V-E-0001).

Acknowledgments: We thank Minh Dang Nguyen for his valuable suggestions on the preparation of the manuscript and Melissa Ariza Gonzalez for her assistance in the revision process.

Conflicts of Interest: The authors declare no conflict of interest.

References

1. Forterre, Y.; Skotheim, J.M.; Dumais, J.; Mahadevan, L. How the Venus Flytrap Snaps. *Nature* **2005**, *433*, 421–425. [CrossRef] [PubMed]
2. Ren, H.; Huang, Y.; Xu, W.; Liu, Y. Electro-Activated Shape Memory Behavior of a Three-Dimensional Lightweight Knitted Tubular Composite. *Compos. Commun.* **2023**, *38*, 101517. [CrossRef]

3. Bhanushali, H.; Amrutkar, S.; Mestry, S.; Mhaske, S. Shape Memory Polymer Nanocomposite: A Review on Structure–Property Relationship. *Polym. Bull.* **2022**, *79*, 3437–3493. [CrossRef]
4. Peng, B.; Yang, Y.; Ju, T.; Cavicchi, K.A. Fused Filament Fabrication 4D Printing of a Highly Extensible, Self-Healing, Shape Memory Elastomer Based on Thermoplastic Polymer Blends. *ACS Appl. Mater. Interfaces* **2020**, *13*, 12777–12788. [CrossRef]
5. Liu, C.; Qin, H.; Mather, P. Review of Progress in Shape-Memory Polymers. *J. Mater. Chem.* **2007**, *17*, 1543–1558. [CrossRef]
6. Rose, A.; Zhu, Z.; Madigan, C.F.; Swager, T.M.; Bulović, V. Sensitivity Gains in Chemosensing by Lasing Action in Organic Polymers. *Nature* **2005**, *434*, 876–879. [CrossRef] [PubMed]
7. Zhang, P.; Wu, B.; Huang, S.; Cai, F.; Wang, G.; Yu, H. UV–Vis–NIR Light-Induced Bending of Shape-Memory Polyurethane Composites Doped with Azobenzene and Upconversion Nanoparticles. *Polymer* **2019**, *178*, 121644. [CrossRef]
8. Li, W.; Liu, Y.; Leng, J. Light-Actuated Reversible Shape Memory Effect of a Polymer Composite. *Compos. Part Appl. Sci. Manuf.* **2018**, *110*, 70–75. [CrossRef]
9. Ramezani, M.; Monroe, M.B.B. Biostable Segmented Thermoplastic Polyurethane Shape Memory Polymers for Smart Biomedical Applications. *ACS Appl. Polym. Mater.* **2022**, *4*, 1956–1965. [CrossRef]
10. Mohr, R.; Kratz, K.; Weigel, T.; Lucka-Gabor, M.; Moneke, M.; Lendlein, A. Initiation of Shape-Memory Effect by Inductive Heating of Magnetic Nanoparticles in Thermoplastic Polymers. *Proc. Natl. Acad. Sci. USA* **2006**, *103*, 3540–3545. [CrossRef] [PubMed]
11. Chen, Y.; Zhao, X.; Li, Y.; Jin, Z.-Y.; Yang, Y.; Yang, M.-B.; Yin, B. Light-and Magnetic-Responsive Synergy Controlled Reconfiguration of Polymer Nanocomposites with Shape Memory Assisted Self-Healing Performance for Soft Robotics. *J. Mater. Chem. C* **2021**, *9*, 5515–5527. [CrossRef]
12. Zeng, C.; Liu, L.; Bian, W.; Liu, Y.; Leng, J. 4D Printed Electro-Induced Continuous Carbon Fiber Reinforced Shape Memory Polymer Composites with Excellent Bending Resistance. *Compos. Part B Eng.* **2020**, *194*, 108034. [CrossRef]
13. Cortés, A.; Cosola, A.; Sangermano, M.; Campo, M.; González Prolongo, S.; Pirri, C.F.; Jiménez-Suárez, A.; Chiappone, A. DLP 4D-Printing of Remotely, Modularly, and Selectively Controllable Shape Memory Polymer Nanocomposites Embedding Carbon Nanotubes. *Adv. Funct. Mater.* **2021**, *31*, 2106774. [CrossRef]
14. Lendlein, A.; Langer, R. Biodegradable, Elastic Shape-Memory Polymers for Potential Biomedical Applications. *Science* **2002**, *296*, 1673–1676. [CrossRef]
15. Jiang, Z.-C.; Xiao, Y.-Y.; Kang, Y.; Pan, M.; Li, B.-J.; Zhang, S. Shape Memory Polymers Based on Supramolecular Interactions. *ACS Appl. Mater. Interfaces* **2017**, *9*, 20276–20293. [CrossRef] [PubMed]
16. Hager, M.D.; Bode, S.; Weber, C.; Schubert, U.S. Shape Memory Polymers: Past, Present and Future Developments. *Prog. Polym. Sci.* **2015**, *49*, 3–33. [CrossRef]
17. Ratna, D.; Karger-Kocsis, J. Recent Advances in Shape Memory Polymers and Composites: A Review. *J. Mater. Sci.* **2008**, *43*, 254–269. [CrossRef]
18. Leng, J.; Lan, X.; Liu, Y.; Du, S. Shape-Memory Polymers and Their Composites: Stimulus Methods and Applications. *Prog. Mater. Sci.* **2011**, *56*, 1077–1135. [CrossRef]
19. Idumah, C.I.; Odera, R.; Ezeani, E.; Low, J.H.; Tanjung, F.; Damiri, F.; Luing, W.S. Construction, Characterization, Properties and Multifunctional Applications of Stimuli-Responsive Shape Memory Polymeric Nanoarchitectures: A Review. *Polym.-Plast. Technol. Mater.* **2023**, *62*, 1247–1272. [CrossRef]
20. Liu, T.; Zhou, T.; Yao, Y.; Zhang, F.; Liu, L.; Liu, Y.; Leng, J. Stimulus Methods of Multi-Functional Shape Memory Polymer Nanocomposites: A Review. *Compos. Part Appl. Sci. Manuf.* **2017**, *100*, 20–30. [CrossRef]
21. Meng, H.; Li, G. A Review of Stimuli-Responsive Shape Memory Polymer Composites. *Polymer* **2013**, *54*, 2199–2221. [CrossRef]
22. Hussain, F.; Hojjati, M.; Okamoto, M.; Gorga, R.E. Polymer-Matrix Nanocomposites, Processing, Manufacturing, and Application: An Overview. *J. Compos. Mater.* **2006**, *40*, 1511–1575. [CrossRef]
23. Panahi-Sarmad, M.; Abrisham, M.; Noroozi, M.; Amirkiai, A.; Dehghan, P.; Goodarzi, V.; Zahiri, B. Deep Focusing on the Role of Microstructures in Shape Memory Properties of Polymer Composites: A Critical Review. *Eur. Polym. J.* **2019**, *117*, 280–303. [CrossRef]
24. Boudjellal, A.; Trache, D.; Khimeche, K.; Hafsaoui, S.L.; Bougamra, A.; Tcharkhtchi, A.; Durastanti, J.-F. Stimulation and Reinforcement of Shape-Memory Polymers and Their Composites: A Review. *J. Thermoplast. Compos. Mater.* **2022**, *35*, 2227–2260. [CrossRef]
25. Zhao, W.; Li, N.; Liu, L.; Leng, J.; Liu, Y. Mechanical Behaviors and Applications of Shape Memory Polymer and Its Composites. *Appl. Phys. Rev.* **2023**, *10*, 011306. [CrossRef]
26. Wang, Y.; Li, G.; Yang, L.; Luo, R.; Guo, G. Development of Innovative Biomaterials and Devices for the Treatment of Cardiovascular Diseases. *Adv. Mater.* **2022**, *34*, 2201971. [CrossRef]
27. Godart, F.; Houeijeh, A.; Recher, M.; Francart, C.; Polge, A.-S.; Richardson, M.; Cajot, M.-A.; Duhamel, A. Transcatheter Closure of Atrial Septal Defect with the Figulla® ASD Occluder: A Comparative Study with the Amplatzer® Septal Occluder. *Arch. Cardiovasc. Dis.* **2015**, *108*, 57–63. [CrossRef]

28. Small, W.; Buckley, P.R.; Wilson, T.S.; Benett, W.J.; Hartman, J.; Saloner, D.; Maitland, D.J. Shape Memory Polymer Stent with Expandable Foam: A New Concept for Endovascular Embolization of Fusiform Aneurysms. *IEEE Trans. Biomed. Eng.* **2007**, *54*, 1157–1160. [CrossRef]
29. Xia, Y.; He, Y.; Zhang, F.; Liu, Y.; Leng, J. A Review of Shape Memory Polymers and Composites: Mechanisms, Materials, and Applications. *Adv. Mater.* **2021**, *33*, 2000713. [CrossRef] [PubMed]
30. Gao, H.; Li, J.; Zhang, F.; Liu, Y.; Leng, J. The Research Status and Challenges of Shape Memory Polymer-Based Flexible Electronics. *Mater. Horiz.* **2019**, *6*, 931–944. [CrossRef]
31. Nasseri, R.; Bouzari, N.; Huang, J.; Golzar, H.; Jankhani, S.; Tang, X.; Mekonnen, T.H.; Aghakhani, A.; Shahsavan, H. Programmable Nanocomposites of Cellulose Nanocrystals and Zwitterionic Hydrogels for Soft Robotics. *Nat. Commun.* **2023**, *14*, 6108. [CrossRef]
32. Toncheva, A.; Khelifa, F.; Paint, Y.; Voué, M.; Lambert, P.; Dubois, P.; Raquez, J.-M. Fast IR-Actuated Shape-Memory Polymers Using in Situ Silver Nanoparticle-Grafted Cellulose Nanocrystals. *ACS Appl. Mater. Interfaces* **2018**, *10*, 29933–29942. [CrossRef] [PubMed]
33. Göldel, A.; Marmur, A.; Kasaliwal, G.R.; Pötschke, P.; Heinrich, G. Shape-Dependent Localization of Carbon Nanotubes and Carbon Black in an Immiscible Polymer Blend during Melt Mixing. *Macromolecules* **2011**, *44*, 6094–6102. [CrossRef]
34. Vernon, L.B.; Vernon, H.M. Process of Manufacturing Articles of Thermoplastic Synthetic Resins. U.S. Patent No. 2,234,993, 18 March 1941.
35. Jia, J.; Wang, J.; Wang, Y. Shape Memory Polymer-Based Thermal-Responsive Circuit Switches. *J. Mater. Chem. C* **2023**, *11*, 6276–6289. [CrossRef]
36. Lendlein, A.; Gould, O.E. Reprogrammable Recovery and Actuation Behaviour of Shape-Memory Polymers. *Nat. Rev. Mater.* **2019**, *4*, 116–133. [CrossRef]
37. Rokaya, D.; Skallevold, H.E.; Srimaneepong, V.; Marya, A.; Shah, P.K.; Khurshid, Z.; Zafar, M.S.; Sapkota, J. Shape Memory Polymeric Materials for Biomedical Applications: An Update. *J. Compos. Sci.* **2023**, *7*, 24. [CrossRef]
38. Xie, T. Recent Advances in Polymer Shape Memory. *Polymer* **2011**, *52*, 4985–5000. [CrossRef]
39. Rousseau, I.A.; Mather, P.T. Shape Memory Effect Exhibited by Smectic-C Liquid Crystalline Elastomers. *J. Am. Chem. Soc.* **2003**, *125*, 15300–15301. [CrossRef]
40. Yao, Y.; Xu, Y.; Chen, H.; Kang, Y.; Liu, Y.; Leng, J. Fabrication and Characterization of Shape Memory Auxetic Metamaterial. *J. Intell. Mater. Syst. Struct.* **2023**, *34*, 101–110. [CrossRef]
41. Quadrini, F.; Bellisario, D.; Ciampoli, L.; Costanza, G.; Santo, L. Auxetic Epoxy Foams Produced by Solid State Foaming. *J. Cell. Plast.* **2016**, *52*, 441–454. [CrossRef]
42. Luo, X.; Mather, P.T. Conductive Shape Memory Nanocomposites for High Speed Electrical Actuation. *Soft Matter* **2010**, *6*, 2146–2149. [CrossRef]
43. Ze, Q.; Kuang, X.; Wu, S.; Wong, J.; Montgomery, S.M.; Zhang, R.; Kovitz, J.M.; Yang, F.; Qi, H.J.; Zhao, R. Magnetic Shape Memory Polymers with Integrated Multifunctional Shape Manipulation. *Adv. Mater.* **2020**, *32*, 1906657. [CrossRef]
44. Xing, S.; Wang, P.; Liu, S.; Xu, Y.; Zheng, R.; Deng, Z.; Peng, Z.; Li, J.; Wu, Y.; Liu, L. A Shape-Memory Soft Actuator Integrated with Reversible Electric/Moisture Actuating and Strain Sensing. *Compos. Sci. Technol.* **2020**, *193*, 108133. [CrossRef]
45. Yang, Q.; Zheng, W.; Zhao, W.; Peng, C.; Ren, J.; Yu, Q.; Hu, Y.; Zhang, X. One-Way and Two-Way Shape Memory Effects of a High-Strain Cis-1, 4-Polybutadiene–Polyethylene Copolymer Based Dynamic Network via Self-Complementary Quadruple Hydrogen Bonding. *Polym. Chem.* **2019**, *10*, 718–726. [CrossRef]
46. Qi, X.; Wang, W.; Dai, H.; Zhu, Y.; Dong, Y.; Fu, S.-Y.; Ni, Q.; Fu, Y. Multifunctional Two-Way Shape Memory RGO/Ethylene-Vinyl Acetate Composite Yarns for Electro-Driven Actuators and High Sensitivity Strain Sensors. *Compos. Part Appl. Sci. Manuf.* **2023**, *169*, 107521. [CrossRef]
47. Zare, M.; Prabhakaran, M.P.; Parvin, N.; Ramakrishna, S. Thermally-Induced Two-Way Shape Memory Polymers: Mechanisms, Structures, and Applications. *Chem. Eng. J.* **2019**, *374*, 706–720. [CrossRef]
48. Xiao, H.; Ma, C.; Le, X.; Wang, L.; Lu, W.; Theato, P.; Hu, T.; Zhang, J.; Chen, T. A Multiple Shape Memory Hydrogel Induced by Reversible Physical Interactions at Ambient Condition. *Polymers* **2017**, *9*, 138. [CrossRef]
49. Dayyoub, T.; Maksimkin, A.V.; Filippova, O.V.; Tcherdyntsev, V.V.; Telyshev, D.V. Shape Memory Polymers as Smart Materials: A Review. *Polymers* **2022**, *14*, 3511. [CrossRef] [PubMed]
50. Soto, G.D.; Meiorin, C.; Actis, D.G.; Zélis, P.M.; Londoño, O.M.; Muraca, D.; Mosiewicki, M.A.; Marcovich, N.E. Magnetic Nanocomposites Based on Shape Memory Polyurethanes. *Eur. Polym. J.* **2018**, *109*, 8–15. [CrossRef]
51. Leungpuangkaew, S.; Amornkitbamrung, L.; Phetnoi, N.; Sapcharoenkun, C.; Jubsilp, C.; Ekgasit, S.; Rimdusit, S. Magnetic-and Light-Responsive Shape Memory Polymer Nanocomposites from Bio-Based Benzoxazine Resin and Iron Oxide Nanoparticles. *Adv. Ind. Eng. Polym. Res.* **2023**, *6*, 215–225. [CrossRef]
52. Ren, Y.; Zhang, Z.; Xia, W.; Zhou, Q.; Song, X. Water-Responsive Shape Memory PLLA via Incorporating PCL-(PMVS-s-PAA)-PCL-PTMG-PCL-(PMVS-s-PAA)-PCL. *Eur. Polym. J.* **2021**, *147*, 110252. [CrossRef]

53. Song, L.; Li, Y.; Xiong, Z.; Pan, L.; Xu, X.; Lu, S. Water-Induced Shape Memory Effect of Nanocellulose Papers from Sisal Cellulose Nanofibers with Graphene Oxide. *Carbohydr. Polym.* **2018**, *179*, 110–117. [CrossRef] [PubMed]
54. Wu, M.; Sukyai, P.; Lv, D.; Zhang, F.; Wang, P.; Liu, C.; Li, B. Water and Humidity-Induced Shape Memory Cellulose Nanopaper with Quick Response, Excellent Wet Strength and Folding Resistance. *Chem. Eng. J.* **2020**, *392*, 123673. [CrossRef]
55. Houbben, M.; Sànchez, C.P.; Vanderbemden, P.; Noels, L.; Jérôme, C. MWCNTs Filled PCL Covalent Adaptable Networks: Towards Reprocessable, Self-Healing and Fast Electrically-Triggered Shape-Memory Composites. *Polymer* **2023**, *278*, 125992. [CrossRef]
56. Zhang, Z.; Wang, J.; Nie, X.; Wen, T.; Ji, Y.; Wu, X.; Zhao, Y.; Chen, C. Near Infrared Laser-Induced Targeted Cancer Therapy Using Thermoresponsive Polymer Encapsulated Gold Nanorods. *J. Am. Chem. Soc.* **2014**, *136*, 7317–7326. [CrossRef]
57. Yenpech, N.; Intasanta, V.; Chirachanchai, S. Laser-Triggered Shape Memory Based on Thermoplastic and Thermoset Matrices with Silver Nanoparticles. *Polymer* **2019**, *182*, 121792. [CrossRef]
58. Das, N.; Chaki, T.; Khastgir, D. Effect of Filler Treatment and Crosslinking on Mechanical and Dynamic Mechanical Properties and Electrical Conductivity of Carbon Black-filled Ethylene–Vinyl Acetate Copolymer Composites. *J. Appl. Polym. Sci.* **2003**, *90*, 2073–2082. [CrossRef]
59. Horastani, S.J.; Ghane, M.; Karevan, M. Production and Performance of a Low Temperature Shape-Memory Actuator Based on Twisted-Coiled Spring Mechanics. *Smart Mater. Struct.* **2022**, *31*, 105005. [CrossRef]
60. Kalita, H.; Karak, N. Hyperbranched Polyurethane/Fe_3O_4 Thermosetting Nanocomposites as Shape Memory Materials. *Polym. Bull.* **2013**, *70*, 2953–2965. [CrossRef]
61. Razzaq, M.Y.; Anhalt, M.; Frormann, L.; Weidenfeller, B. Thermal, Electrical and Magnetic Studies of Magnetite Filled Polyurethane Shape Memory Polymers. *Mater. Sci. Eng. A* **2007**, *444*, 227–235. [CrossRef]
62. Du, L.; Xu, Z.-Y.; Fan, C.-J.; Xiang, G.; Yang, K.-K.; Wang, Y.-Z. A Fascinating Metallo-Supramolecular Polymer Network with Thermal/Magnetic/Light-Responsive Shape-Memory Effects Anchored by Fe_3O_4 Nanoparticles. *Macromolecules* **2018**, *51*, 705–715. [CrossRef]
63. Zou, H.; Weder, C.; Simon, Y.C. Shape-Memory Polyurethane Nanocomposites with Single Layer or Bilayer Oleic Acid-Coated Fe_3O_4 Nanoparticles. *Macromol. Mater. Eng.* **2015**, *300*, 885–892. [CrossRef]
64. Issa, B.; Obaidat, I.M.; Albiss, B.A.; Haik, Y. Magnetic Nanoparticles: Surface Effects and Properties Related to Biomedicine Applications. *Int. J. Mol. Sci.* **2013**, *14*, 21266–21305. [CrossRef] [PubMed]
65. Gao, Y.; Zhu, G.; Xu, S.; Ma, T.; Nie, J. Biodegradable Magnetic-sensitive Shape Memory Poly(ε-caprolactone)/Fe_3O_4 Nanocomposites. *J. Appl. Polym. Sci.* **2018**, *135*, 45652. [CrossRef]
66. Ruenpanya, K.; Mora, P.; Karagiannidis, P.; Bunyanuwat, K.; Rimdusit, S. Magnetic-Responsive Triple Shape Memory Polymer from Bio-Based Benzoxazine/Urethane Polymer Alloys with Iron Oxide Nanoparticles. *Adv. Ind. Eng. Polym. Res.* **2024**, *8*, 37–47. [CrossRef]
67. Liu, H.; Wang, F.; Wu, W.; Dong, X.; Sang, L. 4D Printing of Mechanically Robust PLA/TPU/Fe_3O_4 Magneto-Responsive Shape Memory Polymers for Smart Structures. *Compos. Part B Eng.* **2023**, *248*, 110382. [CrossRef]
68. Babaie, A.; Rezaei, M.; Razzaghi, D.; Roghani-Mamaqani, H. Synthesis of Dual-stimuli-responsive Polyurethane Shape Memory Nanocomposites Incorporating Isocyanate-functionalized Fe_3O_4 Nanoparticles. *J. Appl. Polym. Sci.* **2022**, *139*, e52790. [CrossRef]
69. Khasraghi, S.S.; Shojaei, A.; Janmaleki, M.; Sundararaj, U. Efficient Inductively Heated Shape Memory Polyurethane Acrylate Network with Silane Modified Nanodiamond@Fe_3O_4 Superparamagnetic Nanohybrid. *Eur. Polym. J.* **2021**, *159*, 110735. [CrossRef]
70. Huang, J.; Fan, J.; Yin, S.; Chen, Y. Design of Remotely, Locally Triggered Shape-Memory Materials Based on Bicontinuous Polylactide/Epoxidized Natural Rubber Thermoplastic Vulcanizates via Regulating the Distribution of Ferroferric Oxide. *Compos. Sci. Technol.* **2019**, *182*, 107732. [CrossRef]
71. Huang, J.; Cao, L.; Yuan, D.; Chen, Y. Design of Multi-Stimuli-Responsive Shape Memory Biobased PLA/ENR/Fe_3O_4 TPVs with Balanced Stiffness–Toughness Based on Selective Distribution of Fe_3O_4. *ACS Sustain. Chem. Eng.* **2018**, *7*, 2304–2315. [CrossRef]
72. Zhou, Y.; Tan, J.; Chong, D.; Wan, X.; Zhang, J. Rapid Near-infrared Light Responsive Shape Memory Polymer Hybrids and Novel Chiral Actuators Based on Photothermal $W_{18}O_{49}$ Nanowires. *Adv. Funct. Mater.* **2019**, *29*, 1901202. [CrossRef]
73. Bai, Y.; Zhang, J.; Wen, D.; Gong, P.; Liu, J.; Ju, J.; Chen, X. A Reconfigurable, Self-Healing and near Infrared Light Responsive Thermoset Shape Memory Polymer. *Compos. Sci. Technol.* **2020**, *187*, 107940. [CrossRef]
74. Wu, S.; Li, W.; Sun, Y.; Pang, X.; Zhang, X.; Zhuang, J.; Zhang, H.; Hu, C.; Lei, B.; Liu, Y. Facile Fabrication of a CD/PVA Composite Polymer to Access Light-Responsive Shape-Memory Effects. *J. Mater. Chem. C* **2020**, *8*, 8935–8941. [CrossRef]
75. Lu, C.; Shen, Y.; Wang, X.; Xu, S.; Wang, J.; Yong, Q.; Chu, F. Biomimetic Ultra-Strong, Ultra-Tough, Degradable Cellulose-Based Composites for Multi-Stimuli Responsive Shape Memory. *Int. J. Biol. Macromol.* **2023**, *226*, 1468–1476. [CrossRef] [PubMed]
76. Li, L.; Zhao, B.; Wang, H.; Gao, Y.; Hu, J.; Zheng, S. Nanocomposites of Polyhydroxyurethane with Fe_3O_4 Nanoparticles: Synthesis, Shape Memory and Reprocessing Properties. *Compos. Sci. Technol.* **2021**, *215*, 109009. [CrossRef]

77. Zheng, Y.; Mei, H.; Ullah, S.; Saeed, M.U.; Li, L.; Zheng, S. Reprocessing and Reconfigurable Shape Recovery of Epoxy and Fe_3O_4 Nanocomposites Enabled by Crosslinking with a Polymeric Hardener Bearing Disulfide Bonds. *React. Funct. Polym.* **2023**, *193*, 105768. [CrossRef]
78. Zhang, H.; Xia, H.; Zhao, Y. Optically Triggered and Spatially Controllable Shape-Memory Polymer–Gold Nanoparticle Composite Materials. *J. Mater. Chem.* **2012**, *22*, 845–849. [CrossRef]
79. Fang, L.; Fang, T.; Liu, X.; Ni, Y.; Lu, C.; Xu, Z. Precise Stimulation of Near-Infrared Light Responsive Shape-Memory Polymer Composites Using Upconversion Particles with Photothermal Capability. *Compos. Sci. Technol.* **2017**, *152*, 190–197. [CrossRef]
80. Xiang, Z.; Zhang, J.; Zhou, C.; Zhang, B.; Chen, N.; Li, M.; Fu, D.; Wang, Y. Near-Infrared Remotely Controllable Shape Memory Biodegradable Occluder Based on Poly(l-Lactide-Co-ε-Caprolactone)/Gold Nanorod Composite. *ACS Appl. Mater. Interfaces* **2023**, *15*, 42341–42353. [CrossRef]
81. Ngo, N.M.; Tran, H.-V.; Lee, T.R. Plasmonic Nanostars: Systematic Review of Their Synthesis and Applications. *ACS Appl. Nano Mater.* **2022**, *5*, 14051–14091. [CrossRef]
82. Homaeigohar, S.; Elbahri, M. Switchable Plasmonic Nanocomposites. *Adv. Opt. Mater.* **2019**, *7*, 1801101. [CrossRef]
83. Fortenbaugh, R.J.; Lear, B.J. On-Demand Curing of Polydimethylsiloxane (PDMS) Using the Photothermal Effect of Gold Nanoparticles. *Nanoscale* **2017**, *9*, 8555–8559. [CrossRef]
84. Viswanath, V.; Maity, S.; Bochinski, J.R.; Clarke, L.I.; Gorga, R.E. Thermal Annealing of Polymer Nanocomposites via Photothermal Heating: Effects on Crystallinity and Spherulite Morphology. *Macromolecules* **2013**, *46*, 8596–8607. [CrossRef]
85. Li, S.; Jin, X.; Shao, Y.; Qi, X.; Yang, J.; Wang, Y. Gold Nanoparticle/Reduced Graphene Oxide Hybrids for Fast Light-Actuated Shape Memory Polymers with Enhanced Photothermal Conversion and Mechanical Stiffness. *Eur. Polym. J.* **2019**, *116*, 302–310. [CrossRef]
86. Zhang, P.; Huang, Y.; Lu, X.; Zhang, S.; Li, J.; Wei, G.; Su, Z. One-Step Synthesis of Large-Scale Graphene Film Doped with Gold Nanoparticles at Liquid–Air Interface for Electrochemistry and Raman Detection Applications. *Langmuir* **2014**, *30*, 8980–8989. [CrossRef] [PubMed]
87. Fu, X.; Kuang, P.; Wang, S.; Zhang, G.; Yin, H. Controllable Synthesis of Graphene Oxide–Silver (Gold) Nanocomposites and Their Size-Dependencies. *RSC Adv.* **2016**, *6*, 70468–70473. [CrossRef]
88. Kang, S.; Lee, J.; Ryu, S.; Kwon, Y.; Kim, K.-H.; Jeong, D.H.; Paik, S.R.; Kim, B.-S. Gold Nanoparticle/Graphene Oxide Hybrid Sheets Attached on Mesenchymal Stem Cells for Effective Photothermal Cancer Therapy. *Chem. Mater.* **2017**, *29*, 3461–3476. [CrossRef]
89. Wang, Y.; Sachyani Keneth, E.; Kamyshny, A.; Scalet, G.; Auricchio, F.; Magdassi, S. 4D Multimaterial Printing of Programmable and Selective Light-activated Shape-memory Structures with Embedded Gold Nanoparticles. *Adv. Mater. Technol.* **2022**, *7*, 2101058. [CrossRef]
90. Zhang, H.; Zhao, Y. Polymers with Dual Light-Triggered Functions of Shape Memory and Healing Using Gold Nanoparticles. *ACS Appl. Mater. Interfaces* **2013**, *5*, 13069–13075. [CrossRef]
91. Burnworth, M.; Tang, L.; Kumpfer, J.R.; Duncan, A.J.; Beyer, F.L.; Fiore, G.L.; Rowan, S.J.; Weder, C. Optically Healable Supramolecular Polymers. *Nature* **2011**, *472*, 334–337. [CrossRef] [PubMed]
92. Zheng, X.; Fontana, J.; Pevnyi, M.; Ignatenko, M.; Wang, S.; Vaia, R.; Palffy-Muhoray, P. The Effects of Nanoparticle Shape and Orientation on the Low Frequency Dielectric Properties of Nanocomposites. *J. Mater. Sci.* **2012**, *47*, 4914–4920. [CrossRef]
93. Yadav, P.R.; Rizvi, M.H.; Kuttich, B.; Mishra, S.R.; Chapman, B.S.; Lynch, B.B.; Kraus, T.; Oldenburg, A.L.; Tracy, J.B. Plasmon-Coupled Gold Nanoparticles in Stretched Shape-Memory Polymers for Mechanical/Thermal Sensing. *ACS Appl. Nano Mater.* **2021**, *4*, 3911–3921. [CrossRef]
94. Kennedy, L.C.; Bickford, L.R.; Lewinski, N.A.; Coughlin, A.J.; Hu, Y.; Day, E.S.; West, J.L.; Drezek, R.A. A New Era for Cancer Treatment: Gold-nanoparticle-mediated Thermal Therapies. *Small* **2011**, *7*, 169–183. [CrossRef] [PubMed]
95. Huang, X.; El-Sayed, I.H.; Qian, W.; El-Sayed, M.A. Cancer Cell Imaging and Photothermal Therapy in the Near-Infrared Region by Using Gold Nanorods. *J. Am. Chem. Soc.* **2006**, *128*, 2115–2120. [CrossRef]
96. Zhang, H.; Zhang, J.; Tong, X.; Ma, D.; Zhao, Y. Light Polarization-controlled Shape-memory Polymer/Gold Nanorod Composite. *Macromol. Rapid Commun.* **2013**, *34*, 1575–1579. [CrossRef] [PubMed]
97. Ye, H.; De, S. Thermal Injury of Skin and Subcutaneous Tissues: A Review of Experimental Approaches and Numerical Models. *Burns* **2017**, *43*, 909–932. [CrossRef]
98. Jeon, H.; Lee, K. Effect of Gold Nanoparticle Morphology on Thermal Properties of Polyimide Nanocomposite Films. *Colloids Surf. Physicochem. Eng. Asp.* **2019**, *579*, 123651. [CrossRef]
99. Guo, Q.; Bishop, C.J.; Meyer, R.A.; Wilson, D.R.; Olasov, L.; Schlesinger, D.E.; Mather, P.T.; Spicer, J.B.; Elisseeff, J.H.; Green, J.J. Entanglement-Based Thermoplastic Shape Memory Polymeric Particles with Photothermal Actuation for Biomedical Applications. *ACS Appl. Mater. Interfaces* **2018**, *10*, 13333–13341. [CrossRef] [PubMed]

100. Paunović, N.; Marbach, J.; Bao, Y.; Berger, V.; Klein, K.; Schleich, S.; Coulter, F.B.; Kleger, N.; Studart, A.R.; Franzen, D. Digital Light 3D Printed Bioresorbable and NIR-Responsive Devices with Photothermal and Shape-Memory Functions. *Adv. Sci.* **2022**, *9*, 2200907. [CrossRef]
101. Zheng, Y.; Li, J.; Lee, E.; Yang, S. Light-Induced Shape Recovery of Deformed Shape Memory Polymer Micropillar Arrays with Gold Nanorods. *Rsc Adv.* **2015**, *5*, 30495–30499. [CrossRef]
102. Mishra, S.R.; Tracy, J.B. Sequential Actuation of Shape-Memory Polymers through Wavelength-Selective Photothermal Heating of Gold Nanospheres and Nanorods. *ACS Appl. Nano Mater.* **2018**, *1*, 3063–3067. [CrossRef]
103. Lopez-Carrizales, M.; Mendoza-Mendoza, E.; Peralta-Rodriguez, R.D.; Pérez-Díaz, M.A.; Portales-Pérez, D.; Magaña-Aquino, M.; Aragón-Piña, A.; Infante-Martínez, R.; Barriga-Castro, E.D.; Sánchez-Sánchez, R. Characterization, Antibiofilm and Biocompatibility Properties of Chitosan Hydrogels Loaded with Silver Nanoparticles and Ampicillin: An Alternative Protection to Central Venous Catheters. *Colloids Surf. B Biointerfaces* **2020**, *196*, 111292. [CrossRef] [PubMed]
104. Ringwal, S.; Bartwal, A.S.; Sati, S.C. Photo-Catalytic Degradation of Different Toxic Dyes Using Silver Nanoparticles as Photo-Catalyst, Mediated via Citrus Aurantium Peels Extract. *J. Indian Chem. Soc.* **2021**, *98*, 100221. [CrossRef]
105. Sonseca, A.; Madani, S.; Muñoz-Bonilla, A.; Fernández-García, M.; Peponi, L.; Leonés, A.; Rodríguez, G.; Echeverría, C.; López, D. Biodegradable and Antimicrobial PLA–OLA Blends Containing Chitosan-Mediated Silver Nanoparticles with Shape Memory Properties for Potential Medical Applications. *Nanomaterials* **2020**, *10*, 1065. [CrossRef]
106. Jouni, M.; Boudenne, A.; Boiteux, G.; Massardier, V.; Garnier, B.; Serghei, A. Electrical and Thermal Properties of Polyethylene/Silver Nanoparticle Composites. *Polym. Compos.* **2013**, *34*, 778–786. [CrossRef]
107. Dorigato, A.; Pegoretti, A. Shape Memory Epoxy Nanocomposites with Carbonaceous Fillers and In-situ Generated Silver Nanoparticles. *Polym. Eng. Sci.* **2019**, *59*, 694–703. [CrossRef]
108. Zare, M.; Parvin, N.; Prabhakaran, M.P.; Mohandesi, J.A.; Ramakrishna, S. Highly Porous 3D Sponge-like Shape Memory Polymer for Tissue Engineering Application with Remote Actuation Potential. *Compos. Sci. Technol.* **2019**, *184*, 107874. [CrossRef]
109. Qi, X.; Shao, Y.; Wu, H.; Yang, J.; Wang, Y. Flexible Phase Change Composite Materials with Simultaneous Light Energy Storage and Light-Actuated Shape Memory Capability. *Compos. Sci. Technol.* **2019**, *181*, 107714. [CrossRef]
110. Stroganov, V.; Al-Hussein, M.; Sommer, J.-U.; Janke, A.; Zakharchenko, S.; Ionov, L. Reversible Thermosensitive Biodegradable Polymeric Actuators Based on Confined Crystallization. *Nano Lett.* **2015**, *15*, 1786–1790. [CrossRef]
111. Chen, S.; Yang, S.; Li, Z.; Xu, S.; Yuan, H.; Chen, S.; Ge, Z. Electroactive Two-way Shape Memory Polymer Laminates. *Polym. Compos.* **2015**, *36*, 439–444. [CrossRef]
112. Fan, L.F.; Rong, M.Z.; Zhang, M.Q.; Chen, X.D. Dynamic Reversible Bonds Enable External Stress-Free Two-Way Shape Memory Effect of a Polymer Network and the Interrelated Intrinsic Self-Healability of Wider Crack and Recyclability. *J. Mater. Chem. A* **2018**, *6*, 16053–16063. [CrossRef]
113. Yang, Z.; Wang, Q.; Wang, T. Dual-Triggered and Thermally Reconfigurable Shape Memory Graphene-Vitrimer Composites. *ACS Appl. Mater. Interfaces* **2016**, *8*, 21691–21699. [CrossRef] [PubMed]
114. Weems, A.; Raymond, J.; Easley, A.; Wierzbicki, M.; Gustafson, T.; Monroe, M.; Maitland, D. Shape Memory Polymers with Visible and Near-Infrared Imaging Modalities: Synthesis, Characterization and in Vitro Analysis. *RSC Adv.* **2017**, *7*, 19742–19753. [CrossRef]
115. Rimdusit, S.; Lohwerathama, M.; Hemvichian, K.; Kasemsiri, P.; Dueramae, I. Shape Memory Polymers from Benzoxazine-Modified Epoxy. *Smart Mater. Struct.* **2013**, *22*, 075033. [CrossRef]
116. Xiao, X.; Kong, D.; Qiu, X.; Zhang, W.; Liu, Y.; Zhang, S.; Zhang, F.; Hu, Y.; Leng, J. Shape Memory Polymers with High and Low Temperature Resistant Properties. *Sci. Rep.* **2015**, *5*, 14137. [CrossRef] [PubMed]
117. Schäfer, H.; Hartwig, A.; Koschek, K. The Nature of Bonding Matters: Benzoxazine Based Shape Memory Polymers. *Polymer* **2018**, *135*, 285–294. [CrossRef]
118. Soto-Castro, D.; Reyes-Torres, U.; Santos-López, G.; de Jesús Cano-Barrita, P.F.; Karaaslan, M.A.; Renneckar, S.; Hernández-Martínez, Á.R.; Gutiérrez, M.C. Improving the Thermo-Activated Shape Memory of Thermoplastic Potato Starch by Adding Silver Nanoparticles. *J. Mater. Sci.* **2023**, *58*, 15116–15131. [CrossRef]
119. Surendren, A.; Mohanty, A.K.; Liu, Q.; Misra, M. A Review of Biodegradable Thermoplastic Starches, Their Blends and Composites: Recent Developments and Opportunities for Single-Use Plastic Packaging Alternatives. *Green Chem.* **2022**, *24*, 8606–8636. [CrossRef]
120. Selçuk Pekdemir, S.; Karagulle, B.; Pekdemir, M.E.; Taş, R.; Aksoy, E.; Aydin, D. A Novel Green Synthesis Approach for Shape Memory Polymer Nanocomposites Decorated with Silver Nanoparticles. *Polym. Eng. Sci.* **2023**, *63*, 3986–3997. [CrossRef]
121. Li, C.; Jiao, Y.; Lv, X.; Wu, S.; Chen, C.; Zhang, Y.; Li, J.; Hu, Y.; Wu, D.; Chu, J. In Situ Reversible Tuning from Pinned to Roll-down Superhydrophobic States on a Thermal-Responsive Shape Memory Polymer by a Silver Nanowire Film. *ACS Appl. Mater. Interfaces* **2020**, *12*, 13464–13472. [CrossRef] [PubMed]
122. Manthiram, K.; Alivisatos, A.P. Tunable Localized Surface Plasmon Resonances in Tungsten Oxide Nanocrystals. *J. Am. Chem. Soc.* **2012**, *134*, 3995–3998. [CrossRef]

123. Li, B.; Zhang, Y.; Zou, R.; Wang, Q.; Zhang, B.; An, L.; Yin, F.; Hua, Y.; Hu, J. Self-Assembled WO_{3-x} Hierarchical Nanostructures for Photothermal Therapy with a 915 Nm Laser Rather than the Common 980 Nm Laser. *Dalton Trans.* **2014**, *43*, 6244–6250. [CrossRef] [PubMed]
124. Guo, C.; Yin, S.; Yan, M.; Kobayashi, M.; Kakihana, M.; Sato, T. Morphology-Controlled Synthesis of $W_{18}O_{49}$ Nanostructures and Their near-Infrared Absorption Properties. *Inorg. Chem.* **2012**, *51*, 4763–4771. [CrossRef] [PubMed]
125. Tian, G.; Wang, B.; He, X.; Wang, C.; Yang, D.; Ma, J. On Demand Bidirectional Shape Transformations and Novel Chiral Actuators of Photomediated Shape Memory Polymer Film Based on Photothermal OEGy-$W_{18}O_{49}$ Nanowires. *Sci. China Technol. Sci.* **2023**, *66*, 3585–3595. [CrossRef]
126. Hu, X.; Song, X.; Xu, M.; Wang, Y.; Zhu, C.; Yu, W.; Zhao, Y. A Shape-Memory Poly(ε-Caprolactone) Hybridized TiO_2/Poly(l-Lactide) Composite with Antibacterial Properties. *Int. J. Biol. Macromol.* **2023**, *253*, 126567. [CrossRef]
127. Huang, B.; Wang, Z.; Tu, J.; Liu, C.; Xu, P.; Ding, Y. Interfacial Distribution and Compatibilization of Imidazolium Functionalized CNTs in Poly(Lactic Acid)/Polycaprolactone Composites with Excellent EMI Shielding and Mechanical Properties. *Int. J. Biol. Macromol.* **2023**, *227*, 1182–1190. [CrossRef]
128. Ishii, S.; Uto, K.; Niiyama, E.; Ebara, M.; Nagao, T. Hybridizing Poly(ε-Caprolactone) and Plasmonic Titanium Nitride Nanoparticles for Broadband Photoresponsive Shape Memory Films. *ACS Appl. Mater. Interfaces* **2016**, *8*, 5634–5640. [CrossRef]
129. Ishii, S.; Sugavaneshwar, R.P.; Nagao, T. Titanium Nitride Nanoparticles as Plasmonic Solar Heat Transducers. *J. Phys. Chem. C* **2016**, *120*, 2343–2348. [CrossRef]
130. Pekdemir, M.E. Thermal Properties and Shape Memory Behavior of Titanium Carbide Reinforced Poly(Vinyl Chloride)/Poly(ε-Caprolactone) Blend Nanocomposites. *Polym.-Plast. Technol. Mater.* **2022**, *61*, 242–250.
131. Leonés, A.; Peponi, L.; Fiori, S.; Lieblich, M. Effect of the Addition of MgO Nanoparticles on the Thermally-Activated Shape Memory Behavior of Plasticized PLA Electrospun Fibers. *Polymers* **2022**, *14*, 2657. [CrossRef] [PubMed]
132. Wang, X.; He, Y.; Leng, J. Bionic Shape Memory Polyurethane/Prussian Blue Nanoparticle-Based Actuators with Two-Way and Programmable Light-Driven Motions. *ACS Appl. Polym. Mater.* **2023**, *5*, 1398–1408. [CrossRef]
133. Zhai, J.; Zhai, Y.; Wen, D.; Dong, S. Prussian Blue/Multiwalled Carbon Nanotube Hybrids: Synthesis, Assembly and Electrochemical Behavior. *Electroanal. Int. J. Devoted Fundam. Pract. Asp. Electroanal.* **2009**, *21*, 2207–2212. [CrossRef]
134. Shokouhimehr, M.; Soehnlen, E.S.; Hao, J.; Griswold, M.; Flask, C.; Fan, X.; Basilion, J.P.; Basu, S.; Huang, S.D. Dual Purpose Prussian Blue Nanoparticles for Cellular Imaging and Drug Delivery: A New Generation of T 1-Weighted MRI Contrast and Small Molecule Delivery Agents. *J. Mater. Chem.* **2010**, *20*, 5251–5259. [CrossRef]
135. Karyakin, A.A. Prussian Blue and Its Analogues: Electrochemistry and Analytical Applications. *Electroanal. Int. J. Devoted Fundam. Pract. Asp. Electroanal.* **2001**, *13*, 813–819. [CrossRef]
136. Peng, S.; He, Y.; Er, M.; Sheng, Y.; Gu, Y.; Chen, H. Biocompatible CuS-Based Nanoplatforms for Efficient Photothermal Therapy and Chemotherapy in Vivo. *Biomater. Sci.* **2017**, *5*, 475–484. [CrossRef] [PubMed]
137. Li, M.; Fu, S.; Basta, A.H. Light-Induced Shape-Memory Polyurethane Composite Film Containing Copper Sulfide Nanoparticles and Modified Cellulose Nanocrystals. *Carbohydr. Polym.* **2020**, *230*, 115676. [CrossRef]
138. Bao, C.; Guo, Y.; Song, L.; Kan, Y.; Qian, X.; Hu, Y. In Situ Preparation of Functionalized Graphene Oxide/Epoxy Nanocomposites with Effective Reinforcements. *J. Mater. Chem.* **2011**, *21*, 13290–13298. [CrossRef]
139. Wu, G.; Panahi-Sarmad, M.; Van Vlierberghe, S.; Xu, R.; Hou, X.; Cui, Z.; Xiao, X. Multi-Stimuli Responsive Shape Memory Behavior of Dual-Switch TPU/CB/CNC Hybrid Nanocomposites as Triggered by Heat, Water, Ethanol, and pH. *Chem. Eng. J.* **2022**, *450*, 138253. [CrossRef]
140. Srisaard, S.; Amornkitbamrung, L.; Charoensuk, K.; Sapcharoenkun, C.; Jubsilp, C.; Rimdusit, S. Effects of Graphene Nanoplatelets on Bio-Based Shape Memory Polymers from Benzoxazine/Epoxy Copolymers Actuated by near-Infrared Light. *J. Intell. Mater. Syst. Struct.* **2022**, *33*, 547–557. [CrossRef]
141. Song, Y.S.; Youn, J.R. Influence of Dispersion States of Carbon Nanotubes on Physical Properties of Epoxy Nanocomposites. *Carbon* **2005**, *43*, 1378–1385. [CrossRef]
142. Maheshkumar, K.; Krishnamurthy, K.; Sathishkumar, P.; Sahoo, S.; Uddin, E.; Pal, S.; Rajasekar, R. Research Updates on Graphene Oxide-based Polymeric Nanocomposites. *Polym. Compos.* **2014**, *35*, 2297–2310. [CrossRef]
143. Kim, H.; Abdala, A.A.; Macosko, C.W. Graphene/Polymer Nanocomposites. *Macromolecules* **2010**, *43*, 6515–6530. [CrossRef]
144. Jin Yoo, H.; Chae Jung, Y.; Gopal Sahoo, N.; Whan Cho, J. Polyurethane-carbon Nanotube Nanocomposites Prepared by In-situ Polymerization with Electroactive Shape Memory. *J. Macromol. Sci. Part B* **2006**, *45*, 441–451. [CrossRef]
145. Khan, T.; Irfan, M.; Ali, M.; Dong, Y.; Ramakrishna, S.; Umer, R. Insights to Low Electrical Percolation Thresholds of Carbon-Based Polypropylene Nanocomposites. *Carbon* **2021**, *176*, 602–631. [CrossRef]
146. Olalde, B.; Aizpurua, J.M.; García, A.; Bustero, I.; Obieta, I.; Jurado, M.J. Single-Walled Carbon Nanotubes and Multiwalled Carbon Nanotubes Functionalized with Poly(L-Lactic Acid): A Comparative Study. *J. Phys. Chem. C* **2008**, *112*, 10663–10667. [CrossRef]

147. Tekay, E. Preparation and Characterization of Electro-Active Shape Memory PCL/SEBS-g-MA/MWCNT Nanocomposites. *Polymer* **2020**, *209*, 122989. [CrossRef]
148. Gupta, R.; Mittal, G.; Kumar, K.; Pandel, U. Analysing the Shape Memory Behaviour of MWCNT-Enhanced Nanocomposites: A Comparative Study between Experimental and Finite Element Analysis. *Funct. Compos. Struct.* **2024**, *6*, 025007. [CrossRef]
149. Raja, M.; Ryu, S.H.; Shanmugharaj, A. Influence of Surface Modified Multiwalled Carbon Nanotubes on the Mechanical and Electroactive Shape Memory Properties of Polyurethane (PU)/Poly(Vinylidene Diflouride) (PVDF) Composites. *Colloids Surf. Physicochem. Eng. Asp.* **2014**, *450*, 59–66. [CrossRef]
150. Qi, X.; Dong, P.; Liu, Z.; Liu, T.; Fu, Q. Selective Localization of Multi-Walled Carbon Nanotubes in Bi-Component Biodegradable Polyester Blend for Rapid Electroactive Shape Memory Performance. *Compos. Sci. Technol.* **2016**, *125*, 38–46. [CrossRef]
151. Sánchez, C.P.; Houbben, M.; Fagnard, J.-F.; Harmeling, P.; Jérôme, C.; Noels, L.; Vanderbemden, P. Experimental Characterization of the Thermo-Electro-Mechanical Properties of a Shape Memory Composite during Electric Activation. *Smart Mater. Struct.* **2022**, *31*, 095029. [CrossRef]
152. Zhou, Z.; Chen, Y.; Guo, A.; Xue, T.; Li, X.; Yu, C.; Zhang, F. Remotely Fast Response Healing Crosslinked Polyurea Nanocomposites with Recyclability via Two-Step Method. *Compos. Sci. Technol.* **2022**, *224*, 109462. [CrossRef]
153. Feng, Y.; Nie, Z.; Deng, P.; Luo, L.; Hu, X.; Su, J.; Li, H.; Fan, X.; Qi, S. An Effective Approach to Improve the Thermal Conductivity, Strength, and Stress Relaxation of Carbon Nanotubes/Epoxy Composites Based on Vitrimer Chemistry. *Int. J. Mol. Sci.* **2022**, *23*, 8833. [CrossRef] [PubMed]
154. Li, Z.; Guo, Z.; Yang, Y. Development of Cyanate Ester-based Shape Memory Composite Reinforced by Multi-walled Carbon Nanotube Modified with Silicon Dioxide. *J. Appl. Polym. Sci.* **2023**, *140*, e53749. [CrossRef]
155. Namathoti, S.; Vakkalagadda, M.R.K. Mechanical and Shape Recovery Characterization of MWCNTs/HNTs-Reinforced Thermal-Responsive Shape-Memory Polymer Nanocomposites. *Polymers* **2023**, *15*, 710. [CrossRef] [PubMed]
156. Bo, C.; Guo, S.; Sha, Y.; Yuan, L.; Hu, L.; Jia, P.; Zhou, Y.; Feng, G.; Zhang, M. Recyclable Cardanol-Based Benzoxazines with Multi-Stimulus-Responsive Shape-Memory and Their Carbon Nanotubes Composites for Dynamic Force Sensor. *Compos. Sci. Technol.* **2022**, *230*, 109732. [CrossRef]
157. Sun, W.-J.; Sun, H.; Jia, L.-C.; Lei, J.; Lin, H.; Tang, J.-H.; Wang, Y.-Y.; Yan, D.-X. Segregated Conductive Carbon Nanotube/Poly(Ethylene-Co-Vinyl Acetate) Composites for Low-Voltage Reversible Actuators. *Ind. Eng. Chem. Res.* **2022**, *61*, 13912–13920. [CrossRef]
158. Ma, R.-Y.; Sun, W.-J.; Xu, L.; Jia, L.-C.; Yan, D.-X.; Li, Z.-M. Permanent Shape Reconfiguration and Locally Reversible Actuation of a Carbon Nanotube/Ethylene Vinyl Acetate Copolymer Composite by Constructing a Dynamic Cross-Linked Network. *ACS Appl. Mater. Interfaces* **2023**, *15*, 40954–40962. [CrossRef] [PubMed]
159. Pekdemir, M.E.; KÖK, M.; Qader, I.N.; AYDOĞDU, Y. Preparation and Physicochemical Properties of Mwcnt Doped Polyvinyl Chloride/Poly(ε-Caprolactone) Blend. *J. Polym. Res.* **2022**, *29*, 109. [CrossRef]
160. Mosnackova, K.; Mrlík, M.; Micusik, M.; Kleinová, A.; Sasinková, V.; Popelka, A.; Opálková Šišková, A.; Kasák, P.; Dworak, C.L.; Mosnacek, J. Light-Responsive Hybrids Based on Carbon Nanotubes with Covalently Attached PHEMA-g-PCL Brushes. *Macromolecules* **2021**, *54*, 2412–2426. [CrossRef]
161. Huang, B.; Vyas, C.; Roberts, I.; Poutrel, Q.-A.; Chiang, W.-H.; Blaker, J.J.; Huang, Z.; Bártolo, P. Fabrication and Characterisation of 3D Printed MWCNT Composite Porous Scaffolds for Bone Regeneration. *Mater. Sci. Eng. C* **2019**, *98*, 266–278. [CrossRef] [PubMed]
162. Chen, Y.-F.; Tan, Y.-J.; Li, J.; Hao, Y.-B.; Shi, Y.-D.; Wang, M. Graphene Oxide-Assisted Dispersion of Multi-Walled Carbon Nanotubes in Biodegradable Poly(ε-Caprolactone) for Mechanical and Electrically Conductive Enhancement. *Polym. Test.* **2018**, *65*, 387–397. [CrossRef]
163. Wurm, A.; Lellinger, D.; Minakov, A.A.; Skipa, T.; Pötschke, P.; Nicula, R.; Alig, I.; Schick, C. Crystallization of Poly(ε-Caprolactone)/MWCNT Composites: A Combined SAXS/WAXS, Electrical and Thermal Conductivity Study. *Polymer* **2014**, *55*, 2220–2232. [CrossRef]
164. Grady, B.P. Effects of Carbon Nanotubes on Polymer Physics. *J. Polym. Sci. Part B Polym. Phys.* **2012**, *50*, 591–623. [CrossRef]
165. Abdullah, S.A.; Jumahat, A.; Abdullah, N.R.; Frormann, L. Determination of Shape Fixity and Shape Recovery Rate of Carbon Nanotube-Filled Shape Memory Polymer Nanocomposites. *Procedia Eng.* **2012**, *41*, 1641–1646. [CrossRef]
166. Koerner, H.; Price, G.; Pearce, N.A.; Alexander, M.; Vaia, R.A. Remotely Actuated Polymer Nanocomposites—Stress-Recovery of Carbon-Nanotube-Filled Thermoplastic Elastomers. *Nat. Mater.* **2004**, *3*, 115–120. [CrossRef] [PubMed]
167. Hashmi, S.; Prasad, H.C.; Abishera, R.; Bhargaw, H.N.; Naik, A. Improved Recovery Stress in Multi-Walled-Carbon-Nanotubes Reinforced Polyurethane. *Mater. Des.* **2015**, *67*, 492–500. [CrossRef]
168. Tekay, E. Low-Voltage Triggered Electroactive and Heat-Responsive Thermoplastic Elastomer/Carbon Nanotube Polymer Blend Composites. *Mater. Today Commun.* **2023**, *35*, 106443. [CrossRef]
169. Sun, Y.; Chu, M.; Huang, M.; Hegazi, O.; Naguib, H.E. Hybrid Electroactive Shape Memory Polymer Composites with Room Temperature Deformability. *Macromol. Mater. Eng.* **2019**, *304*, 1900196. [CrossRef]

170. Kuester, S.; Barra, G.M.; Demarquette, N.R. Morphology, Mechanical Properties and Electromagnetic Shielding Effectiveness of Poly(Styrene-b-ethylene-ran-butylene-b-styrene)/Carbon Nanotube Nanocomposites: Effects of Maleic Anhydride, Carbon Nanotube Loading and Processing Method. *Polym. Int.* **2018**, *67*, 1229–1240. [CrossRef]
171. Madbouly, S.A.; Lendlein, A. Shape-Memory Polymer Composites. In *Shape-Memory Polymers*; Lendlein, A., Ed.; Springer: Berlin/Heidelberg, Germany, 2010; pp. 41–95.
172. Dong, K.; Panahi-Sarmad, M.; Cui, Z.; Huang, X.; Xiao, X. Electro-Induced Shape Memory Effect of 4D Printed Auxetic Composite Using PLA/TPU/CNT Filament Embedded Synergistically with Continuous Carbon Fiber: A Theoretical & Experimental Analysis. *Compos. Part B Eng.* **2021**, *220*, 108994.
173. Cao, M.-S.; Song, W.-L.; Hou, Z.-L.; Wen, B.; Yuan, J. The Effects of Temperature and Frequency on the Dielectric Properties, Electromagnetic Interference Shielding and Microwave-Absorption of Short Carbon Fiber/Silica Composites. *Carbon* **2010**, *48*, 788–796. [CrossRef]
174. Gopinath, S.; Adarsh, N.; Nair, P.R.; Mathew, S. One-Way Thermo-Responsive Shape Memory Polymer Nanocomposite Derived from Polycaprolactone and Polystyrene-Block-Polybutadiene-Block-Polystyrene Packed with Carbon Nanofiber. *Mater. Today Commun.* **2020**, *22*, 100802. [CrossRef]
175. Gopinath, S.; Adarsh, N.N.; Nair, P.R.; Mathew, S. Carbon Nanofiber-Reinforced Shape Memory Polyurethanes Based on HTPB/PTMG Blend as Anticorrosive Coatings. *Polym.-Plast. Technol. Mater.* **2023**, *62*, 563–581. [CrossRef]
176. Lu, H.; Liang, F.; Yao, Y.; Gou, J.; Hui, D. Self-Assembled Multi-Layered Carbon Nanofiber Nanopaper for Significantly Improving Electrical Actuation of Shape Memory Polymer Nanocomposite. *Compos. Part B Eng.* **2014**, *59*, 191–195. [CrossRef]
177. Andrews, R.; Weisenberger, M. Carbon Nanotube Polymer Composites. *Curr. Opin. Solid State Mater. Sci.* **2004**, *8*, 31–37. [CrossRef]
178. Gojny, F.H.; Wichmann, M.H.G.; Köpke, U.; Fiedler, B.; Schulte, K. Carbon Nanotube-Reinforced Epoxy-Composites: Enhanced Stiffness and Fracture Toughness at Low Nanotube Content. *Compos. Sci. Technol.* **2004**, *64*, 2363–2371. [CrossRef]
179. Lantada, A.D.; Morgado, P.L.; Sanz, J.L.M.; García, J.M.; Munoz-Guijosa, J.M.; Otero, J.E. Intelligent Structures Based on the Improved Activation of Shape Memory Polymers Using Peltier Cells. *Smart Mater. Struct.* **2010**, *19*, 055022. [CrossRef]
180. Uranbey, L.; Unal, H.I.; Calis, G.; Gumus, O.Y.; Katmer, S.; Karatas, C. One-Pot Preparation of Electroactive Shape Memory Polyurethane/Carbon Black Blend. *J. Mater. Eng. Perform.* **2021**, *30*, 1665–1673. [CrossRef]
181. Arun, D.; Santhosh Kumar, K.; Satheesh Kumar, B.; Chakravarthy, P.; Dona, M.; Santhosh, B. High Glass-Transition Polyurethane-Carbon Black Electro-Active Shape Memory Nanocomposite for Aerospace Systems. *Mater. Sci. Technol.* **2019**, *35*, 596–605. [CrossRef]
182. Du, J.; Zhang, Z.; Liu, D.; Ren, T.; Wan, D.; Pu, H. Triple-Stimuli Responsive Shape Memory Effect of Novel Polyolefin Elastomer/Lauric Acid/Carbon Black Nanocomposites. *Compos. Sci. Technol.* **2019**, *169*, 45–51. [CrossRef]
183. Ren, L.; Wang, Z.; Ren, L.; Han, Z.; Zhou, X.L.; Song, Z.; Liu, Q. 4D Printing of Shape-Adaptive Tactile Sensor with Tunable Sensing Characteristics. *Compos. Part B Eng.* **2023**, *265*, 110959. [CrossRef]
184. Wang, L.; Kelly, P.V.; Ozveren, N.; Zhang, X.; Korey, M.; Chen, C.; Li, K.; Bhandari, S.; Tekinalp, H.; Zhao, X. Multifunctional Polymer Composite Coatings and Adhesives by Incorporating Cellulose Nanomaterials. *Matter* **2022**, *6*, 344–372. [CrossRef]
185. Sharma, H.; Rana, S.; Singh, P.; Hayashi, M.; Binder, W.H.; Rossegger, E.; Kumar, A.; Schlögl, S. Self-Healable Fiber-Reinforced Vitrimer Composites: Overview and Future Prospects. *RSC Adv.* **2022**, *12*, 32569–32582. [CrossRef] [PubMed]
186. Sun, J.; Liang, M.; Yin, L.; Rivers, G.; Hu, G.; Pan, Q.; Zhao, B. Interfacial Compatibility of Core–Shell Cellulose Nanocrystals for Improving Dynamic Covalent Adaptable Networks' Fracture Resistance in Nanohybrid Vitrimer Composites. *ACS Appl. Mater. Interfaces* **2023**, *15*, 39786–39796. [CrossRef] [PubMed]
187. Ogunsona, E.O.; Panchal, P.; Mekonnen, T.H. Surface Grafting of Acrylonitrile Butadiene Rubber onto Cellulose Nanocrystals for Nanocomposite Applications. *Compos. Sci. Technol.* **2019**, *184*, 107884. [CrossRef]
188. Alonso-Lerma, B.; Barandiaran, L.; Ugarte, L.; Larraza, I.; Reifs, A.; Olmos-Juste, R.; Barruetabeña, N.; Amenabar, I.; Hillenbrand, R.; Eceiza, A. High Performance Crystalline Nanocellulose Using an Ancestral Endoglucanase. *Commun. Mater.* **2020**, *1*, 57. [CrossRef]
189. Eyley, S.; Thielemans, W. Surface Modification of Cellulose Nanocrystals. *Nanoscale* **2014**, *6*, 7764–7779. [CrossRef]
190. Zhou, Y.; Wang, F.; Yang, Z.; Hu, X.; Pan, Y.; Lu, Y.; Jiang, M. 3D Printing of Polyurethane/Nanocellulose Shape Memory Composites with Tunable Glass Transition Temperature. *Ind. Crops Prod.* **2022**, *182*, 114831. [CrossRef]
191. Djafari Petroudy, S.R.; Shojaeiarani, J.; Chabot, B. Recent Advances in Isolation, Characterization, and Potential Applications of Nanocellulose-Based Composites: A Comprehensive Review. *J. Nat. Fibers* **2023**, *20*, 2146830. [CrossRef]
192. Lin, S.; Huang, J.; Chang, P.R.; Wei, S.; Xu, Y.; Zhang, Q. Structure and Mechanical Properties of New Biomass-Based Nanocomposite: Castor Oil-Based Polyurethane Reinforced with Acetylated Cellulose Nanocrystal. *Carbohydr. Polym.* **2013**, *95*, 91–99. [CrossRef] [PubMed]
193. Swartz, J.L.; Li, R.L.; Dichtel, W.R. Incorporating Functionalized Cellulose to Increase the Toughness of Covalent Adaptable Networks. *ACS Appl. Mater. Interfaces* **2020**, *12*, 44110–44116. [CrossRef]

194. Wang, S.; Wang, X.; Liu, W.; Zhang, L.; Ouyang, H.; Hou, Q.; Fan, K.; Li, J.; Liu, P.; Liu, X. Fabricating Cellulose Nanofibril from Licorice Residues and Its Cellulose Composite Incorporated with Natural Nanoparticles. *Carbohydr. Polym.* **2020**, *229*, 115464. [CrossRef] [PubMed]
195. Wu, G.; Gu, Y.; Hou, X.; Li, R.; Ke, H.; Xiao, X. Hybrid Nanocomposites of Cellulose/Carbon-Nanotubes/Polyurethane with Rapidly Water Sensitive Shape Memory Effect and Strain Sensing Performance. *Polymers* **2019**, *11*, 1586. [CrossRef] [PubMed]
196. Castillo-Paz, A.M.; Londoño-Restrepo, S.M.; Tirado-Mejía, L.; Mondragón, M.; Rodríguez-García, M.E. Nano to Micro Size Transition of Hydroxyapatite in Porcine Bone during Heat Treatment with Low Heating Rates. *Prog. Nat. Sci. Mater. Int.* **2020**, *30*, 494–501. [CrossRef]
197. Gao, H.; Li, J.; Xie, F.; Liu, Y.; Leng, J. A Novel Low Colored and Transparent Shape Memory Copolyimide and Its Durability in Space Thermal Cycling Environments. *Polymer* **2018**, *156*, 121–127. [CrossRef]
198. Kakroodi, A.R.; Cheng, S.; Sain, M.; Asiri, A. Mechanical, Thermal, and Morphological Properties of Nanocomposites Based on Polyvinyl Alcohol and Cellulose Nanofiber from Aloe Vera Rind. *J. Nanomater.* **2014**, *2014*, 903498. [CrossRef]
199. Zhang, W.; Wang, H.; Wang, H.; Chan, J.Y.E.; Liu, H.; Zhang, B.; Zhang, Y.-F.; Agarwal, K.; Yang, X.; Ranganath, A.S. Structural Multi-Colour Invisible Inks with Submicron 4D Printing of Shape Memory Polymers. *Nat. Commun.* **2021**, *12*, 112. [CrossRef]
200. Li, J.; Wang, A.; Qin, J.; Zhang, H.; Ma, Z.; Zhang, G. Lightweight Polymethacrylimide@Copper/Nickel Composite Foams for Electromagnetic Shielding and Monopole Antennas. *Compos. Part Appl. Sci. Manuf.* **2021**, *140*, 106144. [CrossRef]
201. Korkmaz Memiş, N.; Kaplan, S. Production of Thermal and Water Responsive Shape Memory Polyurethane Nanocomposite Filaments with Cellulose Nanowhisker Incorporation. *Cellulose* **2021**, *28*, 7075–7096. [CrossRef]
202. Lindström, T. Aspects on Nanofibrillated Cellulose (NFC) Processing, Rheology and NFC-Film Properties. *Curr. Opin. Colloid Interface Sci.* **2017**, *29*, 68–75. [CrossRef]
203. Li, B.; Xu, W.; Kronlund, D.; Määttänen, A.; Liu, J.; Smått, J.-H.; Peltonen, J.; Willför, S.; Mu, X.; Xu, C. Cellulose Nanocrystals Prepared via Formic Acid Hydrolysis Followed by TEMPO-Mediated Oxidation. *Carbohydr. Polym.* **2015**, *133*, 605–612. [CrossRef]
204. Wang, Q.; Du, H.; Zhang, F.; Zhang, Y.; Wu, M.; Yu, G.; Liu, C.; Li, B.; Peng, H. Flexible Cellulose Nanopaper with High Wet Tensile Strength, High Toughness and Tunable Ultraviolet Blocking Ability Fabricated from Tobacco Stalk via a Sustainable Method. *J. Mater. Chem. A* **2018**, *6*, 13021–13030. [CrossRef]
205. Neufeld, M.J.; Lutzke, A.; Tapia, J.B.; Reynolds, M.M. Metal–Organic Framework/Chitosan Hybrid Materials Promote Nitric Oxide Release from S-Nitrosoglutathione in Aqueous Solution. *ACS Appl. Mater. Interfaces* **2017**, *9*, 5139–5148. [CrossRef] [PubMed]
206. Toivonen, M.S.; Kurki-Suonio, S.; Schacher, F.H.; Hietala, S.; Rojas, O.J.; Ikkala, O. Water-Resistant, Transparent Hybrid Nanopaper by Physical Cross-Linking with Chitosan. *Biomacromolecules* **2015**, *16*, 1062–1071. [CrossRef] [PubMed]
207. Zhu, Y.; Hu, J.; Luo, H.; Young, R.J.; Deng, L.; Zhang, S.; Fan, Y.; Ye, G. Rapidly Switchable Water-Sensitive Shape-Memory Cellulose/Elastomer Nano-Composites. *Soft Matter* **2012**, *8*, 2509–2517. [CrossRef]
208. Correia, C.O.; Mano, J.F. Chitosan Scaffolds with a Shape Memory Effect Induced by Hydration. *J. Mater. Chem. B* **2014**, *2*, 3315–3323. [CrossRef]
209. Meng, D.; Zhao, Q.; Cheng, X.; Ma, J.; Kong, L.; He, X.; Li, J. Water-Induced Shape Memory Cellulose Nanofiber-Based Nanocomposite Membrane Containing Lignin with Quick Water Response and Excellent Wet Mechanical Property. *Eur. Polym. J.* **2022**, *171*, 111204. [CrossRef]
210. Yang, Y.-N.; Lu, K.-Y.; Wang, P.; Ho, Y.-C.; Tsai, M.-L.; Mi, F.-L. Development of Bacterial Cellulose/Chitin Multi-Nanofibers Based Smart Films Containing Natural Active Microspheres and Nanoparticles Formed in Situ. *Carbohydr. Polym.* **2020**, *228*, 115370. [CrossRef] [PubMed]
211. Azarifar, M.; Ghanbarzadeh, B.; Khiabani, M.S.; Basti, A.A.; Abdulkhani, A.; Noshirvani, N.; Hosseini, M. The Optimization of Gelatin-CMC Based Active Films Containing Chitin Nanofiber and Trachyspermum Ammi Essential Oil by Response Surface Methodology. *Carbohydr. Polym.* **2019**, *208*, 457–468. [CrossRef] [PubMed]
212. Hosseinnezhad, R.; Vozniak, I.; Zaïri, F. In Situ Generation of Green Hybrid Nanofibrillar Polymer-Polymer Composites—A Novel Approach to the Triple Shape Memory Polymer Formation. *Polymers* **2021**, *13*, 1900. [CrossRef]
213. Gu, T.; Bi, H.; Sun, H.; Tang, J.; Ren, Z.; Zhou, X.; Xu, M. Design and Development of 4D-Printed Cellulose Nanofibers Reinforced Shape Memory Polymer Composites: Application for Self-Deforming Plant Bionic Soft Grippers. *Addit. Manuf.* **2023**, *70*, 103544. [CrossRef]
214. Yue, C.; Li, M.; Liu, Y.; Fang, Y.; Song, Y.; Xu, M.; Li, J. Three-Dimensional Printing of Cellulose Nanofibers Reinforced PHB/PCL/Fe_3O_4 Magneto-Responsive Shape Memory Polymer Composites with Excellent Mechanical Properties. *Addit. Manuf.* **2021**, *46*, 102146. [CrossRef]
215. Gupta, A.; Mekonnen, T.H. Cellulose Nanocrystals Enabled Sustainable Polycaprolactone Based Shape Memory Polyurethane Bionanocomposites. *J. Colloid Interface Sci.* **2022**, *611*, 726–738. [CrossRef] [PubMed]
216. Du, W.; Zhang, Z.; Yin, C.; Ge, X.; Shi, L. Preparation of Shape Memory Polyurethane/Modified Cellulose Nanocrystals Composites with Balanced Comprehensive Performances. *Polym. Adv. Technol.* **2021**, *32*, 4710–4720. [CrossRef]

217. Fan, W.; Li, Z. In Situ Reaction of Modified Cellulose Nanocrystals in Shape Memory Polyacrylamide/Gelatin Composite Hydrogel with Enhanced Performance. *Polym. Int.* **2023**, *72*, 578–585. [CrossRef]
218. Basak, S.; Bandyopadhyay, A. Solvent Responsive Shape Memory Polymers-Evolution, Current Status, and Future Outlook. *Macromol. Chem. Phys.* **2021**, *222*, 2100195. [CrossRef]
219. Rossetti, A.; Pizzetti, F.; Rossi, F.; Mauri, E.; Borghi, E.; Ottaviano, E.; Sacchetti, A. Synthesis and Characterization of Carbomer-Based Hydrogels for Drug Delivery Applications. *Int. J. Polym. Mater. Polym. Biomater.* **2021**, *70*, 743–753. [CrossRef]
220. Wu, G.; Panahi-Sarmad, M.; Xiao, X.; Dong, K.; Mei, X.; Li, S.; Li, R.; Hou, X. Synthesis and Properties of Multistimuli Responsive Shape Memory Polyurethane Bioinspired from α-Keratin Hair. *Adv. Mater. Technol.* **2021**, *6*, 2001275. [CrossRef]
221. Zhao, L.; Li, W.; Plog, A.; Xu, Y.; Buntkowsky, G.; Gutmann, T.; Zhang, K. Multi-Responsive Cellulose Nanocrystal–Rhodamine Conjugates: An Advanced Structure Study by Solid-State Dynamic Nuclear Polarization (DNP) NMR. *Phys. Chem. Chem. Phys.* **2014**, *16*, 26322–26329. [CrossRef] [PubMed]
222. Liu, Y.; Li, Y.; Yang, G.; Zheng, X.; Zhou, S. Multi-Stimulus-Responsive Shape-Memory Polymer Nanocomposite Network Cross-Linked by Cellulose Nanocrystals. *ACS Appl. Mater. Interfaces* **2015**, *7*, 4118–4126. [CrossRef] [PubMed]
223. Bi, H.; Ye, G.; Sun, H.; Ren, Z.; Gu, T.; Xu, M. Mechanically Robust, Shape Memory, Self-Healing and 3D Printable Thermoreversible Cross-Linked Polymer Composites toward Conductive and Biomimetic Skin Devices Applications. *Addit. Manuf.* **2022**, *49*, 102487. [CrossRef]
224. Tatsi, E.; Fortunato, G.; Rigatelli, B.; Lyu, G.; Turri, S.; Evans, R.C.; Griffini, G. Thermoresponsive Host Polymer Matrix for Self-Healing Luminescent Solar Concentrators. *ACS Appl. Energy Mater.* **2019**, *3*, 1152–1160. [CrossRef]
225. Zhang, F.; Yang, K.; Liu, G.; Chen, Y.; Wang, M.; Li, S.; Li, R. Recent Advances on Graphene: Synthesis, Properties and Applications. *Compos. Part Appl. Sci. Manuf.* **2022**, *160*, 107051. [CrossRef]
226. Kausar, A.; Ahmad, I.; Aldaghri, O.; Ibnaouf, K.H.; Eisa, M. Shape Memory Graphene Nanocomposites—Fundamentals, Properties, and Significance. *Processes* **2023**, *11*, 1171. [CrossRef]
227. Chen, L.; Shen, Y.; Liu, Z.; Song, Q.; Jiang, Y. Experimental and Modeling Investigation on Thermodynamic Effect of Graphene Doped Shape Memory Epoxy Composites. *Polymer* **2022**, *239*, 124430. [CrossRef]
228. Tee, S.Y.; Ye, E.; Teng, C.P.; Tanaka, Y.; Tang, K.Y.; Win, K.Y.; Han, M.-Y. Advances in Photothermal Nanomaterials for Biomedical, Environmental and Energy Applications. *Nanoscale* **2021**, *13*, 14268–14286. [CrossRef]
229. Xu, J.-W.; Yao, K.; Xu, Z.-K. Nanomaterials with a Photothermal Effect for Antibacterial Activities: An Overview. *Nanoscale* **2019**, *11*, 8680–8691. [CrossRef] [PubMed]
230. Punetha, V.D.; Ha, Y.-M.; Kim, Y.-O.; Jung, Y.C.; Cho, J.W. Rapid Remote Actuation in Shape Memory Hyperbranched Polyurethane Composites Using Cross-Linked Photothermal Reduced Graphene Oxide Networks. *Sens. Actuators B Chem.* **2020**, *321*, 128468. [CrossRef]
231. Xu, L.Q.; Yang, W.J.; Neoh, K.-G.; Kang, E.-T.; Fu, G.D. Dopamine-Induced Reduction and Functionalization of Graphene Oxide Nanosheets. *Macromolecules* **2010**, *43*, 8336–8339. [CrossRef]
232. Ghosh, T.; Karak, N. Interpenetrating Polymer Network/Functionalized-reduced Graphene Oxide Nanocomposite: As an Advanced Functional Material. *J. Appl. Polym. Sci.* **2021**, *138*, 50499. [CrossRef]
233. Yang, H.; Li, F.; Shan, C.; Han, D.; Zhang, Q.; Niu, L.; Ivaska, A. Covalent Functionalization of Chemically Converted Graphene Sheets via Silane and Its Reinforcement. *J. Mater. Chem.* **2009**, *19*, 4632–4638. [CrossRef]
234. Yoo, H.J.; Mahapatra, S.S.; Cho, J.W. High-Speed Actuation and Mechanical Properties of Graphene-Incorporated Shape Memory Polyurethane Nanofibers. *J. Phys. Chem. C* **2014**, *118*, 10408–10415. [CrossRef]
235. Wan, B.; Dong, X.; Yang, X.; Zheng, M.-S.; Chen, G.; Zha, J.-W. High Strength, Stable and Self-Healing Copolyimide for Defects Induced by Mechanical and Electrical Damages. *J. Mater. Chem. C* **2022**, *10*, 11307–11315. [CrossRef]
236. Guo, Y.; Wang, Y.; Tao, L.; Wang, T.; Wang, Q.; Zhang, X.; Yang, Z. Engineering Thermal and Light Dual-Triggered Thermosetting Shape Memory Polyimide Nanocomposites with Superior Toughness and Rapid Remote Actuation Properties. *Adv. Eng. Mater.* **2023**, *25*, 2201555. [CrossRef]
237. Ghosh, T.; Voit, B.; Karak, N. Polystyrene/Thermoplastic Polyurethane Interpenetrating Network-Based Nanocomposite with High-Speed, Thermo-Responsive Shape Memory Behavior. *Polymer* **2020**, *200*, 122575. [CrossRef]
238. Sofla, R.L.M.; Rezaei, M.; Babaie, A.; Nasiri, M. Preparation of Electroactive Shape Memory Polyurethane/Graphene Nanocomposites and Investigation of Relationship between Rheology, Morphology and Electrical Properties. *Compos. Part B Eng.* **2019**, *175*, 107090. [CrossRef]
239. Wang, W.; Liu, D.; Liu, Y.; Leng, J.; Bhattacharyya, D. Electrical Actuation Properties of Reduced Graphene Oxide Paper/Epoxy-Based Shape Memory Composites. *Compos. Sci. Technol.* **2015**, *106*, 20–24. [CrossRef]
240. Falqi, F.H.; Bin-Dahman, O.A.; Khair, A.; Al-Harthi, M.A. PVA/PEG/Graphene Shape Memory Composites Responsive to Multi-Stimuli. *Appl. Phys. A* **2022**, *128*, 427. [CrossRef]

241. Lashgari, S.; Karrabi, M.; Ghasemi, I.; Azizi, H.; Messori, M.; Paderni, K. Shape Memory Nanocomposite of Poly(L-Lactic Acid)/Graphene Nanoplatelets Triggered by Infrared Light and Thermal Heating. *Express Polym. Lett.* **2016**, *10*, 349–359. [CrossRef]
242. Falqi, F.H.; Bin-Dahman, O.A.; Hussain, M.; Al-Harthi, M.A. Preparation of Miscible PVA/PEG Blends and Effect of Graphene Concentration on Thermal, Crystallization, Morphological, and Mechanical Properties of PVA/PEG (10 Wt%) Blend. *Int. J. Polym. Sci.* **2018**, *2018*, 8527693. [CrossRef]
243. Qi, X.; Yao, X.; Deng, S.; Zhou, T.; Fu, Q. Water-Induced Shape Memory Effect of Graphene Oxide Reinforced Polyvinyl Alcohol Nanocomposites. *J. Mater. Chem. A* **2014**, *2*, 2240–2249. [CrossRef]
244. Mat Yazik, M.H.; Sultan, M.T.H.; Jawaid, M.; Abu Talib, A.R.; Mazlan, N.; Md Shah, A.U.; Safri, S.N.A. Effect of Nanofiller Content on Dynamic Mechanical and Thermal Properties of Multi-Walled Carbon Nanotube and Montmorillonite Nanoclay Filler Hybrid Shape Memory Epoxy Composites. *Polymers* **2021**, *13*, 700. [CrossRef] [PubMed]
245. Kojima, Y.; Usuki, A.; Kawasumi, M.; Okada, A.; Kurauchi, T.; Kamigaito, O. One-pot Synthesis of Nylon 6–Clay Hybrid. *J. Polym. Sci. Part Polym. Chem.* **1993**, *31*, 1755–1758. [CrossRef]
246. Okada, A.; Usuki, A. The Chemistry of Polymer-Clay Hybrids. *Mater. Sci. Eng. C* **1995**, *3*, 109–115. [CrossRef]
247. Rafiee, R.; Shahzadi, R. Mechanical Properties of Nanoclay and Nanoclay Reinforced Polymers: A Review. *Polym. Compos.* **2019**, *40*, 431–445. [CrossRef]
248. Yazik, M.M.; Sultan, M.; Mazlan, N.; Talib, A.A.; Naveen, J.; Shah, A.; Safri, S. Effect of Hybrid Multi-Walled Carbon Nanotube and Montmorillonite Nanoclay Content on Mechanical Properties of Shape Memory Epoxy Nanocomposite. *J. Mater. Res. Technol.* **2020**, *9*, 6085–6100. [CrossRef]
249. Mat Yazik, M.H.; Hameed Sultan, M.T.; Jawaid, M.; Mazlan, N.; Abu Talib, A.R.; Md Shah, A.U.; Safri, S.N.A. Shape Memory Properties of Epoxy with Hybrid Multi-Walled Carbon Nanotube and Montmorillonite Nanoclay Nanofiller. *Polym. Bull.* **2024**, *81*, 951–968. [CrossRef]
250. Sun, Y.C.; Cai, S.; Ren, J.; Naguib, H.E. Room Temperature Deformable Shape Memory Composite with Fine-tuned Crystallization Induced via Nanoclay Particles. *J. Polym. Sci. Part B Polym. Phys.* **2017**, *55*, 1197–1206. [CrossRef]
251. Cao, F.; Jana, S.C. Nanoclay-Tethered Shape Memory Polyurethane Nanocomposites. *Polymer* **2007**, *48*, 3790–3800. [CrossRef]
252. Coativy, G.; Gautier, N.; Pontoire, B.; Buléon, A.; Lourdin, D.; Leroy, E. Shape Memory Starch–Clay Bionanocomposites. *Carbohydr. Polym.* **2015**, *116*, 307–313. [CrossRef]
253. Arash, S.; Akbari, B.; Ghaleb, S.; Kaffashi, B.; Marouf, B. Preparation of PLA-TPU-Nanoclay Composites and Characterization of Their Morphological, Mechanical, and Shape Memory Properties. *J. Mech. Behav. Biomed. Mater.* **2023**, *139*, 105642. [CrossRef] [PubMed]
254. Mi, H.-Y.; Salick, M.R.; Jing, X.; Jacques, B.R.; Crone, W.C.; Peng, X.-F.; Turng, L.-S. Characterization of Thermoplastic Polyurethane/Polylactic Acid (TPU/PLA) Tissue Engineering Scaffolds Fabricated by Microcellular Injection Molding. *Mater. Sci. Eng. C* **2013**, *33*, 4767–4776. [CrossRef]
255. Zhang, X.; Li, J.; Liang, Z.; Kan, Q. Design and Finite Element Simulation of Shape Memory Polyurethane Self-Deforming Structures. *Eng. Fail. Anal.* **2022**, *139*, 106446. [CrossRef]
256. Jafari Horastani, S.; Karevan, M.; Ghane, M. Structural, Thermal, and Viscoelastic Response of Nanoclay Reinforced Polylactic Acid/Thermoplastic Polyurethane Shape-memory Nanocomposites of Low Transition Temperature. *Polym. Adv. Technol.* **2022**, *33*, 2720–2735. [CrossRef]
257. Gu, S.; Chang, K.; Jin, S. A Dual-induced Self-expandable Stent Based on Biodegradable Shape Memory Polyurethane Nanocomposites (PCLAU/Fe_3O4) Triggered around Body Temperature. *J. Appl. Polym. Sci.* **2018**, *135*, 45686. [CrossRef]
258. Biswas, A.; Aswal, V.K.; Maiti, P. Tunable Shape Memory Behavior of Polymer with Surface Modification of Nanoparticles. *J. Colloid Interface Sci.* **2019**, *556*, 147–158. [CrossRef]
259. Feng, X.; Zhang, G.; Zhuo, S.; Jiang, H.; Shi, J.; Li, F.; Li, H. Dual Responsive Shape Memory Polymer/Clay Nanocomposites. *Compos. Sci. Technol.* **2016**, *129*, 53–60. [CrossRef]
260. Dai, S.; Yue, S.; Ning, Z.; Jiang, N.; Gan, Z. Polydopamine Nanoparticle-Reinforced Near-Infrared Light-Triggered Shape Memory Polycaprolactone–Polydopamine Polyurethane for Biomedical Implant Applications. *ACS Appl. Mater. Interfaces* **2022**, *14*, 14668–14676. [CrossRef] [PubMed]
261. Yi, J.; Nguyen, K.-C.T.; Wang, W.; Yang, W.; Pan, M.; Lou, E.; Major, P.W.; Le, L.H.; Zeng, H. Mussel-Inspired Adhesive Double-Network Hydrogel for Intraoral Ultrasound Imaging. *ACS Appl. Bio Mater.* **2020**, *3*, 8943–8952. [CrossRef] [PubMed]
262. Jin, Z.; Yang, L.; Shi, S.; Wang, T.; Duan, G.; Liu, X.; Li, Y. Flexible Polydopamine Bioelectronics. *Adv. Funct. Mater.* **2021**, *31*, 2103391. [CrossRef]
263. Thomas, R.J.; Rockwell, B.A.; Marshall, W.J.; Aldrich, R.C.; Zimmerman, S.A.; Rockwell, R.J., Jr. A Procedure for Laser Hazard Classification under the Z136. 1-2000 American National Standard for Safe Use of Lasers. *J. Laser Appl.* **2002**, *14*, 57–66. [CrossRef]
264. Chen, Y.; Zhao, X.; Luo, C.; Shao, Y.; Yang, M.-B.; Yin, B. A Facile Fabrication of Shape Memory Polymer Nanocomposites with Fast Light-Response and Self-Healing Performance. *Compos. Part Appl. Sci. Manuf.* **2020**, *135*, 105931. [CrossRef]

265. Atsuta, Y.; Takeuchi, K.; Shioda, N.; Hamada, W.; Hirai, T.; Nakamura, Y.; Oaki, Y.; Fujii, S. Colloidally Stable Polypyrrole Nanoparticles Synthesized by Surfactant-Free Coupling Polymerization. *Langmuir* **2023**, *39*, 14984–14995. [CrossRef]
266. Chen, J.; Sun, D.; Gu, T.; Qi, X.; Yang, J.; Lei, Y.; Wang, Y. Photo-Induced Shape Memory Blend Composites with Remote Selective Self-Healing Performance Enabled by Polypyrrole Nanoparticles. *Compos. Sci. Technol.* **2022**, *217*, 109123. [CrossRef]
267. Wang, Y.; Huang, L.; Wang, X.; Lu, X.; Wang, B.; Qin, Y.; Huang, C. Photoresponsive Triple Shape Memory Polymers with a Self-Healing Function Based on Poly(Lactic Acid)/Polycaprolactone Blends. *Polym. Test.* **2023**, *120*, 107966. [CrossRef]
268. Lashkari, R.; Zare, S.; Tabatabaei-Nezhad, S.A.; Husein, M.M. Geothermal Drilling Using Reprocessable Shape Memory Polymer Nanocomposite. *Colloids Surf. Physicochem. Eng. Asp.* **2023**, *673*, 131809. [CrossRef]
269. Kango, S.; Kalia, S.; Celli, A.; Njuguna, J.; Habibi, Y.; Kumar, R. Surface Modification of Inorganic Nanoparticles for Development of Organic–Inorganic Nanocomposites—A Review. *Prog. Polym. Sci.* **2013**, *38*, 1232–1261. [CrossRef]
270. Liu, M.; Fan, M.; Zhu, S.; Liu, W.; Yang, L.; Ge, D. Dual Manipulation of Light and Shape Based on Nanoparticle-Induced Shape Memory Composites. *J. Mater. Chem. C* **2023**, *11*, 4570–4575. [CrossRef]
271. Wang, F.; Jiang, M.; Pan, Y.; Lu, Y.; Xu, W.; Zhou, Y. 3D Printing Photo-Induced Lignin Nanotubes/Polyurethane Shape Memory Composite. *Polym. Test.* **2023**, *119*, 107934. [CrossRef]
272. Zhang, H.; Huang, S.; Sheng, J.; Wang, C.; Zhang, J.; Zhu, M.; Agyenim-Boateng, E.; Liang, C.; Xue, B.; Yang, H. 4D Printing of Shape Memory Polymer Nanocomposites for Enhanced Performances and Tunable Response Behavior. *Eur. Polym. J.* **2023**, *201*, 112568. [CrossRef]
273. Zou, Y.; Guo, J.; Liu, Y.; Du, Y.; Pu, Y.; Wang, D. Process Intensified Synthesis of Luminescent Poly(9,9-Dioctylfluorene-Alt-Benzothiadiazole) and Polyvinyl Alcohol Based Shape Memory Polymeric Nanocomposite Sensors toward Cold Chain Logistics Information Monitoring. *Polym. Chem.* **2023**, *14*, 1275–1281. [CrossRef]
274. Xu, X.; Skelly, J.D.; Song, J. Chemically Crosslinked Amphiphilic Degradable Shape Memory Polymer Nanocomposites with Readily Tuned Physical, Mechanical, and Biological Properties. *ACS Appl. Mater. Interfaces* **2023**, *15*, 2693–2704. [CrossRef] [PubMed]
275. Jalal, Z.; Hascoet, S.; Baruteau, A.-E.; Iriart, X.; Kreitmann, B.; Boudjemline, Y.; Thambo, J.-B. Long-Term Complications after Transcatheter Atrial Septal Defect Closure: A Review of the Medical Literature. *Can. J. Cardiol.* **2016**, *32*, 1315.e11–1315.e18. [CrossRef] [PubMed]
276. Liu, S.-J.; Peng, K.-M.; Hsiao, C.-Y.; Liu, K.-S.; Chung, H.-T.; Chen, J.-K. Novel Biodegradable Polycaprolactone Occlusion Device Combining Nanofibrous PLGA/Collagen Membrane for Closure of Atrial Septal Defect (ASD). *Ann. Biomed. Eng.* **2011**, *39*, 2759–2766. [CrossRef]
277. Wertman, B.; Azarbal, B.; Riedl, M.; Tobis, J. Adverse Events Associated with Nickel Allergy in Patients Undergoing Percutaneous Atrial Septal Defect or Patent Foramen Ovale Closure. *J. Am. Coll. Cardiol.* **2006**, *47*, 1226–1227. [CrossRef]
278. Lin, C.; Liu, L.; Liu, Y.; Leng, J. 4D Printing of Bioinspired Absorbable Left Atrial Appendage Occluders: A Proof-of-Concept Study. *ACS Appl. Mater. Interfaces* **2021**, *13*, 12668–12678. [CrossRef]
279. Lin, C.; Lv, J.; Li, Y.; Zhang, F.; Li, J.; Liu, Y.; Liu, L.; Leng, J. 4D-printed Biodegradable and Remotely Controllable Shape Memory Occlusion Devices. *Adv. Funct. Mater.* **2019**, *29*, 1906569. [CrossRef]
280. Lin, C.; Liu, L.; Liu, Y.; Leng, J. Recent Developments in Next-Generation Occlusion Devices. *Acta Biomater.* **2021**, *128*, 100–119. [CrossRef] [PubMed]
281. Wei, H.; Zhang, Q.; Yao, Y.; Liu, L.; Liu, Y.; Leng, J. Direct-Write Fabrication of 4D Active Shape-Changing Structures Based on a Shape Memory Polymer and Its Nanocomposite. *ACS Appl. Mater. Interfaces* **2017**, *9*, 876–883. [CrossRef] [PubMed]
282. Zhao, W.; Zhang, F.; Leng, J.; Liu, Y. Personalized 4D Printing of Bioinspired Tracheal Scaffold Concept Based on Magnetic Stimulated Shape Memory Composites. *Compos. Sci. Technol.* **2019**, *184*, 107866. [CrossRef]
283. Senatov, F.S.; Niaza, K.V.; Zadorozhnyy, M.Y.; Maksimkin, A.; Kaloshkin, S.; Estrin, Y. Mechanical Properties and Shape Memory Effect of 3D-Printed PLA-Based Porous Scaffolds. *J. Mech. Behav. Biomed. Mater.* **2016**, *57*, 139–148. [CrossRef] [PubMed]
284. Hanif, M.; Zhang, L.; Shah, A.H.; Chen, Z. Mechanical Analysis and Biodegradation of Oxides-Based Magneto-Responsive Shape Memory Polymers for Material Extrusion 3D Printing of Biomedical Scaffolds. *Addit. Manuf.* **2024**, *86*, 104174. [CrossRef]
285. Zhao, W.; Huang, Z.; Liu, L.; Wang, W.; Leng, J.; Liu, Y. Porous Bone Tissue Scaffold Concept Based on Shape Memory PLA/Fe_3O_4. *Compos. Sci. Technol.* **2021**, *203*, 108563. [CrossRef]
286. Zhang, F.; Wang, L.; Zheng, Z.; Liu, Y.; Leng, J. Magnetic Programming of 4D Printed Shape Memory Composite Structures. *Compos. Part Appl. Sci. Manuf.* **2019**, *125*, 105571. [CrossRef]
287. Doostmohammadi, H.; Baniassadi, M.; Bodaghi, M.; Baghani, M. 4D Printing of Magneto-Thermo-Responsive PLA/PMMA/Fe_3O_4 Nanocomposites with Superior Shape Memory and Remote Actuation. *Macromol. Mater. Eng.* **2024**, *309*, 2400090. [CrossRef]
288. Liu, X.; Zhao, K.; Gong, T.; Song, J.; Bao, C.; Luo, E.; Weng, J.; Zhou, S. Delivery of Growth Factors Using a Smart Porous Nanocomposite Scaffold to Repair a Mandibular Bone Defect. *Biomacromolecules* **2014**, *15*, 1019–1030. [CrossRef] [PubMed]

289. Xie, R.; Hu, J.; Hoffmann, O.; Zhang, Y.; Ng, F.; Qin, T.; Guo, X. Self-Fitting Shape Memory Polymer Foam Inducing Bone Regeneration: A Rabbit Femoral Defect Study. *Biochim. Biophys. Acta BBA-Gen. Subj.* **2018**, *1862*, 936–945. [CrossRef] [PubMed]
290. Vakil, A.U.; Ramezani, M.; Monroe, M.B.B. Magnetically Actuated Shape Memory Polymers for On-Demand Drug Delivery. *Materials* **2022**, *15*, 7279. [CrossRef]
291. Ahn, J.; Gu, J.; Choi, J.; Han, C.; Jeong, Y.; Park, J.; Cho, S.; Oh, Y.S.; Jeong, J.; Amjadi, M. A Review of Recent Advances in Electrically Driven Polymer-Based Flexible Actuators: Smart Materials, Structures, and Their Applications. *Adv. Mater. Technol.* **2022**, *7*, 2200041. [CrossRef]
292. Booth, R.E.; Khanna, C.; Schrickx, H.M.; Siddika, S.; Al Shafe, A.; O'Connor, B.T. Electrothermally Actuated Semitransparent Shape Memory Polymer Composite with Application as a Wearable Touch Sensor. *ACS Appl. Mater. Interfaces* **2022**, *14*, 53129–53138. [CrossRef]
293. Yoon, J.; An, Y.; Hong, S.B.; Myung, J.H.; Sun, J.; Yu, W. Fabrication of a Highly Stretchable, Wrinkle-Free Electrode with Switchable Transparency Using a Free-Standing Silver Nanofiber Network and Shape Memory Polymer Substrate. *Macromol. Rapid Commun.* **2020**, *41*, 2000129. [CrossRef]
294. Booth, R.E.; Schrickx, H.M.; Hanby, G.; Liu, Y.; Qin, Y.; Ade, H.; Zhu, Y.; O'Connor, B.T. Silver Nanowire Composite Electrode Enabling Highly Flexible, Robust Organic Photovoltaics. *Sol. RRL* **2022**, *6*, 2200264. [CrossRef]
295. Kim, C.-L.; Lee, J.-J.; Oh, Y.-J.; Kim, D.-E. Smart Wearable Heaters with High Durability, Flexibility, Water-Repellent and Shape Memory Characteristics. *Compos. Sci. Technol.* **2017**, *152*, 173–180. [CrossRef]
296. Luo, H.; Li, Z.; Yi, G.; Wang, Y.; Zu, X.; Wang, H.; Huang, H.; Liang, Z. Temperature Sensing of Conductive Shape Memory Polymer Composites. *Mater. Lett.* **2015**, *140*, 71–74. [CrossRef]
297. Zhang, J.; Cao, L.; Chen, Y. Mechanically Robust, Self-Healing and Conductive Rubber with Dual Dynamic Interactions of Hydrogen Bonds and Borate Ester Bonds. *Eur. Polym. J.* **2022**, *168*, 111103. [CrossRef]
298. Li, L.; Shi, P.; Hua, L.; An, J.; Gong, Y.; Chen, R.; Yu, C.; Hua, W.; Xiu, F.; Zhou, J. Design of a Wearable and Shape-Memory Fibriform Sensor for the Detection of Multimodal Deformation. *Nanoscale* **2018**, *10*, 118–123. [CrossRef] [PubMed]
299. Alipour, S.; Pourjavadi, A.; Hosseini, S.H. Magnetite Embedded κ-Carrageenan-Based Double Network Nanocomposite Hydrogel with Two-Way Shape Memory Properties for Flexible Electronics and Magnetic Actuators. *Carbohydr. Polym.* **2023**, *310*, 120610. [CrossRef] [PubMed]
300. Yu, Z.; Zhang, Q.; Li, L.; Chen, Q.; Niu, X.; Liu, J.; Pei, Q. Highly Flexible Silver Nanowire Electrodes for Shape-memory Polymer Light-emitting Diodes. *Adv. Mater.* **2011**, *23*, 664–668. [CrossRef]
301. Yu, Z.; Niu, X.; Liu, Z.; Pei, Q. Intrinsically Stretchable Polymer Light-emitting Devices Using Carbon Nanotube-polymer Composite Electrodes. *Adv. Mater.* **2011**, *23*, 3989–3994. [CrossRef]
302. Wang, T.; Zhao, J.; Weng, C.; Wang, T.; Liu, Y.; Han, Z.; Zhang, Z. Three-Dimensional Graphene Coated Shape Memory Polyurethane Foam with Fast Responsive Performance. *J. Mater. Chem. C* **2021**, *9*, 7444–7451. [CrossRef]
303. Wang, J.; Zheng, Y.; Qiu, S.; Song, L. Ethanol Inducing Self-Assembly of Poly-(Thioctic Acid)/Graphene Supramolecular Ionomers for Healable, Flame-Retardant, Shape-Memory Electronic Devices. *J. Colloid Interface Sci.* **2023**, *629*, 908–915. [CrossRef]
304. Wang, M.; Zhang, Q.; Bo, Y.; Zhang, C.; Lv, Y.; Fu, X.; He, W.; Fan, X.; Liang, J.; Huang, Y. Highly Stretchable Shape Memory Self-Soldering Conductive Tape with Reversible Adhesion Switched by Temperature. *Nano-Micro Lett.* **2021**, *13*, 124. [CrossRef] [PubMed]
305. Shi, Y.; Han, J.; Jin, X.; Miao, W.; Zhang, Y.; Duan, P. Chiral Luminescent Liquid Crystal with Multi-State-Reversibility: Breakthrough in Advanced Anti-Counterfeiting Materials. *Adv. Sci.* **2022**, *9*, 2201565. [CrossRef] [PubMed]
306. Xu, M.; Xu, Z.; Soto, M.A.; Xu, Y.; Hamad, W.Y.; MacLachlan, M.J. Mechanically Responsive Circularly Polarized Luminescence from Cellulose Nanocrystal-based Shape-Memory Polymers. *Adv. Mater.* **2023**, *35*, 2301060. [CrossRef]
307. Gu, T.; Ji, T.; Bi, H.; Ding, K.; Sun, H.; Zhai, W.; Ren, Z.; Wei, Y.; Xu, M. 4D Printed and Multi-Stimulus Responsive Shape Memory Polymer Nanocomposites Developed on Hydrogen Bonding–Metal-Phenolic Sacrificial Network: Application for Hazardous Chemical Operations Soft Robots. *Appl. Mater. Today* **2023**, *35*, 102009. [CrossRef]
308. Liu, J.A.-C.; Gillen, J.H.; Mishra, S.R.; Evans, B.A.; Tracy, J.B. Photothermally and Magnetically Controlled Reconfiguration of Polymer Composites for Soft Robotics. *Sci. Adv.* **2019**, *5*, eaaw2897. [CrossRef] [PubMed]
309. Wei, H.; Cauchy, X.; Navas, I.O.; Abderrafai, Y.; Chizari, K.; Sundararaj, U.; Liu, Y.; Leng, J.; Therriault, D. Direct 3D Printing of Hybrid Nanofiber-Based Nanocomposites for Highly Conductive and Shape Memory Applications. *ACS Appl. Mater. Interfaces* **2019**, *11*, 24523–24532. [CrossRef] [PubMed]
310. Kim, D.; Song, S.; Jang, S.; Kim, G.; Lee, J.; Lee, Y.; Park, S. Untethered Gripper-Type Hydrogel Millirobot Actuated by Electric Field and Magnetic Field. *Smart Mater. Struct.* **2020**, *29*, 085024. [CrossRef]
311. Xu, Z.; Ding, C.; Wei, D.-W.; Bao, R.-Y.; Ke, K.; Liu, Z.; Yang, M.-B.; Yang, W. Electro and Light-Active Actuators Based on Reversible Shape-Memory Polymer Composites with Segregated Conductive Networks. *ACS Appl. Mater. Interfaces* **2019**, *11*, 30332–30340. [CrossRef]

312. Sun, W.-J.; Guan, Y.; Wang, Y.-Y.; Wang, T.; Xu, Y.-T.; Kong, W.-W.; Jia, L.-C.; Yan, D.-X.; Li, Z.-M. Low-Voltage Actuator with Bilayer Structure for Various Biomimetic Locomotions. *ACS Appl. Mater. Interfaces* **2021**, *13*, 43449–43457. [CrossRef] [PubMed]
313. Peng, Q.; Wei, H.; Qin, Y.; Lin, Z.; Zhao, X.; Xu, F.; Leng, J.; He, X.; Cao, A.; Li, Y. Shape-Memory Polymer Nanocomposites with a 3D Conductive Network for Bidirectional Actuation and Locomotion Application. *Nanoscale* **2016**, *8*, 18042–18049. [CrossRef]
314. Goudar, N.; Vanjeri, V.N.; Kasai, D.; Gouripur, G.; Malabadi, R.B.; Masti, S.P.; Chougale, R.B. ZnO NPs Doped PVA/Spathodea Campanulata Thin Films for Food Packaging. *J. Polym. Environ.* **2021**, *29*, 2797–2812. [CrossRef]
315. Pekdemir, M.E.; Aydin, D.; Selçuk Pekdemir, S.; Erecevit Sönmez, P.; Aksoy, E. Shape Memory Polymer-Based Nanocomposites Magnetically Enhanced with Fe_3O_4 Nanoparticles. *J. Inorg. Organomet. Polym. Mater.* **2023**, *33*, 1147–1155. [CrossRef] [PubMed]
316. Korkmaz Memiş, N.; Kaplan, S. Smart Polyester Fabric with Comfort Regulation by Temperature and Moisture Responsive Shape Memory Nanocomposite Treatment. *J. Ind. Text.* **2022**, *51*, 7920S–7941S. [CrossRef]
317. Xie, Y.; Meng, Y.; Wang, W.; Zhang, E.; Leng, J.; Pei, Q. Bistable and Reconfigurable Photonic Crystals—Electroactive Shape Memory Polymer Nanocomposite for Ink-free Rewritable Paper. *Adv. Funct. Mater.* **2018**, *28*, 1802430. [CrossRef]
318. Wu, P.; Shen, X.; Schäfer, C.G.; Pan, J.; Guo, J.; Wang, C. Mechanochromic and Thermochromic Shape Memory Photonic Crystal Films Based on Core/Shell Nanoparticles for Smart Monitoring. *Nanoscale* **2019**, *11*, 20015–20023. [CrossRef]
319. Wang, S.; Wang, W.; Chi, Z.; Long, Z.; Xu, H.; Dong, Y. Development of Electric-and near-Infrared Light-Driven CNTs/EVA Shape Memory Composite Actuators with Strain Sensing and Encrypted Information Transmitting Functionalities. *Sens. Actuators Phys.* **2023**, *360*, 114547. [CrossRef]
320. Li, W.; Liu, Y.; Leng, J. Programmable and Shape-Memorizing Information Carriers. *ACS Appl. Mater. Interfaces* **2017**, *9*, 44792–44798. [CrossRef]
321. Wang, Y.; Xu, G.; Yu, H.; Hu, C.; Yan, X.; Guo, T.; Li, J. Comparison of Anti-Corrosion Properties of Polyurethane Based Composite Coatings with Low Infrared Emissivity. *Appl. Surf. Sci.* **2011**, *257*, 4743–4748. [CrossRef]
322. Jacobson, N.D.; Iroh, J. Shape Memory Corrosion-Resistant Polymeric Materials. *Int. J. Polym. Sci.* **2021**, *2021*, 5558457. [CrossRef]
323. Charlon, M.; Heinrich, B.; Matter, Y.; Couzigné, E.; Donnio, B.; Avérous, L. Synthesis, Structure and Properties of Fully Biobased Thermoplastic Polyurethanes, Obtained from a Diisocyanate Based on Modified Dimer Fatty Acids, and Different Renewable Diols. *Eur. Polym. J.* **2014**, *61*, 197–205. [CrossRef]
324. Al-Humairi, S.N.S.; Majdi, H.S.; Al-Humairi, A.N.S.; Al-Maamori, M. Future Prospects: Shape Memory Features in Shape Memory Polymers and Their Corresponding Composites. In *Smart and Functional Soft Materials*; IntechOpen: Rijeka, Croatia, 2019; ISBN 1-78984-717-6.
325. Melly, S.K.; Liu, L.; Liu, Y.; Leng, J. Active Composites Based on Shape Memory Polymers: Overview, Fabrication Methods, Applications, and Future Prospects. *J. Mater. Sci.* **2020**, *55*, 10975–11051. [CrossRef]
326. Khalid, M.Y.; Arif, Z.U.; Noroozi, R.; Zolfagharian, A.; Bodaghi, M. 4D Printing of Shape Memory Polymer Composites: A Review on Fabrication Techniques, Applications, and Future Perspectives. *J. Manuf. Process.* **2022**, *81*, 759–797. [CrossRef]
327. Li, F.; Liu, Y.; Leng, J. Progress of Shape Memory Polymers and Their Composites in Aerospace Applications. *Smart Mater. Struct.* **2019**, *28*, 103003. [CrossRef]
328. Ma, J.; Zhang, T.-Y.; Sun, S. Machine Learning-Assisted Shape Morphing Design for Soft Smart Beam. *Int. J. Mech. Sci.* **2024**, *267*, 108957. [CrossRef]
329. Sliozberg, Y.R.; Kröger, M.; Henry, T.C.; Datta, S.; Lawrence, B.D.; Hall, A.J.; Chattopadhyay, A. Computational Design of Shape Memory Polymer Nanocomposites. *Polymer* **2021**, *217*, 123476. [CrossRef]